Nikola Stanić

Assessment Methods for
Structural and Hydraulic Properties of
Concrete Sewer Pipes

ASSESSMENT METHODS FOR STRUCTURAL AND HYDRAULIC PROPERTIES OF CONCRETE SEWER PIPES

NIKOLA STANIĆ

ASSESSMENT METHODS FOR STRUCTURAL AND HYDRAULIC PROPERTIES OF CONCRETE SEWER PIPES

Proefschrift

ter verkrijging van de graad van doctor
aan de Technische Universiteit Delft,
op gezag van de Rector Magnificus prof. ir. K.C.A.M. Luyben;
voorzitter van het College voor Promoties,
in het openbaar te verdedigen op
dinsdag 26 januari 2016 om 15:00 uur

door

Nikola STANIĆ

Diplomirani Građevinski Inženjer, Universiteit van Belgrado, Servië
Master of Science in Municipal Water and Infrastructure, UNESCO-IHE
geboren te Kragujevac, Servië, Joegoslavië

Dit proefschrift is goedgekeurd door de

promotor: Prof.dr.ir. F.H.L.R. Clemens
copromotor: Dr.ir. J.G. Langeveld

Samenstelling promotiecommissie:

Rector Magnificus	voorzitter
Prof.dr.ir. F.H.L.R. Clemens	Technische Universiteit Delft, promotor
Dr.ir. J.G. Langeveld	Technische Universiteit Delft, copromotor
Prof.dr.ir. T.A.M. Salet	Technische Universiteit Eindhoven

Onafhankelijke leden:

Prof.dr. M. Maurer	ETH Zürich
Prof.dr. K.V. Horoshenkov	University of Sheffield
Prof.dr.ir. A.R.M. Wolfert	Technische Universiteit Delft
Dr. P. Le Gauffre	INSA de Lyon
Prof.dr.ir. L.C. Rietveld	Technische Universiteit Delft, reservelid

Typeset by the author with the LaTeX Documentation System.

'Experience has shown, and a true philosophy
will always show, that a vast, perhaps
the larger portion of the truth arises
from the seemingly irrelevant.'

— Edgar Allan Poe

PREFACE

Four and a half years ago I started my journey towards this book. It was an enriching experience that had its ups and downs but overall it was gratifying. As long as I can remember engineering has fascinated me. Perhaps due to the fact that almost everyone in my family is an engineer, it was just a genetic love of technology. My background and previous experiences have shown me that I enjoy facing and overcoming the challenge of research on urban drainage.

However, passion alone is not enough. This research would not have been possible without the support of the *Knowledge Programme Urban Drainage*. The aim of the project was to (*i*) identify the required information on the structural and hydraulic performance of the sewer pipes, (*ii*) quantify the uncertainties of information and (*iii*) improve the quality of this information in order to further understand the changes in processes/status. I tried my best to do as much as possible and scratch under the vast surface of sewer asset management.

A PhD is a lonely endeavor, which is not possible without the support of others. My gratitude goes to my promoter Prof. François Clemens for his patience, motivation, enthusiasm, and immense knowledge. I could not have imagined having a better promoter for my PhD study. My copromoter, Dr. Jeroen Langeveld, has always been there to listen and give advice. I am grateful to him for the long discussions that helped me to better structure my thoughts and work. I would like to thank Dr. Mathieu Lepot for his keen interest, involvement and assistance in the research, especially the experiments. Furthermore, I would like to thank my TU Delft colleagues and friends (too many to list here but you know who you are!) for their support and care, which helped me to overcome setbacks and stay focused on my work. Special thanks go to the staff of the Municipality of The Hague, the Municipality of Breda, vandervalk+degroot, Deltares and to the staff of the structure laboratory of TU Eindhoven for their assistance with the experiments, as well as to all participants in the HAZOP sessions. Finally, I would like to thank everyone who participated in this research project with interest and enthusiasm.

Most importantly, I would like to express my heartfelt gratitude to my family, especially my parents Mirjana and Milan, and my lovely fiancée Tijana. They have been a constant source of love, concern, support and strength all these years. I dedicate this book to you.

Nikola Stanić
2016

CONTENTS

1

INTRODUCTION

Throughout history, urban drainage systems have evolved and today they are viewed as a vital component of a sustainable urban system (see *e.g.* Burian & Edwards, 2002). Sewer systems can be branched or looped, consisting of various structures located in various environments *i.e.* soil types, terrain, climate conditions, urban areas. Furthermore, numerous complex and still somewhat unknown processes happen in sewers (*e.g.* Kleijwegt, 1993). Overall, sewerage and urban drainage systems are capital-intensive infrastructures characterised by process and structure complexity. In order to protect these investments, to ensure the delivery of a sewerage service and to extend the serviceability of the infrastructure, such systems have to be properly operated and maintained together with adequate rehabilitation (*i.e.* repair, renovation or replacement) (Delleur *et al.*, 1998; Marsalek & Schilling, 1998).

Sewer asset management aims at maintaining a certain minimum level of service at the lowest cost for rehabilitation and maintenance while meeting environmental/sanitary requirements. In general, asset management relies on a cost-benefit analysis between the required physical condition and the expected serviceability (Le Gauffre *et al.*, 2007). In developed countries, about 80% of the available budget for sewer asset management is spent on the rehabilitation of sewers. In the Netherlands, for instance, the municipalities spent around €1.2 billion on sewerage (or €151/per household/annum) in 2009 (Walder, 2011). Therefore, cost-effective sewer asset management is necessary to attain a preferred service level at lowest public costs.

Decisions on rehabilitation are mainly made on the basis of a limited amount of information, which is often of disputable quality (Dirksen *et al.* 2013). In addition, decisions are affected by uncertainties due to changing policies, climate conditions and future urban development (Dirksen *et. al.*, 2009). On the other hand, Ashley *et al.*, (2003) argue that such decisions should be made on a relatively limited set of economic and technical criteria, mainly related to costs, risk, environmental impact and maintaining structural integrity. In practice, there is seldom enough information available to take all these aspects into account.

Currently, decisions are mostly made based on the information on the sewer's physical status and serviceability. For instance, the primary sources of information used in decision making are pipe age and closed-circuit television (CCTV) inspections; sometimes monitored hydraulic performance is also taken into consideration (Halfawy *et al.*, 2008). While pipe age and hydraulic models are generally regarded as being an insufficient basis for asset management (Ana & Bauwens, 2007; Stone *et al.*, 2002), new models for pipe replacement based only on pipe age are still introduced and applied in practice (see, *e.g.* Carrión *et al.*, 2010). The information obtained from CCTV is limited due to the fact that only defects from within the sewer are taken into account (European Committee for Standardization, 2003).

Furthermore, Dirksen *et al.*, (2009) concluded that more information is needed for proper decision making because of insufficient quality of visual inspection results. Destructive methods like drill core sampling can provide additional valuable information about the strength properties of the sewer. Core samples, however, provide information on the material properties of only a few locations. Stanić *et al.*, (2013a) showed that uncertainties related to the application of core sampling analysis in today's practice are considerable. Core classification parameters and their classification range are not well defined. In other words, decisions on sewer management are based on partial knowledge due to scarcity of information on the functioning and conditions of urban drainage systems (Elachachi *et al.*, 2006).

1.1   INFORMATION IN DECISION MAKING

In order to meet the serviceability requirements at acceptable costs systematically, sewer managers ask questions such as 'What pipes have a greater predisposition to early failure than others?' and 'What is the range of consequences?' The answers to these and similar questions can be found using an implementation of risk analysis (Faber & Stewart, 2003). Risk analysis can be considered to consist of three main stages: failure identification, probability of the occurrence of failure and its consequences (estimation) and acceptability of the risk (evaluation) (Frosdick, 1997). Numerous techniques and methodologies for the implementation of risk analysis are known and applied in practice and scientific research (Faber & Stewart, 2003). As Montague (1990, p. 52) has stated, 'However, selecting the right method that will answer the manager's questions is an art rather than a science'. Therefore, a rather subjective, but motivated choice has to be made on which method to apply.

The first task on risk analysis of urban drainage infrastructure is to identify the potential performance failures. Overall, the main question is what information is needed to enhance a rational decision process. A first step towards an improved decision process is to have insight into the failure mechanisms. The term failure mechanism refers to a complete systematic description of how, when, and why the failure comes about, and if any other failure occurs in the chain of events. Many failures, as a qualitative change, of sewer elements emerge due to gradual build-up of conditions leading to the problem. Some of them appear due to sudden incidents. For example, clogging of sewers usually results from a gradual build-up of sediment or grease caused by different kind of factors influencing the hydraulic performance of the sewer, or from structural failures which are caused by different kinds of factors that influence sewer structural stability (Marsalek & Schilling, 1998). Once these mechanisms are known it will be more clear what chain of events lead to each particular failure. Consequently, the required information for each mechanism can be defined. For the aforementioned reasons, further research needs to be done to define a method for assessing sewer failure mechanisms as a first step to identify the required information for sewer asset management.

Table 1.1: Classification of the main sources of information for sewer asset management.

	Sources of information	Examples
	Final design reports	hydraulic design report, structural design report
Reports	As-built reports	construction report
	System performance reports	operation report, maintenance report
	All underground infrastructure reports	master plan
	Surveys	complaint surveys
	Soil characteristics measurements	soil, texture/structure, aeration, aggressivity
Measurements	Asset condition investigations	CCTV inspection, person-entry, laser scanning, core sampling, ground-penetrating radar (GPR), advanced systems (*e.g.* KARO, PIRAT, SSET)
	Hydraulic measurements	water level, velocity
	Hydrological measurements	groundwater table, rainfall measurements
	Water quality measurements	temperature, turbidity, conductivity, pH, H_2S consecrations *etc.*
	External load measurements	traffic load

There are many different sources of information that can help in explaining failure occurrences and expanding the knowledge on the actual sewer conditions. Table 1.1 summarises the main sources of information from which asset management could benefit. It can be seen from Table 1.1 that some information required already exists and only needs to be extracted (*e.g.* as-built reports). However, there are situations when the information must be collected actively.

For instance, to assess current sewer conditions, it is necessary to conduct an investigation with available inspection techniques.

Furthermore, decisions on sewer asset management could be made based on data/information with an appropriate quality. Data and information are often used synonymously. In practice, managers differentiate information from data intuitively, and describe information as data that have been processed in some manner (Pipino *et al.*, 2002; Wang, 1998). As Juran (1964) has stated, 'Data are of high quality if they are fit for their intended use in operations, decision making and planning'. What numerous studies in the field of management information systems have confirmed is that data quality is a multidimensional concept (English, 1999; Naumann & Rolker, 2000; Redman, 1996; Wang & Strong, 1996).

Data quality will differ for specific user groups. From the sewer asset management perspective, they can be characterised by six data quality dimensions, as suggested here (Table 1.2) based on already mapped dimensions (Kahn *et al.*, 2002; Wang & Strong, 1996). First of all, for the management of sewer data, it is important to know the characteristics of data sources. Data should be obtained from the representative parts of the system and should be easily accessible. The amount of data should be sufficient to meet the data processing requirement. In addition, data should be complete, reliable enough and accurate enough for the task at hand. Apart from this, data should be up-to-date, making data actuality an important data quality dimension.

Table 1.2: Data quality dimensions from the perspective of sewer asset management.

	Dimensions	Definitions
Sewer Data Quality	Source and Accessibility	where data comes from and the extent to which data is available, or easily and quickly retrieved
	Appropriate Amount of Data	the extent to which the volume of data is appropriate for the task at hand
	Completeness	he extent to which data is not missing and is of sufficient breadth and depth for the task at hand
	Believability	the extent to which data is regarded as true and credible
	Accuracy	the extent to which data are correct, reliable, and certified free of error
	Timeliness	the extent to which data is sufficiently up-to-date for the task at hand

There are numerous sources of information that can be used, but individually they do not solve the major issues of asset management. Each of these possible sources of information has its own characteristics - advantages and disadvantages (*e.g.* CCTV inspection, drill core analysis). For example, one important parameter related to the structural condition is the wall thickness, which can be measured directly by *e.g.* core sampling, but also estimated indirectly by calculating the wall losses based on a measurement of the interior shape of the pipe. A laser profiler, as an adjunct to CCTV, can identify the profile of a circular sewer and also wall loss from corrosion (Thomson *et al.*, 2010). The advantage of laser profilers is speed. Duran *et al.*, (2003) state that the main difficulty in laser profiling is the alignment and orientation of the sensor in the harsh sewer environment. Even small misalignments and shift in position can cause a significant systematic error in the measured internal geometry.

Furthermore, wall roughness has a direct influence on the hydraulic performance of the system. Increased hydraulic roughness, due to aging of the pipe material, reduces flow capacity overall influencing systems' hydraulic performance (Bennis *et al.*, 2003). Pegram and Pennington (1996) have developed a method for the *in situ* determination of hydraulic friction loss coefficients of bored tunnels, using high accurate laser scan measurements. In conclusion, there is potential in combining these two laser-based methods into one *i.e.* using the laser profiler to measure interior shape and physical roughness in order to better estimate both structural and operational conditions of sewer pipes.

1.2   RESEARCH OBJECTIVES AND CHALLENGES

Asset management strategies can be reactive and/or proactive: in a reactive approach, problems are dealt with on a corrective basis, whereas in a proactive approach potential problems are dealt with prior to failure (Butler & Davies, 2004). The current practice attempts to achieve a balance between these two approaches (Davies *et al.*, 2001b). Achieving an appropriate balance between proactive and reactive approaches depends on a number of critical factors that indicate a potential future failure (Sægrov *et al.*, 1999). Further research needs to be carried out to determine what the critical factors are and their relationships with the structural and/or operational failures of sewer elements. The Dutch RIONED Foundation statistics (2009) shows that the majority of urban drainage systems (about 72%) are made of concrete, thus making studying concrete sewer pipes the most essential.

For instance, when a concrete sewer pipe collapses, it must be replaced. But what leads to complete loss of structural integrity? Collapse of structural elements is caused by structure overloading and/or by loss of strength. The principle of structural behaviour of buried concrete pipes is fairly well understood (see, *e.g.* Kim *et al.*, 2010; Trautmann & O'Rourke, 1985), except for how material deterioration affects structural behaviour and performance. Consequently, information on the structural behaviour of deteriorated sewer pipes will contribute to better understanding of the changes in status, which is essential for achieving the desired efficiency gains for urban drainage systems. Therefore, it is necessary to define new methods that will allow this information to be collected.

Furthermore, decision making on rehabilitation or replacement should preferably be based on the actual functionality of a sewer system. In order to judge the ability of a sewer system to transport sewage, hydrodynamic models are used. One of the key parameters used in these models is the hydraulic roughness. For new pipes, this is well known, but for aged pipes, with uneven deterioration along the cross section, information on the hydraulic roughness is lacking. Therefore, it is necessary to define methods that enable the collection of this information.

CCTV as as predominantly applied inspection technique is effective only for detecting gross defects (Wirahadikusumah *et al.*, 1998). Further, Dirksen *et al.*, (2013) notes that currently applied visual inspection coding systems are too complex to give consistent, reproducible results. The same applies for the core sampling analysis. There are many other methods new developments for sewer condition assessment e.g. infra-red (IR) thermography systems, ground-penetrating radar (GPR), ultrasonic-based systems, and laser-based systems. However, interpretation of IR thermography and GPR still presents some difficulties. On the other hand, laser- and ultrasonic-based systems can quickly collect information only on the pipe surface, and they still have some problems with the accuracy of collected data (Duran *et al.*, 2002; 2003). Overall, there is a need for a new inspecting approach, which is not limited by coding and is able with an appropriate accuracy to assess sewer conditions. Moreover, with a better quantification of inspection uncertainties sewer operators should be able to judge the impact of the uncertainties on their decisions in order to justify their choices properly.

This research aims at (*i*) identifying the required information on the structural and hydraulic performance of the sewer pipes, (*ii*) quantifying the uncertainties of information and (*iii*) improving the quality of this information in order to further understand the changes in processes/status. For this purpose, the structural and hydraulic behaviour of the pipes is studied in more depth. Finally, this research is a first step towards determining the remaining load bearing capacity of a sewer pipe and it determines the type of information needed for proper decision making, which is essential to minimize the pipe replacement costs. Moreover, providing an input for the hydrodynamic sewer models enables an accurate estimation of actual hydraulic characteristics and thus may serve as a basis for a sewer asset management based on actual functionality.

The outline of the thesis is structured as follows. **Chapter 1** gives an introduction to the limitations and potentials of different information sources on concrete pipe structural and operational conditions in sewer asset management. In order to identify the failure mechanisms involved, the HAZard and Operability (HAZOP) approach is applied (Frosdick, 1997). This is a first step in identifying required information for sewer asset management. With HAZOP analysis, failure mechanisms can be identified, as well as sources of information to detect and quantify these mechanisms. This approach determines the site-specific relevant failure mechanisms and information needed on structural and hydraulic performance of sewer pipes (**Chapter 2**). The HAZOP study presented here yields an extensive failure tree structure and large amounts of potential sources of information.

Part I presents the limitations and potentials of different techniques for structural condition assessment of concrete sewer pipes. These techniques are potential information sources on the pipe collapse failure mechanism. In sewer systems where pipe corrosion is the dominant failure mechanism, visual inspection by CCTV and core sampling are among the methods mostly applied to assess sewer pipe condition. Large uncertainties are currently associated with both methods and there is no obvious correlation between them **(Chapter 3)**. Therefore, new inspection approaches should be applied. Important structural characteristics, such as interior shape and related to this the remaining wall thickness are measured using an inspection concept employing a laser-based profiler coupled to a CCTV camera **(Chapter 4)**. Based on the uncertainty analysis revealed to this technique, an improvement of the available laser profiling technique is proposed and tested (Prototype v1.0). Moreover, the structural behaviour of the pipes is studied in more depth. No attempt was made to evaluate the structural response of deteriorated concrete sewer pipes. A simple test set-up is designed and adopted to see whether it is possible to simulate a structural response of deteriorated concrete sewer pipes **(Chapter 5)**. A geometry of the pipes is defined (laser profiling) as well as certain concrete material properties (core sampling). The most significant parameters are identified and their impacts to the remaining load bearing capacity of a sewer pipe (collapse) quantified.

Part II presents the limitations and potentials of a technique for hydraulic condition assessment of concrete sewer pipes. Pegram and Pennington (1996) have developed a laser-based method for linking hydraulic roughness to measured physical roughness of an irregular surface. There is potential in applying this methodology in order to obtain an accurate estimation for the hydraulic condition of sewer pipes; *i.e.* quantifying physical (wall) roughness, quantifying the attached and/or settled deposits roughness **(Chapter 6)**. For the deteriorated concrete pipe surfaces a low-resolution laser scan is able to measure physical roughness and consequently the hydraulic roughness.

Laser profiling offers a new and challenging perspective for measuring sewer pipe structural characteristics, such as interior shape and, related to this, the remaining wall thickness and hydraulic properties, such as wall roughness **(Chapter 7)**. A new improved version of the laser profiling technique (Prototype v2.0) and its potential applications are presented.

Chapter 8 presents conclusions of this study and recommendations for future work. In this thesis we show the successful design of a new and collaborative technique for sewer pipe inspection (Prototype v2.0), which can provide accurate information on concrete pipe conditions. Moreover, we determine the critical parameters that provide the lowest uncertainties and highest information content on the status of deteriorated concrete sewer pipes. This new technique and defined parameters can significantly contribute to future decision making.

2

IDENTIFICATION OF INFORMATION REQUIREMENTS FOR SEWER ASSET MANAGEMENT

Due to sewer systems' processes and structure complexity, it is difficult to achieve a well-established relation between required asset management efforts and the level of service provided (Ashley & Hopkinson, 2002). Further, it is not clear what type of information of what quality is necessary to fully benefit from sewer asset management. Information on the physical status and the serviceability by themselves are not sufficient for identifying a trend towards failure. An understanding of changes in processes and/or status is essential for achieving effective sewer asset management. This can be achieved through an increased understanding of sewer failure mechanisms. In this chapter a method is described for assessing sewer failure mechanisms as a first step to identify the required information for sewer asset management.

The first section of the chapter presents the HAZard and OPerability (HAZOP) approach. The HAZOP analysis allows failure mechanisms to be identified, as well as sources of information to detect and quantify the identified failure mechanisms. In the second section the failure mechanisms, as well as sources of information to detect and quantify the identified failure mechanisms are identified. The third section discusses possibilities for filling the gaps in the information, followed by a section on the information needed on the structural and hydraulic performance of concrete sewer pipes and the concluding remarks.

2.1   METHOD FOR IDENTIFYING SEWER FAILURE MECHANISMS

The first task on risk analysis of urban drainage infrastructure is to identify the potential performance failures. One of the techniques for risk identification of sewer systems, HAZOP analysis, was used in this study. HAZOP analysis was developed in Britain by ICI (Imperial Chemical Industries, Ltd) in the late 1960s for risk identification in chemical plants. HAZOP is a well-established structured 'brain-storming' technique in engineering risk assessment (Frosdick, 1997; Kirwan, 1992). It uses special guidewords combined with process conditions to systematically consider all possible deviations from normal conditions (Figure 2.1).
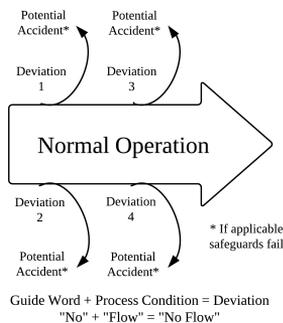
Figure 2.1: Schematic diagram of the HAZOP analysis.

In a HAZOP study, a multidisciplinary group of sewerage experts have to serve as the review team (Montague, 1990). The reason to choose HAZOP for this research is that this technique allows for input from practitioners, specialists and scientists, and gives the opportunity for interaction between the three groups, which enhances a comprehensive description of failure mechanisms. Team members have to bring knowledge of the sewer design and construction, experience in system and equipment operations, experience in equipment testing and maintenance, knowledge on hydraulic and/or hydrological and/or geohydrological processes and knowledge of safety objectives and procedures.

This qualitative technique was carried out during a set of meetings. The expert team first determined the top events causing sewer failure, and then reviewed each top event using the HAZOP analysis steps given in Figure 2.2. Results from a HAZOP analysis are summarised in tabular form. Overall, this extensive screening of the possible failures/risks with numerous expert groups makes this technique strongly suitable for the sewer risk analysis. In order to avoid bias of HAZOP sessions, an independent expert who did not participate in the actual HAZOP meetings reviewed the final documentation. However, a disadvantage of the risk identification techniques is that they rely on expert subjective judgements based on hindsight; HAZOP cannot predict new failure/risks - which we are not yet aware of (Frosdick, 1997).
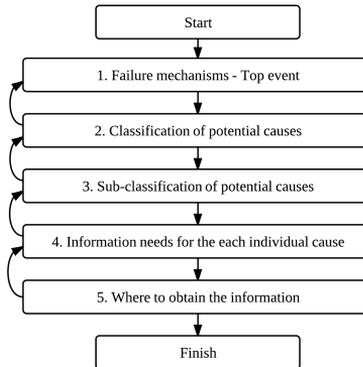
Figure 2.2: Procedural outline followed in sewer failure assessment.

2.2 FAILURE TREE AND POTENTIAL SOURCES OF INFORMATION

2.2.1 *Failure mechanisms - top events*

A long list of processes and defects responsible for the structural/operational failures of sewer systems in this study was identified, as well as the possibility of obtaining the information about them. Table 2.1 shows the top failure events that affect the sewer system serviceability and the principle causes why these events are occurring.

Failures are differentiated into two main groups, system and element performance. System failure is defined as failing to meet serviceability requirements with respect to system performance, such as urban flooding. Element failures are defined as the failure of a specific sewer object or element, either collapse or breakdown. Element failures not necessarily lead to system failure. For example, if one pipe in a mazed sewer system is fully clogged, it will most likely not have a significant effect on overall system performances as wastewater will find another route to flow downstream, the systems serviceability is likely to be effected only marginally (partial

failure). Top events occur as soon as the load (*e.g.* hydraulic loading of system and traffic loading of sewer pipe) exceeds the capacity or strength.

2.2.2 *Classification of potential causes*

The HAZOP study resulted in extensive failure tree structures and large amounts of potential sources of information. The HAZOP results are presented in detail in Appendix A. One example is presented in some detail here. Flooding is caused by hydraulic overloading of the system when the system is not capable of completely conveying the hydraulic load. Figure 2.3 shows the logic tree structure for flooding, top event. Flooding due to a decrease in capacity may be caused by human errors, external effects or by their combination.

Table 2.1: Top failure events of sewer systems and their main causes.

	Top event	Cause
System Performance Failures	Flooding Frequent CSOs	load ↗ and/or capacity ↘
	Soil contamination	load ↗ and/or strength ↘
	Exposure to health hazards	load ↗ and/or protection ↘
Element Performance Failures	Collapse of structural elements Breakdown of mechanical elements	load ↗ and/or strenght ↘

Note: CSOs: Combined Sewer Overflows

2.2.3 *Sub-classification of causes*

Each cause defined in Figure 2.3 is explained by a number of sub-causes. For instance, root intrusion and ingress of soil are external effects that may cause flooding of the system. Furthermore, these causes can also cause element performance failures. Root intrusion may affect the structural strength of the elements and eventually initiate sewer collapse. On the other hand, ingress of soil may contribute to the formation of a sinkhole, which can also cause collapse of the sewer. Figure 2.4 shows the sewer with root intrusion and ingress of soil.

Root intrusion is a known major sewer maintenance problem that is generally easily detected with visual inspection (Duran *et al.*, 2002; Randrup *et al.*, 2001). In contrast, there is very limited knowledge on ingress of soil (Korving *et al.*, 2003); and ingress of soil is barely noted during visual inspection of sewer (Ibrahim *et al.*, 2009). The possible sub-classification of causes of root intrusion and ingress of soil derived in the HAZOP is given in Tables 2.2 and 2.3.

2.2.4 *Information needed per individual cause*

The information needed per individual cause is shown in Tables 2.2 and 2.3. A number of these needs are discussed hereafter. Tree species and their distance from the sewer (A-2.1.1.) are factors that may contribute to root intrusion and consequently sewer damage and blockage. Some tree species have a higher potential to cause damage to urban infrastructures such as sewers (McPherson & Pepér, 1995). Furthermore, trees that are located close to the sewer may represent a treat to sewer (Randrup *et al.*, 2001). Information on characteristics of the trees and their distance to the sewer would contribute to the root intrusion prediction.

Environmental factors (A-2.1.2.) can increase the root growth and thus increase the possibility of root intrusion. Soil characteristics, *e.g.* texture, structure, moisture, aeration, temperature, toxic material, bacteria, fungi and soil-inhabiting animals, may influence root growth (Feldman, 1984; Gregory, 1988; Waisel *et al.*, 1991). Atmospheric conditions, namely light intensity and amount of CO_2 in air, and their effect on the treetops can have indirect effect on the root growth. Furthermore, in case of a low groundwater table, roots will search for water and will eventually reach
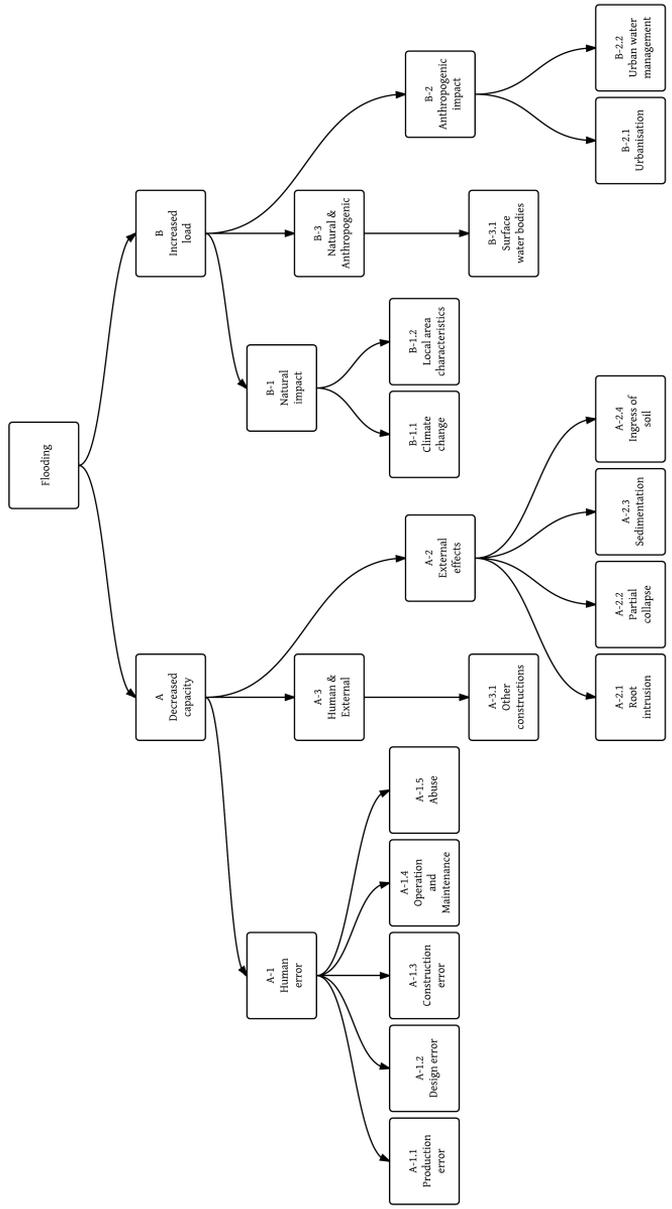
Figure 2.3: Classification of potential causes of flooding.
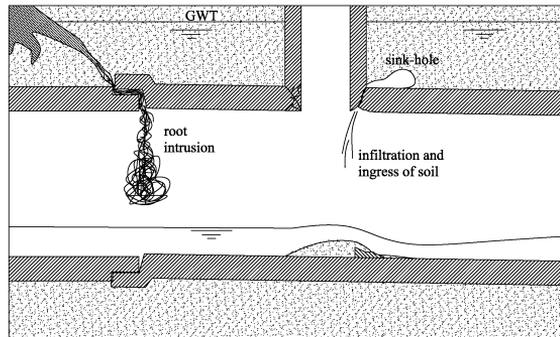
Figure 2.4: Sewer with root intrusion and ingress of soil.

the sewer and cause problems (Comery 2007). Information on the overall local environmental characteristics would help in determining the possibility of occurrence of root intrusion.

Workmanship errors (A-2.1.3. and A-2.4.1.-2.4.4.) contribute to a large extent to the occurrence of root intrusion and ingress of soil. Applying poor practice during the sewer construction may be the cause of different kinds of defects such as openings/leakage at joints and even a complete structural failure (Boden *et al.*, 1975). Roots may enter through the joint openings. In addition, infiltration of groundwater, and potentially, ingress of soil into the sewer will most likely happen through the pipe joint rather than through some other defect in the pipeline (Fenner, 1990). The amount of soil entered due to infiltration depends on the soil characteristics of the backfill. Finer particles of soil can be flushed out easily into the sewer. Therefore, it is very important for pipes to be properly connected and for the backfill to be of proper quality. Improper compaction of the backfill can also contribute to ingress of soil into the sewer. Fenner (1991) showed that the intensity of water and soil migration into the sewer is influenced by the bedding and/or foundation characteristics. Improper bedding/foundation would allow pipe settlement, enabling infiltration of water and soil. Information on the construction process and an as-built report would help in determining the possibility of occurrence of root intrusion and of ingress of soil.

Lack of supervision (A-2.1.3. and A-2.4.1.-2.4.4.) is an important issue when it comes to a construction of connections and joint placement. Formally, after a sewer construction field testing should be done to ensure that the joints are watertight and constructed satisfactorily (European Committee for Standardization, 2011). The same kind of check should be carried out on the constructed connections. However, a lack of supervision minimizes enforcement of these checks. The presence of openings in the pipes or structure should be prevented, because if they are present, roots, water and, possibly, soil, will be allowed to enter the sewer. Improvisations during construction due to local conditions can be important in influencing structural stability of a sewer. Lack of professionalism during construction and improper improvisation can create cracks and holes in the pipe structure through which roots and soil will be able to pass. As mentioned earlier, information on construction process and as-built report would be useful.

The selection of pipe and joint type and/or material (A-2.1.4. and A-2.4.5.) can also significantly influence the possibility of soil intrusion. Pipe durability depends among others on pipe materials due to different structural characteristics (Sousa *et al.*, 2009). For instance, if a sewer is built using plastic material, a potential pipe defect is deformation (Water Services Association and Foundation for Water Research, 1993). Openings at the location of connections may occur allowing the passage of soil into the sewer. Furthermore, joint type and/or material must be resistant to root intrusion (Davies *et al.*, 2001a). Inspection could provide valuable information about the current status of the drain and sewer system and its components for prevention of possible root intrusion and ingress of soil. The major cause of joint-related structural defects is an improper selection of joint type (Park & Lee, 1998). An improper selection of the joint type or selection of poor quality

Table 2.2: Classification of possible causes of root intrusion and their information needs.

2.1. Root intrusion	Cause	Information needed on cause	Where to get information
2.1.1. Tree species and their position	- trees with deep roots - trees located close-by the sewer	1. type of trees 1. location of trees	a. from the local community a. from the local community
2.1.2. Characteristics of the local environment	- low groundwater table	1. measurement of groundwater table	a. from measuring programs (groundwater table)
	- poor soil conditions	1. soil texture/structure, moisture, aeration, temperature and root competition	a. from measuring programs
	- climate conditions	1. light intensity, CO_2	a. from the meteorological department
	- pollution and infection	1. toxic material, bacteria fungi and soil-inhabiting animals	a. from measuring programs
2.1.3. Wrongly constructed connections and/or joints	- lack of professionalism during construction	1. as-built report 2. inspection results	a. from the constructor
	- lack of supervision	1. who and if there was supervised	a. from the municipality
	- improvisation due to local conditions	1. as-built report 2. inspection results	a. from the constructor
2.1.4. Improper choice of joint type and/or material	- un/experienced engineers -lack of quality check -lack of appropriate data	1. checking of design protocol 1. checking of final report 1. checking the quality of initial data necessary for the design	a. inside the design company a. from the contractor a. sources of initial data: (*e.g.* material → manufacture)
2.1.5. Weakened structural elements	- low strength properties of plastic pipes	1. deformation of pipes	a. from the inspection (*e.g.* CCTV)
	- sever pipe deterioration	1. sever cracks, pipe brakes, infiltration	a. from the inspection (*e.g.* CCTV)
2.1.6. Sewer maintenance practices	- improper root removal	1. maintenance procedure	a. from the maintenance team

may easily result in a short period of time of root intrusion and infiltration of water and consequently soil. Assessing final reports and the quality of the material could give useful information for estimating the possibility of appearance of ingress of soil and root intrusion.

With time drainage systems deteriorate (A-2.1.5. and A-2.4.6.) due to ageing, overloading, misuse and mismanagement. The more deteriorated pipes are, the more likely the occurrence of root intrusion and ingress of soil become. Sewer inspection (*e.g.* CCTV inspection) can provide valuable information about the physical status of the system and on rate of the deterioration.

Control and removal of roots (A-2.1.6.) in a sewer is an important on-going maintenance operation. The cutting frequency and methodology affect their growth. After cutting, roots tend to grow faster and more than before. There exist several maintenance options for controlling root growth (Randrup *et al.*, 2001). Information on conducted maintenance would be useful.

Groundwater (A-2.4.7.) intrusion can occur when the groundwater table (GWT) is above sewer invert level. Soil particles can be flushed in through the existing defect with the infiltration of groundwater as a result of erosion and suffusion which could cause ground loss and subsequent lack of support to the sewer through the loss in soil density or the formation of cavities (Davies *et al.*, 2001b). However, erosion of cohesive soil through the defect can occur due to strong changes of hydraulic conditions in the sewers. Over time, voids formed by internal erosion can enlarge to the point of total loss of structural integrity. Furthermore, groundwater in highly corrosive soil may have adverse effects on some sewer joint materials (Davies *et al.*, 2001b). In the course of time, the joint material could deteriorate to such an extent to allow passage of soil into the sewer. Information on groundwater level and quality is necessary to be able to determine groundwater infiltration and possible soil passage.

Root intrusion (A-2.1.1.-2.1.6. and A-2.4.8.) may contribute to migration of soil by expanding existing openings in the sewer, allowing surrounding soil to enter through the defect (Water

Table 2.3: Classification of possible causes of ingress of soil and their information needs.

2.4. Ingress of soil	Cause	Information needed on cause	Where to get information
2.4.1. Improper pipe positioning	- improper quality of backfill	1. soil characteristics of backfill	a. from the constructor
			b. from the measuring
	- lack of supervision	1. who and if there was supervision	a. from the municipality
	- pipes barely connected	1. position of pipes	a. from the constructor
			b. from the inspection
2.4.2. Damaging during refilling and/or compaction	- cores material in backfill	1. soil characteristics of backfill	a. from the constructor
		2. how it was compacted	
	- lack of supervision	1. who and if there was supervised	a. from the municipality
2.4.3. Improper bedding and/or foundation	- improper consolidation of bedding	1. characteristics of bedding	a. from the constructor
	- improper foundation	1. soil characteristics of foundation	a. from the constructor
	- lack of supervision	1. who and if there was supervised	a. from the municipality
2.4.4. Wrongly constructed connections and/or joints	- lack of professionalism during construction	1. as-built report	a. from the constructor
		2. inspection results	
	- lack of supervision	1. who and if there was supervised	a. from the municipality
	- improvisation due to local conditions	1. as-built report	a. from the constructor
		2. inspection results	
2.4.5. Improper choice of pipe and joint type/material	- un/experienced engineer	1. checking of design protocol	a. inside the design company
	- lack of quality check	1. checking of final report	a. from the contractor
	- lack of appropriate data	1. checking the quality of initial data necessary for the design	a. sources of initial data: (*e.g.* material $\rightarrow$ manufacture)
2.4.6. Weakened structural elements	- low strength properties of plastic pipes	1. deformation of pipes	a. from the inspection (*e.g.* CCTV)
	- sever pipe deterioration	1. sever cracks, pipe brakes, infiltration	a. from the inspection (*e.g.* CCTV)
2.4.7. Groundwater table	- high groundwater table	1. measurement of groundwater table	a. from measuring programs (groundwater table)
	- aggressive ground water	1. ground water quality	a. from measuring programs
2.4.8. Root intrusion	$\Longrightarrow$ Table Flooding A-2.1	$\Longrightarrow$ Table Flooding A-2.1	$\Longrightarrow$ Table Flooding A-2.1
2.4.9. Inappropriate load transfer	- improper traffic load	1. nature and density of the traffic	a. from the municipality
	- load due to construction around the sewer	1. if proper measures were taken during construction	a. from the constructor
		2. structure conditions	b. from the inspection

Environment Federation, 1994). Information on characteristics of the trees and their location in the area around sewers would contribute to root intrusion prevention.

Inappropriate load transfer (A-2.4.9.) may cause different kinds of damage to the sewer (textite.g. cracks, break, collapse) as well as ingress of soil. A sewer can be affected by a variety of loads, such as traffic load, and load too close to the construction; Davies *et.al.*, (2001b) showed that traffic load damage increases with the number of vehicles passing over the sewer. Cracks may appear and on-going deterioration may induce infiltration, provided that the GWT is above the sewer. Furthermore, vibrations due to near-by construction activities may cause severe damage to sewers within a very short period of time. Information on the traffic frequency and construction activity would help in assessing sewer damage. damage.

2.2.5 *Filling gaps*

The HAZOP results showed that there are a lot of different sources of information that can help in explaining failure occurrences and expanding the knowledge on the actual sewer conditions. There are two major approaches of data collection that can be distinguished as follows: primary and secondary sources of information. Sometimes, information required needs to be collected *i.e.* primary sources (measurements); however, there are times when information is already available and needs only to be retrieved *i.e.* secondary sources (reports) (Kumar, 2005).

Table 2.4: Possible sources of information needed for assessment of root intrusion and ingress of soil.

	Reports		Measurements				
	As-built	System performance	Surveys	Soil charact.	Asset cond.	Hydrologic	External load
Tree species and their position			+				
Characteristics of the local environment				+		++	
Wrongly constructed connections/joints	+						
Improper choice of joint type/material	+						
Weakened structural elements					++		
Sewer maintenance practices		+	+				
Improper pipe positioning	+			+			
Damaging during refilling/compaction	+			+			
Improper bedding/foundation	+			+			
Inappropriate load transfer							+

Legend: + possible sources of information, ++ possible sources that are most commonly used in practise

Table 2.4 shows clearly that there are seven groups of possible sources of information for assessment of root intrusion and ingress of soil. Table 2.4 shows that asset condition investigations (*e.g.* CCTV inspection) and hydrological measurements (*e.g.* GWT measurements) are the most common sources of information used in practice for assessment of root intrusion and ingress of soil. These relatively cheap sources of data give only a limited amount of information and of sometimes questionable data quality. There are numerous sources of information that can be used, but individually they do not solve the full information need for asset management. Each of these possible sources of information has their own characteristics - advantages and disadvantages (Table 2.5).

First, it is important to find the answer to 'What factors most influence the failure occurrence?'. There have been numerous attempts to answer this and other failure related question (see *e.g.*, Hahn, *et. al.*, 2002). What is specific for this analysis is that considers the Netherlands settings, such as issue of the soil settlement.

This research showed that greater number of failure causes contributing to root intrusion and ingress of soil is linked to human activity especially during the construction phase. The extent to which the environment influences the sewer system (controlled system) depends on the condition of the system and *vice versa*. Information on the construction practices can be found in as-built reports. As a secondary source of information, as-built reports provide detailed information on the conducted construction practices and on the locations where the construction deviated most from the final design. This information can help pinpointing locations that most likely will suffer from root intrusion and ingress of soil, and thus help future investigation planning. Studying of as-built reports is time consuming and should be done by sewer experts.

Maintenance reports could provide information on sewer defects and their location, and information about maintenance practices. Sewer management decisions (control), *e.g.* maintenance policies, influence both the controlled system and the environment. In CCTV inspection, roots are generally easily noticed, opposite to ingress of soil (Ibrahim *et al.*, 2009). Maintenance reports

Table 2.5: Characteristics of the possible sources of information needed for assessment of root intrusion and ingress of soil (the quality indications given are subjective).

Sources of information	Use	Data quality	Scale	Cost	Time
As-built reports	- construction reports, structural reports	2-3	1-3	1-2	2-3
System performance reports	- maintenance reports	1-2	1-3	1-2	2-3
Surveys	- observations, interviews, questioners	1-3	1-3	2-3	1-2
Soil characteristics measurements	- taking soil samples, field measurements	2-3	1-2	1-3	2-3
Asser condition investigations	- CCTV inspections, person entry, GPR, infra-red thermography	1-3	1-3	1-3	1-3
Hydrological measurements	- field GWT measure, local climate inform.	2-3	1-2	1-3	2-3
External load measurements	- traffic density, field measurements	2-3	1-2	2-3	2-3

Legend: 1 - low; 2 - moderate; 3 - high

are a relatively good source of information as long as they are complete and up-to-date. Like in the case of as-built reports, it is expected that information in the reports to be objective.

Furthermore, surveys can easily provide information on a local environment, *e.g.* tree species and their distance from the sewer. Together with knowledge of the local climate conditions and the soil type, the extent of the root growth the behaviour of root growth can be anticipted ergo the root intrusion can be predicted. There are numerous measurements on soil conditions, pollution and/or infections that provide information about the local environment on a small scale. Moreover, they do not provide enough relevant information needed for estimating sewer root intrusion and ingress of soil.

Ingress of soil is not easily noticed by CCTV. Therefore, there is a need for changing the investigation method. Sewer inspection techniques that can detect ingress of soil include, for example, infrared (IR) thermography, ground-penetrating radar (GPR) and advanced systems (*e.g.* KARO) (Costello *et al.*, 2007; Duran *et al.*, 2002; Makar, 1999). These are all relatively advanced investigation technologies and relatively expensive in comparison with CCTV inspection; hence, these technologies should be used only when it is required. One possible approach is, when there is enough suspicion that there is a problem of ingress of soil at a particular location based on the secondary sources of information, surveys and GWT values, only then one of these techniques should be applied to confirm the suspicion.

2.3 INFORMATION NEEDED ON STRUCTURAL AND HYDRAULIC PERFORMANCE OF CONCRETE SEWER PIPES

For practical applications, it is unlikely that all possible failure mechanisms will or even can be taken into account, because of the vast amount of information that is involved. Another example of top events is presented in some detail here. Collapse of structural elements is caused by static and/or dynamic overloading of the structure when the structure is not able to withstand the load and loses its structural integrity. Figure 2.5 shows the logic tree structure for collapse of structural elements. When comparing Figure 2.3 with Figure 2.5 repetition of the sub-causes can be observed. Furthermore, Appendix A shows that the greater number of possible failure causes is linked to human activity - around 65% (*e.g.* workmanship errors, design errors). Overall, the assumption that a newly built sewer is perfect is hampering effective and efficient sewer maintenance strategies. Information on these causes falls generally under the category of secondary
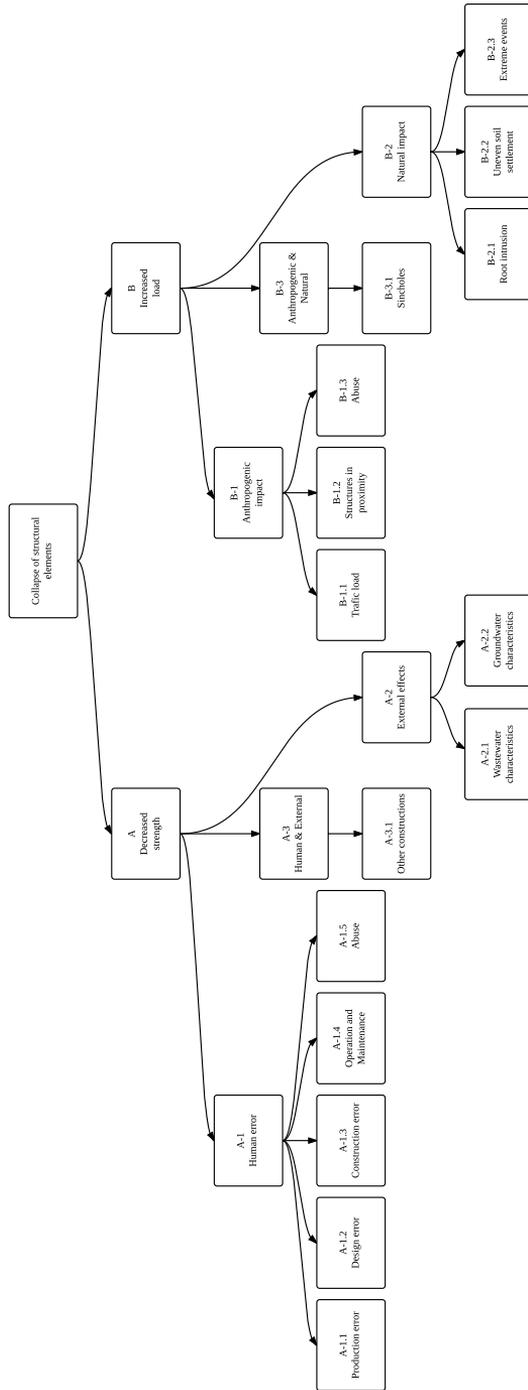
Figure 2.5: Classification of potential causes of collapse of structural elements.

sources (reports). The reports like as-built reports provide valuable information on the initial status of the system. However, they do not provide information on the current state of the system. In order to better understand the changes in the condition of the assets, it is essential to gather information (measurements) on relevant deterioration. This can be achieved generally by using sewer inspection techniques.

Information on structural and hydraulic failures of sewer pipes is one of the most relevant due to the fact that this is the basic unit (element) of the system. In The Netherlands the majority of urban drainage systems are made of concrete elements (about 72%) thus making information on concrete sewer pipes the most essential (RIONED, 2009). Overall, possible sources of information, necessary for assessing impacts of sewer pipe structural and hydraulic failures on meeting the serviceability requirement, were determined based on knowledge of the chain events of sewer failure and information needed on their initial causes.

With time, concrete sewer pipes deteriorate due to characteristics of wastewater (*i.e.* nature and concentration of pollutants) and groundwater (*i.e.* aggressive groundwater) (Hobbs, 2001; Polder, 1987). Material corrodes due to the effect of chemical, biological and/or mechanical (erosion) attack (A-2.1-2.). In addition, evidence shows that an inappropriate maintenance practices (*i.e.* sewer cleaning) can accelerate sewer deterioration (A-1.4.). For instance, the high water pressure sometimes involved in jetting, a sewer cleaning technique, may cause damage to sewer infrastructure (Davies *et al.*, 2001a). Concrete degenerates and disappears with time and at some point can lead to the structural collapse due to decreased material strength and decreased wall thickness. Consequently, collecting information on the pipe geometry (*i.e.* loss of wall thickness), material properties and structural defects (*e.g.* cracks) become imperative.

Table 2.6 shows existing inspection techniques that can collect this information along with their characteristics (see, *e.g.* Duran *et al.*, 2002; Guo *et al.*, 2009; Kirkham *et al.*, 2000; Makar, 1999; Wirahadikusumah *et al.*, 1998). Each of the inspection techniques has its own advantages and disadvantages. Furthermore, they provide limited information about the sewer condition due to the fact that each method measures different physical properties and, consequently, only specific features of the material defects are recognized. For instance, drill core analysis provides information on the material properties of a few locations only. Further, the SewerBatt$^{\textcircled{R}}$, acustis inspection technique, can quickly and economically provide information on the defects over the whole sewer stretch. In other respect, the disadvantage of sewerbatt technique is its inability to distinguish between a single or the multiple defects present at scanned location. With a view to informing prioritisation, this technique can precede higher resolution techniques which are carried out where it is most critical, and not where it is not required (Long & Faram, 2014; Plihal *et al.*, 2015).

CCTV inspection, as commonly used technique, is relatively cheap and quick regarding application. However, Dirksen *et al.*, (2013) shows that visual inspections have a significant uncertainty. Besides, visual inspection will not reveal invisible deterioration, like corrosion on the outside wall of a sewer. Destructive methods like core sampling can provide additional valuable information about the strength properties of the sewer. Drill core analysis can provide more information on the material properties (*e.g.* density, splitting tensile strength, water absorption) as well as on the soil properties compared with other techniques used for inspection of pipe structure and bedding condition. Their inspection costs are of the same order. Furthermore, one important parameter related to the structural condition is the wall thickness, which can be measured directly by *e.g.* core sampling, but also estimated indirectly (through estimation of loss of the wall thickness) with an inspection concept employing a laser-based profiler coupled to a CCTV camera. Laser profiling, as well as sonar, is capable of providing a quick, quantitative assessment of sewer deformation and other problems, indicating not just the presence of the defect, but also its severity and location more accurately then visual inspection. However, laser technique is a somewhat cheaper for application compered to sonar because a laser profiler is an adjunct to CCTV (Thomson *et al.*, 2010). Other advanced system (*e.g.* SSET, PIRAT) provide a lot of valuable information on the pipe geometry (profile), nonetheless, their initial cost are high for practical application.

Table 2.6: Characteristics of the possible inspection techniques for assessment of structural properties of the concrete sewer pipes (the quality indications given are subjective and based on experts' judgment).

Inspection technique	Use	Availability	Scale	Cost	Time
CCTV inspection	- examine pipe wall surface (*e.g.* visible deformation, surface crack, fracture, break and/or collapse)	3	1-3	1-2	1-2
Drill core analysis	- strength properties of pipe, pipe thickness, carbonation depth	2-3	1	2-3	2-3
Laser profiling	- examine pipe wall surface (*e.g.* visible deformation, surface crack, loss of the wall thickness)	2-3	1-3	2	1-2
Sonar	- shape, defects, material thickness and attenuation	2-3	1-3	2	1-2
Impact echo	- pipe wall integrity, combined pipe and soil condition, regions of cracking	1-2	1-3	2-3	1-3
Spectral Analysis of Surface Waves (SASW)	- pipe wall integrity, surrounding soil conditions	1-2	1-3	2-3	1-3
Microdeflections	- overall mechanical strength	1-2	1-3	2-3	1-3
Natural vibrations	- pipe wall and bedding condition	1-2	1-3	2-3	1-3
SewerBatt®	- detects crack, break and/or collapse	2-3	1-3	2	1
Advanced systems (KARO, PIRAT, SSET)	- detect the type, location and size of defects in and out sewer lines	1-2	1-3	3	2

Legend: 1 - low; 2 - moderate; 3 - high

Of all the techniques for the assessment of the pipe structural properties core sampling and laser profiling are the most promising techniques when taking into account the amount of information that they provide, the costs of the application and their availability. Therefore, further study of these techniques, their perspective for quantifying a sewer pipe's structural characteristics and uncertainties related to them, will contribute to a better understanding of structural status which is essential for achieving the desired serviceability of the infrastructure.

Further, the principle of structural behaviour of buried concrete pipes is fairly well understood (see, *e.g.* Kang *et al.*, 2007; Kim *et al.*, 2010; Krizek & McQuade, 1978; Trautmann & O'Rourke, 1985), except for how material deterioration affects the structural behaviour and performance. Consequently, information on the structural behaviour of deteriorated sewer pipes will contribute to better understanding of the changes in status, which is essential for achieving the desired efficiency gains for urban drainage systems. Therefore, it is necessary to define new methods that will allow this information to be collected.

With respect to hydraulic performance of concrete sewer pipes in practise there is a lack of reliable information on the actual hydraulic roughness of aged pipes; the roughness will change over time due to *e.g.* corrosion processes, joint eccentricity, protruding objects and subsidence. Increased hydraulic roughness, due to aging of the pipe material, reduces the flow capacity of the pipe, resulting in decreasing systems' hydraulic performance consequently causing flooding (Bennis *et al.*, 2003). Furthermore, sewer repairs (A-1.4.), like sewer relining, alter the hydraulic resistance mainly due to a decrease in diameter and, depending on the material used, the hydraulic roughness. Consequently, it is important to know the actual status of the asset - pipes, such as hydraulic roughness and the exact interior geometry in order to determine whether or not a given pipe has adequate hydraulic capacity.

In literature, some attempts to this end are reported. For instance, Romanova *et al.*, (2014) developed a novel, non-invasive and *in situ* acoustic method and instrumentation to measure the water surface pattern and hence determine the resistance and then the pipe wall roughness. Romanova *et al.*, (2014), however, does not measure the actual wall roughness and above all suggests further research. For example, the presence of sediments or other objects can also induce

the formation of patterns at the surface; hence it is hard to state that the actual roughness can always be measured using this method. Therefore, it is necessary to define methods that enable the collection of this information.

Pegram and Pennington (1996) have developed a method for the *in situ* determination of hydraulic friction loss coefficients of bored tunnels, using high accurate laser scan measurements. There is potential in applying this methodology in order to obtain an accurate estimation for the hydraulic condition of sewer pipes; *i.e.* quantifying physical (wall) roughness, quantifying the attached and/or settled deposits roughness.

2.4 CONCLUSIONS

The HAZOP technique confirmed that it could be used as a first indication for determining the basic information needed for sewer asset management. The main processes and defects responsible for the structural and operational failures of sewer elements were identified, as well as the possibility of obtaining information about them. A comprehensive description of the failure mechanisms is obtained as well as failure trees that describe the failure process; these are used as a basis from which to prioritise research aimed at obtaining proper information on sewer failure. It is possible that, due to expert subjective judgment based on hindsight, some failure causes were not identified. In order to avoid this the experts from various fields of work and expertise were interviewed. Moreover, the same failure mechanism were discussed with different experts eventually leading to the same conclusions.

In addition, it is expected that the results of this HAZOP study will allow for determining the site-specific relevant failure mechanisms. For example, when a sewer system is constructed using PVC pipes, the most of failure mechanisms related to chemical corrosion will be irrelevant, or when due to substantial ground settlement, sewer rehabilitation is necessary within 25 years, failure mechanisms related to ageing of material will be less relevant (Dirksen *et al.*, 2012). Furthermore, the presented method ultimately helps to define what information is required to be able to detect and quantify any given failure mechanism. This gives the possibility to judge the added value of newly introduced inspection techniques.

Part I

STRUCTURAL CONDITIONS

CONVENTIONAL INSPECTION TECHNIQUES FOR CONCRETE SEWER PIPES: CCTV AND CORE SAMPLING

As concluded in Chapter 2, various inspection techniques can be taken into consideration for the assessment of sewer pipe conditions while also taking into account the amount of information that they provide, the costs of the application and their availability. In this chapter an overview and comparison of currently applied techniques for assessing structural conditions (*i.e.* CCTV inspection and drill core analysis) and their uncertainties are presented. Finally it is concluded that the quality of visual inspection and drill core results are an insufficient basis for proper decision making.

3.1 INTRODUCTION

As many sewer systems were constructed between the 1950s and 1970s, the societal costs of managing the sewer systems have increased strongly over the past years. For instance, Oosterom and Hermans (2005) showed that the replacement value of the sewerage system in the Netherlands is around €58 billion. They also estimated the 2005 average annual sewerage tax per household in the Netherlands to be €125, covering 87% of the costs. Consequently, maintaining physical integrity and serviceability of the asset has become a priority. An understanding of the actual status of the assets is a prerequisite for adequate sewer asset management.

Many municipalities in the Netherlands determine sewer conditions by visual inspection, but only a few municipalities (depending on their needs and decisions) are combining that information with drill core analysis. For instance, the Sewerage Department of the Municipality of The Hague is determining the condition of the sewer system using visual inspection (CCTV) and drill core analysis. This is done to ensure that as little as possible of the sewer is replaced before the end of its service life, as well as to reduce the risk of sewer collapse before the scheduled replacement moment.

The city of The Hague has a relatively old sewer compared to the rest of the cities in the Netherlands. Approximately 37% of the existing sewer system was built before 1950 and it still functions (Gemeente Den Haag, 2011). The sewer system in The Hague is mainly a combined system. The greatest part of the sewer consists of concrete (95%; this is approximately 2.4% renovated) and plastic (3.4%). The rest of the sewer (around 1.6%) consists of materials such as glass-fibre reinforced plastic, masonry, cast iron, stoneware, steel and asbestos cement (Chan 2011). The old part of the city of The Hague is located on an area of old and young dunes. This whole area has a stabile soil, whereas the newer parts of The Hague are built in areas where soil settles at a faster rate, thus becoming the limiting factor of the sewers' service life. In the older parts of the city, sewer corrosion is the main failure mechanism leading to sewer rehabilitation. The sewers in this part of the city are typically replaced when they are about 70-100 years old. This is considerably later than in many other municipalities in the Netherlands (Gemeente Den Haag, 2011).

The Municipality of The Hague manages approximately 1,400 km of sewers with a replacement value of around €2 billion, which requires a rational and planned care. The moment of replacement is determined by age, hydraulic improvements and activities in the public space, such as road maintenance and redesign. The quality of the sewer largely determines the replacement strategy. Therefore, knowledge of the sewer condition is necessary. This can be achieved only by conducting inspections and proper recording of them (Chan, 2011). Deterioration of sewer pipes

is one of the most important criteria for determining if replacement of the sewer is required, due to the fact that there is little settlement occurring in the city area (Gemeente Den Haag, 2011). Particularly decisions for replacement are made based on 'surface damage' BAF coding (see 'Visual inspection' section) (Nederlands Normalisatie Instituut, 2004a).

Recent research (Korving, 2004; Korving & Clemens, 2004; Dirksen *et al.*, 2013) has shown that inspections are inherently unreliable, apart from the fact that visual inspection will not reveal invisible deterioration, like corrosion on the outside wall of a sewer. Polder (1987) described deterioration processes of sewer pipes especially from a chemical and materials point of view, but did not give practical advice on how to deal with inspection and did not address the relationship between visual inspection and the quality of the concrete. On the other hand, Stein (2001) tried to describe this relationship. Based on the already mentioned situation in today's practice it can be seen that decisions on financial and social risks are linked mostly to visual inspection. Destructive methods like core sampling can provide additional valuable information about the strength properties of the sewer (de Silva *et al.*, 2002). The potential gains of combining drill core analysis and video inspection should be assessed. However, no attempt to combine these two methods and to study the consistency of their results has been reported so far. This chapter compares the results of the assessment of sewer corrosion based on CCTV inspection and core sampling, taking the uncertainty of both methods into account.

3.2   METHODOLOGY

The study was conducted in a sewer that according to the municipal sewer rehabilitation plans was expected to be replaced within a few years. The sewer is located in a domestic housing area around old dunes. In this area the groundwater is below the sewer invert level (Gemeente Den Haag, 2011).The sewer system in this catchment is a combined sewer, consisting of concrete egg-shaped pipes with dimensions of 300/450 mm. The first stretch of this sewer (about 274 m) was constructed in 1931 and the second part (about 42 m) was constructed in 1960.

In the selected location, first a visual inspection was performed to determine the condition of the inner surface of the sewer. Second, core sampling was applied to determine the strength properties of pipes through mechanical testing of samples.

3.2.1   *Visual inspection*

Specifically for this study, a commercial waste management company, was assigned to conduct visual inspection using CCTV. The Dutch RIONED guidelines for sewage system operations management firmly establish the manner in which visual inspection needs to take place, as well as condition assessment (RIONED, 2004; Chan, 2011). The registration of defects was done according to the visual inspection coding Standard EN 13508-2, while the Standard NEN 3399 was used for condition assessment (Table 3.1) (European Committee for Standardization, 2003; Nederlands Normalisatie Instituut, 2004a). All visual inspection reports from the field have gone through a cross-check (re-evaluation) by the inspector from the Municipality of The Hague who makes the final decision on the existing sewer condition. This re-evaluation is based on the same coding system.

The most common condition aspects of sewer systems noted by the Municipality of The Hague are: surface damage by internal chemical (corrosion) or mechanical action (BAF) and cracks (BAB). Based on the investigation results certain replacement decisions and/or additional investigations are made. Table 3.2 shows the action plan under different sewer conditions. It should be noted that 'replacement decisions and/or additional investigations' is the method used within the Municipality of The Hague and it is not completely in line with the NEN 3398 norm (Nederlands Normalisatie Instituut, 2004b). This study focused only, due to good soil conditions, on the surface damage classification. Based on the Municipality's Inspection and Assessment Plan (action

Table 3.1: Codes condition aspects for the visual inspection of the sewer (Nederlands Normalisatie Instituut, 2004a).

Code	Description	Class	Class description
BAF	surface damage	1	not found
		2	crumbling of the surface, visible aggregates, deterioration material on the surface
		3	aggregates that protrude beyond the surface or visible reinforcement
		4	missing aggregates or reinforcement outside the surface protrudes
		5	wall missing or damaged wall reinforcement
BAB	fissure	1	not found
		2	surface crack - a crack in the surface only
		4	crack - crack visible lines on the pipe wall, chunks still in place
		5	fracture - visible cracks open in the pipe wall, chunks still in place

plan), at the places where there is estimated to be more than 50% of severe surface damage (class BAF 4) drill core samples are taken (Chan 2011).

Table 3.2: CCTV classification for BAF/BAB with associated action (Chan, 2011).

Classification	1	2	3	4	5
BAF	no	no	no	drill core	replacement
BAB	no	no	no	replacement	replacement

3.2.2 Drill core analysis

In each section, between two manholes, four core samples of 100 mm diameter were taken by the contractor Meeuwisse Nederland BV. The cores are taken by drilling directly from the street. The samples were transported to the VLG laboratory of the Municipality of Rotterdam and tested for splitting tensile strength, specific mass and water absorption, to determine the quality of the concrete. All tests mentioned were carried out according to standard EN 12390-6 'Testing of hardened concrete' (European Committee for Standardization, 2009c).

Core classification was based on the INTRON (Institute for Materials and Environmental Research) report (INTRON, 1997). Table 3.3 shows the classification applied in The Hague. The final core classification is based on the highest score of the three criteria shown in Table 3.3. Sewer replacement is scheduled only for the pipes classified as class 5 (Chan, 2011), *i.e.* when one of the criteria is five.

Table 3.3: Drill core classification according to "The Hague" (Chan, 2011).

	class 1	class 2	class 3	class 4	class 5
Splitting tensile strength (N/mm^2)	>6	5-6	2.6-4.9	2.5-2	<2
Water absorption (%)	<8	8-9	9-11	11-13.5	>13.5
Specific weight (kg/m^3)	>2275	2230-2275	2190-2229	2150-2189	<2150

Statistical analysis was carried out on the experimental result. To determine the homogeneity and independence of the core results Mann-Whitney and Wald-Wolfowitz tests were used. The Mann-Whitney test (U test) is a non-parametric statistical test that evaluates whether the medians

on a test variable differ significantly between two groups. This test uses the ranks of the data rather than their raw values to calculate the statistic. The Mann-Whitney U statistic is defined by the following, for each group:

$$U_1 = N_1 N_2 + \frac{N_1(N_1+1)}{2} - R_1 \tag{3.1}$$

$$U_2 = N_1 N_2 + \frac{N_2(N_2+1)}{2} - R_2 \tag{3.2}$$

where N_1 and N_2 are the sample sizes for the group 1 and 2, and R_1 and R_2 are the sums of the ranks assigned to the group 1 and 2. Knowing that $R_1 + R_2 = N(N+1)/2$ and $N = N_1 + N_2$, between these statistics, there is a relationship:

$$U_1 + U_2 = N_1 N_2 \tag{3.3}$$

The Wald-Wolfowitz test (runs test) is a non-parametric statistical test that assesses if the number of 'runs' in an ordering is random or not. A 'run' $\bar{R}$ of a sequence is a maximal non-empty segment of the sequence consisting of adjacent equal elements. For the sample x_i size of N, the runs test observes statistic $\bar{R}$ as:

$$\bar{R} = \sum_{i=1}^{N-1} x_i x_{i+1} \tag{3.4}$$

In the case that the elements of the sequence are mutually independent, statistics $\bar{R}$ follows normal distribution (μ, σ^2); where μ is mean and σ^2 is variance.

3.3 RESULTS AND DISCUSSION

Firstly, sewer condition - surface damage - was assessed by CCTV over the whole studied length. Figure 3.1 shows the (field) inspection results and results with re-evaluation from 2011 at the studied location. From the results it can be seen that CCTV results are not entirely in line with the re-evaluated results. For example, in sections 1 and 2 surface damage was estimated differently by the field inspector (results) and the municipal inspector (re-evaluated results). Overall, the results suggest that subjective visual assessment introduces uncertainties in the overall surface damage assessment, confirming earlier research (Dirksen & Clemens, 2008). Furthermore, Dirksen *et al.*, (2013) found that the probability that an inspector fails to recognise the presence of a defect is around 25% and the probability that a defect is reported, although it is not present, is in the order of a few percent. In addition, the probability of incorrect coding for the surface damage is significant (around 40%).

Secondly, sewer conditions were assessed based on the experimental results of core samples taken on selected locations and INTRON core classification. From the results (Figure 3.2) it can be seen that there is a significant variation in classification between parameters selected by the Municipality of The Hague. For example, in Sections 2 and 5 it can be seen that the difference between specific mass and splitting tensile strength is three classes. As mentioned earlier, core classification is based on the criterion with the highest score. This implies that classification results could be changed with the exclusion of even one parameter. For example, if the results of splitting tensile strength were excluded the classification results would change.

The experimental results of specific mass, water absorption and splitting tensile strength were analysed on the presence of mutual correlation. The coefficients of determination (R^2) given in
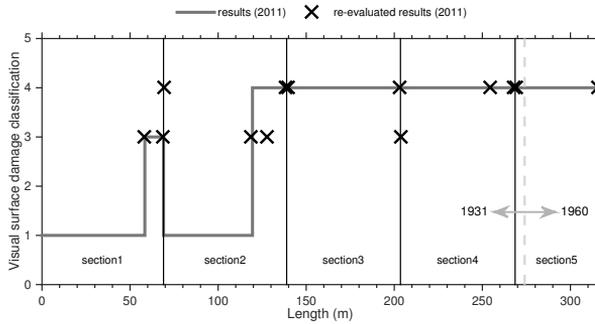
Figure 3.1: Classification (see Table 3.1) of visual impairment conditions using CCTV at the studied location as a function of time.
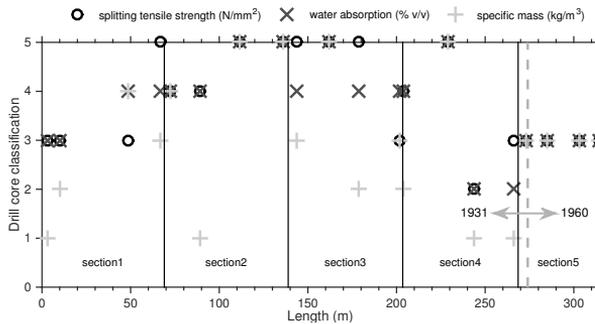

Figure 3.2: Classification (see Table 3.3) of the experimental results of core sample from the crown of the sewer.

Figure 3.3 (a)-(b) show that there was a weak correlation between specific mass and splitting tensile strength results and between splitting tensile strength and water absorption results. On the other hand, the correlation coefficient (Figure 3 (c)) suggests that values of specific mass and water absorption are interdependent. Therefore, according to the studied correlations, core conditions could be assessed by either studying specific mass or water absorption or they could act as control measurement.

As mentioned earlier, core samples were taken from the invert and the crown of the sewer. Experimental results showed (Table 3.4) that invert samples have a lower average density and a higher water absorption values compared with crown results. This suggests that the specific mass of the concrete in the sewer invert decreased over the years and deteriorated more than the crown region. Factors influencing structural deterioration of concrete are numerous, *e.g.* sewage characteristics (pH, sulphate concentration, conductivity, temperature, turbulence, velocity variation, dissolved oxygen) and initial concrete quality (Hvitved-Jacobsen *et al.*, 2000; Parande *et al.*, 2006; Zhang *et al.*, 2008). Therefore, it was not possible to determine which process precisely influenced the durability of concrete. For example, a sewer invert might have been physically damaged due to the effect of the difference between external soil temperature and wastewater temperature. Furthermore, an adverse effect on concrete durability in the sewer invert could have been caused by the transport of fluid through the concrete (Neville, 1995). Chemical attack on concrete by wastewater could increase the fluid transport through the concrete. The larger aggre-
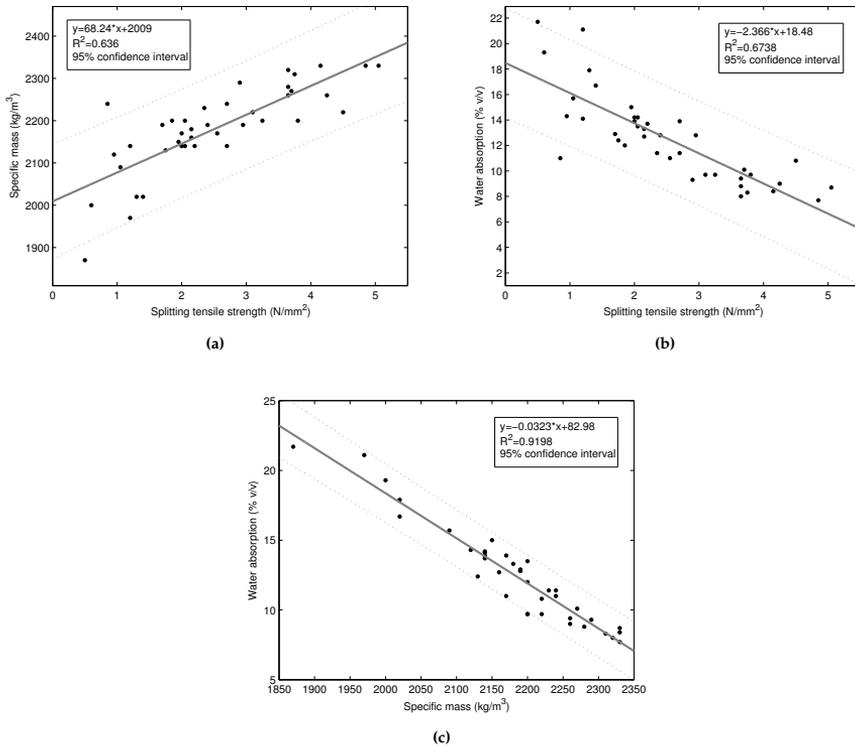
Figure 3.3: Correlation between: (a) specific mass and splitting tensile strength results; (b) splitting tensile strength and water absorption results; (c) specific mass and water absorption results.

gate size and its inert nature may have influenced the concrete degradation to the largest extent (Neville, 1995; de Belie *et al.*, 2004).

Before conducting any statistical analysis on the experimental results it was first necessary to determine their independence and homogeneity. The non-parametric statistical test of Wald-Wolfowitz and Mann-Whitney confirmed that subjectivity can be removed (the data could not be distinguished from a random normal distribution) which was also confirmed by the field experiments.

From Table 3.4 a few observations can be made. The variation of sample results from the sewer invert is higher when compared to results from the crown. This could imply that concrete on the invert was affected by processes other than in the crown region. In addition, skewness showed that there was non-constant (asymmetric) deterioration of the concrete over the length of the studied sewer. The coefficient of variation has the highest value for the results of the splitting tensile strength test. This high value is probably influenced by several factors. Non-uniform deterioration over time influences the results of the splitting test. An important parameter which influences the results of the splitting tests is the aggregate size. A larger aggregate size was observed in the core samples, thus increasing the measurement uncertainties related to the splitting test. Another influencing factor on the recorded strength is height/diameter ratio of the cylinder, which was, in the studied case, lower than 1, suggesting that results were unreliable (Neville 1995). Also, it should be emphasised that the core strength, even under excellent experimental

conditions, is unlikely to exceed 70-85% of standard test specimens (Neville, 1995). Moreover, based on the previous testing of the laboratory the uncertainty of the splitting tensile strength results is 2 N/mm^2. When this is compared with the average values of the splitting tensile strength given in Table 3.4, it can be seen that uncertainty of the results is relatively high. Consequently, when considering all these different factors, it could be regarded that the results of the splitting tensile strength are unreliable. On the other hand, based on the previous testing by the laboratory the measurement uncertainties related to concrete density and water absorption tests are in the order of a few percent, thus making these test results more reliable.

Table 3.4: Statistical characteristics of the selected core parameters from invert and crown of sewer at the studied location with average classification value.

	Sample thickness (mm)		Specific mass (kg/m^3)		Splitting tensile strength (N/mm^2)		Water absorption (% v/v)	
	invert	crown	invert	crown	invert	crown	invert	crown
μ	64.3	66.0	2164.5	2198	2.45	2.59	13.35	11.68
σ	2.0	2.2	119.80	81.21	1.24	1.18	4.03	2.59
C_v	0.03	0.03	0.06	0.04	0.50	0.46	0.30	0.22
C_s	0.81	0.23	-0.75	-0.73	0.35	0.31	0.57	0.94
$class_{avg}$	-	-	4	3	4	3	4	4

Legend: μ - average, σ - standard deviation, C_v - coefficient of variation, C_s - skewness, $class_{avg}$ - average classification over the sewer length

It is noted that there is a difference in the condition assessment between the invert and crown pipe region (Figure 3.4). A general acknowledged assumption is that concrete in the crown region has a poorer quality than the concrete in the invert region, due to the classical H_2S-induced crown corrosion process (see, *e.g* Bielecki & Schremmer, 1987), and based on this implicit assumption the current condition assessment is done in practice. Results showed that concrete conditions at the sewer invert were more severe than conditions at the crown. This contradicts the general idea that sewer corrosion caused by biological H_2S is the dominant degradation process. Consequently, more attention should be given to the sewer invert in future practice.
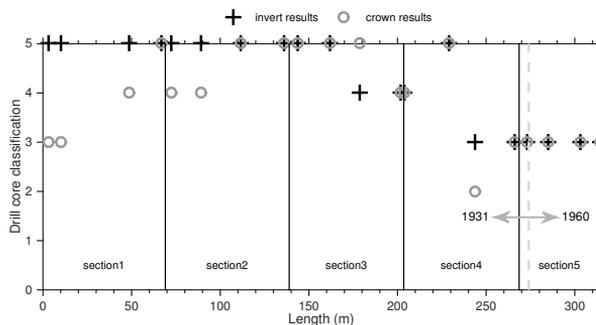
Figure 3.4: Comparison of drill core sample results from sewer invert and crown at the studied location.

In the Municipality of The Hague final sewer condition assessment is based on the re-evaluated CCTV results and drill core experimental results from the crown region of the sewer only. Figure 3.5 shows the difference between results of two inspection techniques in estimation of current conditions at the studied location. Based on the current The Hague inspection regulation, Sections 2-3 and one part of Section 4 should be replaced. On the other hand, sewer conditions in Section 5 are better when looking at the core results. For Section 5, these were expected results

because the last 80% of the section is 29 years younger compared to the rest of the studied sewer. Further, dotted line on Figure 3.5 shows the core sample uncertainty; thus demonstrating once again the results unreliability. In addition, as mentioned earlier the probability of incorrect coding for CCTV is substantial. Moreover, re-evaluated CCTV results are not consistent with the drill core results, *i.e.* the relative severity of the sewer condition should be similar irrespective of the boundaries of the classes, but it is not. Overall, this study shows that the assumption that core sampling will produce results that are in line with the visual inspection results is not correct, due to uncertainties related to the application of both techniques.
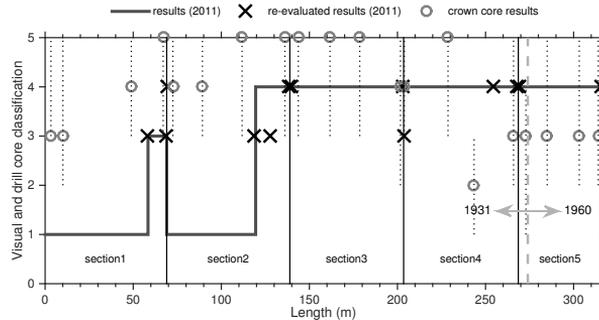
Figure 3.5: Comparison of visual inspection and drill core analysis results at the studied location. Dotted lines represent the error bar ± sample uncertainty.

The Dutch RIONED foundation issues frequently a publication (RIONED, 2007) on cost figures for design and management of sewer systems. These cost figures are based on questionnaires and give prices with a bandwidth of ±30%. CCTV inspection is normally combined with sewer cleaning. Based on an average daily production of 500 m for normal-sized sewers (400-600 mm), the general cost price for CCTV + cleaning will be €5.30 per metre sewer length. Testing a drill core in the laboratory costs €65 per sample, while sampling costs amount to €210 per sample for sewers above the groundwater table and €335 per sample for sewer below the groundwater table. The inspection costs for the sewer described in this paper would, based on the general cost figures, amount to €1.670 for the CCTV inspection combined with cleaning, and €5.500 for sampling of 20 cores from the crown region. However, the number of core samples for this length of sewer would not have exceeded three if it were not for research purposes, resulting in a total cost of €855. When comparing these costs, one should realise that CCTV provides information on the status of the pipe for a range of aspects over the total length, and core samples provide information on the material properties of a few locations only.

3.4 CONCLUSIONS

This study was carried out to further understand the limitations and potentials of both visual inspection and drill core analysis. The following conclusions transpired from the study.

- Core classification is based on a number of different criteria/parameters. The quality of the final core classification depends on selection of parameters and their classification range.
- Specific mass and water absorption show a high correlation. As a consequence, it is unnecessary to analyse both parameters, unless this is required to detect measurement errors.
- Different factors like non-uniform deterioration, height/diameter ratio, experimental uncertainty and damage during drilling influence the proper estimation of the splitting tensile strength, which makes results unreliable.

- The quality of concrete at the sewer invert was lower in comparison to the concrete quality at the crown region.
- There is no obvious correlation between results of visual inspection and results of drill core analysis.

Overall, the understanding of the uncertainty of inspection data is relevant for future decision making and model development. Uncertainties related to application of both CCTV inspection and core analysis in today's practice could be and should be decreased, as the results are inconsistent when compared to each other. Proper selection of core classification parameters and their classification range will provide more reliable results. Further, cores should not be damaged during collection and they should have proper dimension. Moreover, the current core sampling method is more suitable for the pipes of bigger diameter ($D \geqslant 1$ m) due to available drill sizes in practice. Finally, there is need for further study of material property parameters of core sampling in order to be able to assess the associated uncertainties and the optimal parameter to assess the concrete quality of the pipe.

4

QUANTIFICATION OF THE INTERIOR GEOMETRY OF CONCRETE SEWER PIPES

In Chapter 2 the potential of the laser profiling method for an accurate, non-invasive assessment of changes in the inner pipe profile was discussed. However, the main difficulty in laser profiling is the alignment and orientation of the sensor in the harsh sewer environment. Even small misalignments and shifts in position can cause a significant systematic error in the measured internal geometry. As concluded in Chapter 3 an understanding of the uncertainty of inspection results is relevant for future decision making. Therefore, in this chapter the uncertainties associated with the application of laser profiling in order to obtain a 3D profile of corroded concrete (sewer) pipes are analysed.

In the first section of the chapter, the current use of the laser profiling technique and currently quantified uncertainty are presented, and after that the possible sources of uncertainties are defined. In the third section an improvement of the available laser profilers is proposed (Prototype v1.0) and tested in a full scale pilot using a corroded egg-shaped concrete sewer pipe. The fourth section discusses a method for correction of misalignment and orientation of the camera and profiling systems, relative to the pipe coordinate system which is presented together with an uncertainty analysis, followed by concluding remarks and recommendations for further improvements.

4.1 INTRODUCTION

For gravity sewers, three main classes of failures can be distinguished: water tightness, structural stability and operational reliability. The latter two are considered to be the most important failure classes for decisions on sewer rehabilitation. In order to overcome the limitations of visual inspection, several new techniques have been developed over the past two decades and are applied in practice (Wirahadikusumah *et al.*, 1998), like radar (*e.g.* Olhoeft, 2000), acoustic techniques (*e.g.* Feng *et al.*, 2012) or sonar (Kirkham *et al.*, 2000), laser profiling (Duran *et al.*, 2003) or a combination of these technologies in order to benefit from the strengths of each technology (Duran *et al.*, 2007; Environmental Protection Agency, 2010). A recent and comprehensive review of existing techniques for condition assessment of underground infrastructure, including sewer systems, can be found in Hao *et al.*, (2012).

Laser profiling of (sewer) pipes is a technology that is introduced and applied in practice for some years. Main applications are checks on ovality or other significant deformations of the geometry and the detection of damages such as cracks or obstacles (see, *e.g.* Arsénio *et al.*, 2013; Duran *et al.*, 2003; Gooch *et al.*, 1996). In addition, some authors also claim that the laser profiling technique is capable of measuring the wall losses due to corrosion (Kirkham *et al.*, 2000) with a relative uncertainty of 0.5%. This implies that in a 600 mm circular sewer, wall losses higher than 3 mm could potentially be measured. Given the typical wall thickness of 80 mm for a 600 mm concrete sewer, this 3 mm seems to be sufficiently accurate as input for the purpose of assessing the constructional strength and stability.

However, amongst others, Duran *et al.*, (2003) state that the main difficulty in laser profiling is the alignment and orientation of the sensor in the harsh sewer environment. Even small misalignments and shift in position can cause a significant systematic error in the measured in-

ternal geometry (Stanić *et al.*, 2013b; van der Schoot, 2015). In current practice, uncertainties due to unknown misalignments remain unnoticed, rendering the laser profiling technique without correction of the alignment and position unsuitable for measuring the exact internal geometry.

In this chapter, the uncertainties associated with the application of laser profiling in order to obtain a 3D profile of corroded concrete (sewer) pipes are analysed. The uncertainty analysis revealed the significance of the different sources of errors in the laser profiler monitoring results. Based on this, an improvement of the available laser profiling techniques is proposed and tested in a full scale pilot using a corroded egg-shaped concrete sewer pipe and one new egg-shaped pipe that has not been in service. Based on laboratory experiments and theoretical analysis, future developments are defined.

4.2   LASER PROFILING: MEASURING UNCERTAINTIES

Laser profiling of sewer pipes is based on a combination of projecting rings of light on the sewer pipe wall and capturing the images by a digital camera. Laser profilers are commonly placed on top of a CCTV camera tractor in order to be able to move them through the sewer pipe, as shown in Figure 4.1.

Figure 4.1: Photograph of the experimental set-up.

The accuracy of the results obtained by laser profiling is determined by: (1) the quality of the camera, *i.e.* the number of pixels, the pixel size and the number of frames per second that can be recorded, (2) the quality of the circular laser projection, which determines the width of the projected rings of light, (3) the method used to determine the position of the camera during its movement through the sewer, which determines the position of each recorded frame and consequently the distance between the frames and (4) the alignment of the laser and camera, which determine the angle of the projection and consequently the extent of deformation of the projection.

The impact of the quality of the camera and lasers on the uncertainties can be assessed by checking the specifications of the equipment by practical tests. The position of the camera and laser is normally determined by measuring the rotation of the wheels of the camera tractor or of the cable that is used to pull the camera tractor through the sewer. As the wheels of the camera tractor are likely to skid in the sewer, the position of the laser and camera can be rather imprecise (Dirksen *et al.* 2014). Another bias could be introduced by the use of the cable to estimate distance: the cable follows the path of the tractor (not necessarily parallel to the pipe) and the flexion of the cable. Moreover, the alignment of the camera and laser is normally not accounted for. As a consequence, this adds to the unknown bias related to the position.

4.3   MATERIAL AND METHODS

4.3.1   *Measuring set-up*

To assess the uncertainties associated with laser profiling, the measuring set-up shown in Figure 4.2 has been designed with all the monitoring equipment placed on a mobile platform. The set-up consists, like for ordinary laser profilers, of a laser projector combined with a camera, referred to as cam_{FRONT}. The laser uses a reflecting cone to produce a laser sheet which projects a line perpendicular to the main axis of the platform on the inner pipe wall. The mobile platform moves at a, not necessarily constant, speed of approximately 0.05 m/s through the pipe, the recording frequency of cam_{FRONT} is 30 frames/s, implying that each frame is about 1.7 mm apart along the length of the pipe. The images recorded by cam_{FRONT} are stored on a measuring computer for further processing.

Accurately measuring the position and alignment of the camera and laser requires that information is available on the x, y and z positions and rotation around these axes. In the experiments, this information is obtained by using a set-up comprising of three parallel lasers with a fixed position, each measuring the distance between the parallel lasers and a reflection board. A second camera, referred to as cam_{BACK}, records the position of the three points projected by the parallel lasers on the reflection board. The frame rate of cam_{BACK} is 8 frames/s, implying that every 6.25 µm there is a recording of the distance between reflection board and the three lasers.
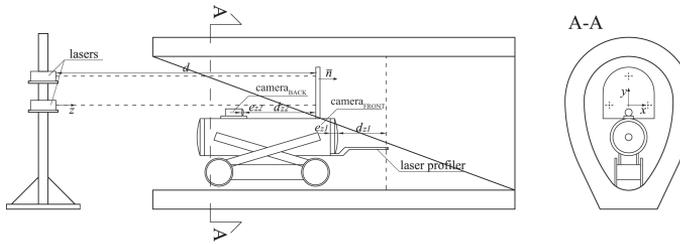
Figure 4.2: Sketch of the experimental set-up, details on the dimensions and materials used can be found in Tables 4.1 and 4.2.

Table 4.1: Specifications and their standard uncertainties (obtained by repeated measurement) of the instrumentation.

	Brand / Model	Standard uncertainty σ
cam_{FRONT} and the tractor	Panoramo / 3D optical Pipeline scanner	13 µm
cam_{BACK}	D link / DCS 2310 L	5.6 µm
Laser distance meters	Fluke/ 414D	0.5 mm
Circular projected laser	Ibak / ILP	-
Dimensions of the measuring set-up	-	0.25 mm

The three parallel lasers have a fixed position and define a reference coordinate system, with the z-axis being parallel to the main axis of the pipe. A left-handed coordinate system is applied, while the rotation angles are defined in the Tait-Bryan formalism (Figure 4.3) see, *e.g.* Baranowski, (2013). The images recorded by cam_{BACK} and the readings from the laser distance meters are stored on the same measuring computer as cam_{FRONT}.

For each frame recorded by the front camera, the exact position and orientation of this camera should be known; therefore, for each frame, the position of the three laser points projected on the reflection board has to be known. It is important that the synchrony of the images recorded with the front camera and the back camera is guaranteed. Synchrony is guaranteed by the fact

Table 4.2: Dimensions of the measuring set-up.

| Measure	Value (in m)
$d_{z_{FRONT}}$	0.4760
$d_{z_{BACK}}$	0.3540
$e_{z_{FRONT}}$	0.003440
$e_{z_{BACK}}$	0.002860
$camoff_x$	0.0020 (0.0022)
$camoff_y$	-0.2307 (-0.2248)
$camoff_z$	0.1647 (0.16466)

Note: The figures between brackets for the camera offset values are
valid for the old pipe, and the other values are valid for the new pipe.

that both cameras were connected to the same data-acquisition system, which enforced both data sources into the same time base.
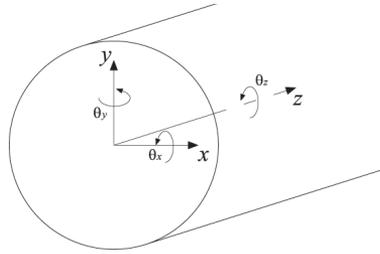
Figure 4.3: Left-handed coordinate system and definition of the Tait-Bryan angles.

Accuracy of camera sensors. The measuring error of the 2D projection of the wall of the pipe is calculated using the average number of pixels that are illuminated on the sensor of cam_{FRONT}, depending on the scale factor, defined by the ratio between the distance between the laser sheet and the lens and the distance between the lens and sensor plane. The sensor used in cam_{FRONT} is a 2/3" sensor with 1024 × 760 pixels, pixel dimensions are 6.45 μm × 6.45 μm. Based on an analysis of 20 repetitive samples in 20 different video frames, in which the measuring system was stationary, all rotation angles were equal to zero and the camera positioned in the axis of the conduit revealed that the laser sheet illuminated about 9-10 pixels. Figure 4.4 shows the results of the distribution of the recorded light intensity across the projected line on the camera sensor, which was obtained using image processing and analysis. Based on these experiments, the standard deviation in the position was estimated to be $\sigma_{x,y\ cam_{FRONT}} = 13$ μm.

cam_{BACK} is used to keep track of the position of the three points projected on the reflection board by the three stationary lasers. The obtained image of these points is transferred into contour lines using standard image processing routines. On these contour lines, an ellipse is fitted from which the intersection point of both axes defined as the x and y location of the point (in sensor coordinates) is derived. Analysing 30 independent frames resulted in a standard deviation in both x and y directions of about 2 pixels. The sensor of cam_{BACK} is a 1/4" sensor with a resolution of 1280 x 800 pixels with a pixel width of 2.8 μm × 2.8 μm, resulting in estimated standard deviation of $\sigma_{x,y\ cam_{BACK}} = 5.6$ μm. The cameras were tested on lens distortion effects (*e.g.* barrel distortion), for cam_{FRONT} these proved to be not observable, for cam_{BACK} there was some distortion at the far corners of the image. During the experiments, care was taken to avoid that the laser dots were recorded in these (slightly) distorted areas.

Accuracy of laser alignment. The alignment of the lasers was determined by repeated measurement of the distance between the three projected points at a distance of 30 m, the maximum
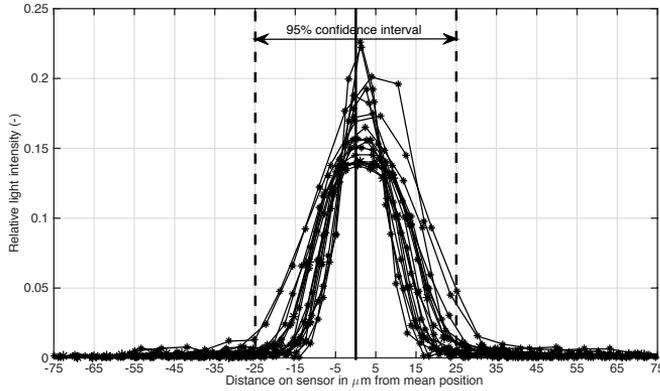
Figure 4.4: Distribution of the light intensity on the sensor of cam_{FRONT}, shown as normalised pixel intensity on the camera sensor.

mutual deviation over this distance between the projected points was ±3 mm (95% confidence interval in 30 repeated measurements) when compared with their position at the origin. This implies that the standard deviation of the alignment was estimated to be 2.5×10^{-5} radials.

4.3.2 *Data processing*

Processing of raw data consists of five steps as follows:

1. Determine the x, y and z positions of the three laser points projected on the reflection board.
2. Determine the position and orientation of the mobile platform.
3. Correct the recorded image from cam_{FRONT} for misalignment and orientation.
4. Calculate the inaccuracy interval for each recorded point in x, y and z directions.
5. Generate images.

These steps have been incorporated in Matlab$^{\circledR}$ platform for post-processing the raw data.

Correction for misalignment and orientation of the camera/profiling systems relative to the pipe coordinate system. The recorded 2D images on the camera sensor have to be translated into 3D information based on the exact position of cam_{FRONT} and the orientation of the mobile platform (*i.e.* the exact position and the axis along which the system is 'looking'). The three stationary laser distance meters (having known and fixed positions $p_{R,i} = [x_i, y_i, 0]$, $i = 1, 2, 3$) define a reference coordinate system $\mathfrak{R}^{(3)}$ see Figure 4.5. From the projected three points and their measured distances along the z-axis (d_1, d_2 and d_3), between the fixed stand and the projection board, the position and orientation of the mobile platform and especially that of cam_{FRONT} can be calculated. The three laser points define a plane in the reference coordinate system $\mathfrak{R}^{(3)}$ with a normal vector $\underline{n}$:

$$\underline{n} = \begin{bmatrix} a \\ b \\ c \end{bmatrix} = \begin{bmatrix} x_1 & y_1 & d_1 \\ x_2 & y_2 & d_2 \\ x_3 & y_3 & d_3 \end{bmatrix}_{\mathfrak{R}^{(3)}}^{-1} \begin{bmatrix} 1 \\ 1 \\ 1 \end{bmatrix}_{\mathfrak{R}^{(3)}} \tag{4.1}$$

which is normalised:

$$n_n = \frac{n}{\| n \|} \tag{4.2}$$
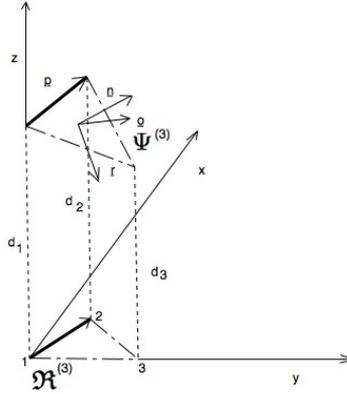
Figure 4.5: Definition sketch coordinate systems.

Additional to this normal vector, a normalised orthogonal basis for the rotated camera system is defined with two vectors o_n and r_n (see, *e.g.* Gruber, 2000):

$$\begin{cases} \underline{o} = \underline{j} - (\underline{j} \cdot \underline{n_n}) \cdot \underline{n_n} \\ \underline{j} = \begin{bmatrix} 0 & 1 & 0 \end{bmatrix} \\ \underline{r} = \underline{o} \times \underline{n_n} \\ \underline{o}_n = \frac{\underline{o}}{\|\underline{o}\|} \\ \underline{r}_n = \frac{\underline{r}}{\|\underline{r}\|} \end{cases} \tag{4.3}$$

These three vectors define a transformation matrix ($\underline{\underline{R}}_{\psi^{(3)}}$) for the camera space $\Psi^{(3)}$:

$$\underline{\underline{R}}_{\psi^{(3)}} = \begin{bmatrix} r_n(1) & o_n(1) & n_n(1) \\ r_n(2) & o_n(2) & n_n(2) \\ r_n(3) & o_n(3) & n_n(3) \end{bmatrix} \tag{4.4}$$

Since the projection on the reflection board is in a plane, the transformation of the position of the laser points as recorded by cam_{BACK} to the x-y plane in $\mathfrak{R}^{(2)}$ (transformation $\Psi^{(2)} \rightarrow \mathfrak{R}^{(2)}$) uses the following transformation matrix ($\underline{\underline{R}}_{\psi^{(2)}}$):

$$\underline{\underline{R}}_{\psi^{(2)}} = \begin{bmatrix} r_n(1) & o_n(1) \\ r_n(2) & o_n(2) \end{bmatrix} \tag{4.5}$$

Using this matrix, coordinate transformations between the spaces $\mathfrak{R}^{(2)}$ and $\Psi^{(2)}$ for a point $p_{c_{BACK}} = [b_{x_{BACK}}, b_{y_{BACK}}]$ as recorded on the sensor of cam_{BACK} can be made, taking into account the scaling factor (s_{BACK}) of cam_{BACK}[i]:

---

i The scaling factor is the ratio between the measure of an object and the size of its projection through the lens on the optical sensor in the camera.

$$s_{BACK} = \frac{d_{z_{BACK}}}{e_{z_{BACK}}} \tag{4.6}$$

and:

$$p_{\mathfrak{R}^{(2)}} = s_{BACK} \cdot \underline{R}_{\psi^{(2)}} \cdot p_{cBACK} \tag{4.7}$$

Note that this is a non-orthogonal transformation, *i.e.* angles and distances are not conserved. This is due to the fact that the laser beams are stationary and the reflection board is shifted and rotated. As a consequence a deformation (stretch) of the original positions of the projected points occurs. Therefore prior to rotation, the shift and scale should be applied. As a first step it is necessary to do a coordinate transform from the projected points in the coordinate system $\Psi^{(2)}$ to the reference coordinate system $\mathfrak{R}^{(2)}$.

$$p_{\mathfrak{R}^{(2)}_{i=1,2,3}} = s_{BACK} \cdot \underline{R}_{\psi^{(2)}} \cdot p_{cBACK_{i=1,2,3}} \tag{4.8}$$

Subsequently, the projected points are corrected for the shift in x, y and z directions. The correction in the z-direction is equal to $1/c$ (being the distance between the reference stand and the reflection board), the shift in x and y directions are made based on the coordinates of the origin[ii] $(x_1, y_1)_{\mathfrak{R}^{(2)}} = (0,0)_{\mathfrak{R}^{(2)}}$:[iii]

$$\begin{cases} \begin{bmatrix} \triangle x \\ \triangle y \end{bmatrix}_{\mathfrak{R}^{(2)}} = \triangle^{(2)}_{orig} = p_{\mathfrak{R}^{(2)}_1} \\ (T)p_{\mathfrak{R}^{(2)}_{i=1,2,3}} = p_{\mathfrak{R}^{(2)}_{i=1,2,3}} - p_{\mathfrak{R}^{(2)}_1} \end{cases} \tag{4.9}$$

At this stage, the points are defined in the z = 0 plane of the reference coordinate system $\mathfrak{R}^{(2)}$, not corrected for the rotation around the z-axis however. Two points (*e.g.* $(T)p_{\mathfrak{R}^{(2)}_1}$ and $(T)p_{\mathfrak{R}^{(2)}_2}$, or any other combination of two points), define a vector $(T)\underline{p}_{\mathfrak{R}^{(2)}_{1 \rightarrow 2}}$ that can be used to define the rotation around the z-axis:

$$\theta_z = sign\left[p_{\mathfrak{R}^{(2)}_{reference,2}}(1) - (T)p_{\mathfrak{R}^{(2)}_2}(1)\right] arccos\left[\frac{\underline{p}_{\mathfrak{R}^{(2)}_{reference,1 \rightarrow 2}} \cdot (T)\underline{p}_{\mathfrak{R}^{(2)}_{1 \rightarrow 2}}}{\left\|\underline{p}_{\mathfrak{R}^{(2)}_{reference,1 \rightarrow 2}}\right\| \left\|(T)\underline{p}_{\mathfrak{R}^{(2)}_{1 \rightarrow 2}}\right\|}\right] \tag{4.10}$$

The first term determines the direction of the rotation (counter-clockwise is positive). The next step is to rotate $(T)p_{\mathfrak{R}^{(2)}_{i=1,2,3}}$ with $-\theta_z$:

$$p_{\mathfrak{R}^{(2)}_{i=1,2,3}} = \underline{R}_{z^{(2)}} (T)p_{\mathfrak{R}^{(2)}_{i=1,2,3}} \tag{4.11}$$

with

$$\underline{R}_{z^{(2)}} = \begin{bmatrix} cos(-\theta_z) & sin(-\theta_z) \\ -sin(-\theta_z) & cos(-\theta_z) \end{bmatrix} = \begin{bmatrix} cos(\theta_z) & -sin(\theta_z) \\ sin(\theta_z) & cos(\theta_z) \end{bmatrix} \tag{4.12}$$
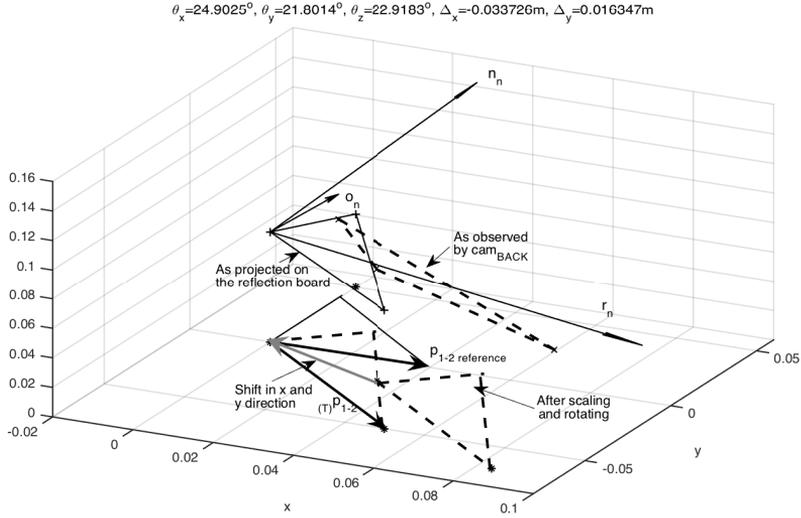
Figure 4.6: Successive steps in the calculation of orientation and shift.

Figure 4.6 presents an example of the successive operations defined in Equations (4.1) to (4.12). At this point, the orientation for x, y and z axes as well as the shift of the position x, y and z of the moving camera platform are known, allowing the position of cam_{FRONT} to be determined:

$$
\begin{bmatrix} x_{FRONT} \\ y_{FRONT} \\ z_{FRONT} \end{bmatrix}_{\Re(3)} = \underline{\underline{R}}_{\psi(3)}\underline{\underline{R}}_{z(3)} \begin{bmatrix} camoff_x \\ camoff_y \\ camoff_z \end{bmatrix}_{\psi(3)} + \begin{bmatrix} \triangle_{orig}^{(2)}(1) \\ \triangle_{orig}^{(2)}(2) \\ c^{-1} \end{bmatrix} \tag{4.13}
$$

with

$$
\underline{\underline{R}}_{z(3)} = \begin{bmatrix} \cos(\theta_z) & \sin(\theta_z) & 0 \\ -\sin(\theta_z) & \cos(\theta_z) & 0 \\ 0 & 0 & 1 \end{bmatrix} \tag{4.14}
$$

The first term in Equation (4.13) is the rotation of the camera relative to the origin followed by the shift of the origin along the x-, y- and z-axis of the reference coordinate system. Finally, an observed point (reflection from the pipe wall) $p_{c_{FRONT}} = [b_{x_{FRONT}}, b_{y_{FRONT}}]$ on the sensor of cam_{FRONT} with camera coordinates $[b_{x_{FRONT}}, b_{y_{FRONT}}]$ translates into the (corrected) x, y and z positions in the reference coordinate system $\Re^{(3)}$:

---

ii Laser number 1 defines the origin of the reference coordinate systems $\Re^{(3)}$ and $\Re^{(2)}$.

iii The prefix (T) indicates the vector is shifted.

$$
\begin{cases}
p_{\mathfrak{R}^{(3)}_{corrected}} = \underline{\underline{R}}_{\psi(3)}\,\underline{\underline{R}}_{z(3)} \begin{bmatrix} s_{FRONT}\,b_{x_{FRONT}} \\ s_{FRONT}\,b_{y_{FRONT}} \\ 0 \end{bmatrix} + \begin{bmatrix} camoff_x \\ camoff_y \\ camoff_z \end{bmatrix}_{\mathfrak{R}^{(3)}} + \\[2em]
\begin{bmatrix} 0 \\ 0 \\ \cos(\theta_x)\cos(\theta_y)d_{z_{FRONT}} \end{bmatrix} = \underline{\underline{R}}_{\psi(3)}\,\underline{\underline{R}}_{z(3)} \begin{bmatrix} s_{FRONT}\,b_{x_{FRONT}} \\ s_{FRONT}\,b_{y_{FRONT}} \\ 0 \end{bmatrix} + \\[2em]
\underline{\underline{R}}_{\psi(3)}\,\underline{\underline{R}}_{z(3)} \begin{bmatrix} camoff_x \\ camoff_y \\ camoff_z \end{bmatrix}_{\psi(3)} + \begin{bmatrix} \triangle^{(2)}_{orig}(1) \\ \triangle^{(2)}_{orig}(2) \\ c^{-1} \end{bmatrix} + \\[2em]
\begin{bmatrix} 0 \\ 0 \\ \cos(\theta_x)\cos(\theta_y)d_{z_{FRONT}} \end{bmatrix} = \underline{\underline{R}}_{\psi(3)}\,\underline{\underline{R}}_{z(3)} \begin{bmatrix} s_{FRONT}\,b_{x_{FRONT}} \\ s_{FRONT}\,b_{y_{FRONT}} \\ 0 \end{bmatrix} + \\[2em]
\underline{\underline{R}}_{\psi(3)}\,\underline{\underline{R}}_{z(3)} \begin{bmatrix} camoff_x \\ camoff_y \\ camoff_z \end{bmatrix}_{\psi(3)} + \begin{bmatrix} \triangle^{(2)}_{orig}(1) \\ \triangle^{(2)}_{orig}(2) \\ c^{-1} + d_{z_{FRONT}}\frac{c}{\sqrt{a^2+b^2+c^2}} \end{bmatrix}
\end{cases}
\tag{4.15}
$$

with

$$
\begin{cases}
\cos(\theta_x) = \left[\dfrac{\sqrt{a^2+b^2}}{\sqrt{a^2+b^2+c^2}} \right] \\[1.5em]
\cos(\theta_y) = \left[\dfrac{c}{\sqrt{a^2+c^2}} \right]
\end{cases}
\tag{4.16}
$$

and

$$
s_{FRONT} = \frac{d_{z_{FRONT}}}{e_{z_{FRONT}}}
\tag{4.17}
$$

denotes the scaling factor for cam_{FRONT}.

The term $d_{z_{FRONT}} = \frac{c}{\sqrt{a^2+b^2+c^2}}$ in Equation (4.15) is the projection of the distance between cam_{FRONT} and the laser sheet on the z-axis in the reference coordinate system $\mathfrak{R}^{(3)}$.

Uncertainties analysis. The overall uncertainty of the position of a point projected on the pipe wall is determined as follows:

- The uncertainty of the recorded images in cam_{FRONT} and cam_{BACK}.
- The uncertainty of the measured distances $d_{1,2,3}$.
- The uncertainty of the alignment of the lasers.
- The uncertainty of the fixed distances in the measuring set-up.

Assuming that the measuring uncertainties in the parameters mentioned are mutually independent, hence neglecting covariance terms, the law of propagation of uncertainties (JCGM 104, 2009) applies for the measured points:

$$\sigma^2_{p_{corrected}} = \sum_{i=1}^{i=19} \sigma^2_{v_c(i)} \left[\frac{\partial p_{corrected}}{\partial v_c(i)} \right]^2 \qquad (4.18)$$

in which:

$$\underline{v}_c = \begin{pmatrix} d_{i=1,2,3}, x_{i=1,2,3}, y_{i=1,2,3}, b_{x_{FRONT}}, b_{y_{FRONT}}, b_{x_{BACK}}, b_{y_{BACK}}, \\ camoff_x, camoff_y, camoff_z, d_{z_{FRONT}}, d_{z_{BACK}}, \\ e_{z_{FRONT}}, e_{z_{BACK}}, \alpha_{misal} \end{pmatrix} \qquad (4.19)$$

The uncertainty of the uncorrected point is calculated in the same manner:

$$\sigma^2_p = \sum_{i=1}^{i=8} \sigma^2_{v_i} \left[\frac{\partial p}{\partial v_i} \right]^2 \qquad (4.20)$$

with

$$\underline{v} = (d_{i=1,2,3}, b_{x_{FRONT}}, b_{y_{FRONT}}, d_{z_{FRONT}}, e_{z_{FRONT}}, \alpha_{misal}) \qquad (4.21)$$

where α_{misal} is the misalignment of the lasers. Due to the very complicated analytical expressions that would result for most of the terms in Equations (4.18) and (4.20), the quantification has been done numerically using partial differences estimates.

4.4 EXPERIMENTAL RESULTS

Two concrete sewer pipes were subjected to the analysis as described before, one new egg-shaped pipe (*i.e.* P01) with an inner nominal geometry of 400/600 mm[iv] and one egg-shaped pipe - P08 (400/600 mm) that was in service for more than 89 years in the municipality of the Hague, showing clear marks of crown corrosion and concretions of sediments at the sides.
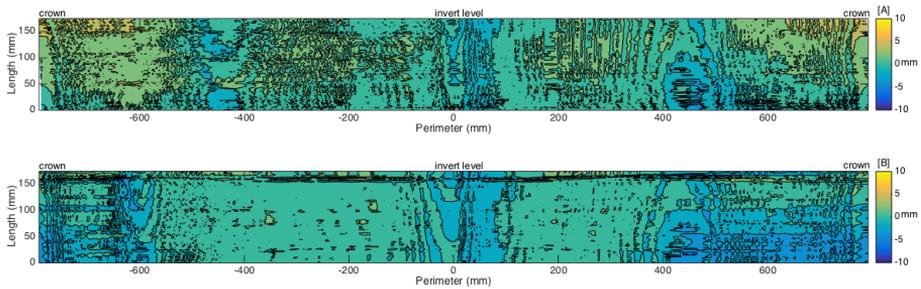
Figure 4.7: Difference between theoretical and measured geometry for the new pipe (P01). The upper chart shows the uncorrected result, and the lower chart shows the result after correction for position and orientation of the measuring platform. [A] uncorrected; [B] corrected measurements.

Figure 4.7 depicts the results for the new pipe. The charts indicate the difference between the profiles measured following the procedures as described before minus the theoretical profile. In

iv The new pipe was produced in accordance with the Dutch Standard NEN 7126 (Nederlands Normalisatie Instituut, 2004c).

the upper chart, the result is shown without correcting for position and orientation of the mobile platform, while in the lower chart, the correction has been applied. As can be seen, the differences between measurement and theoretical profiles are, overall, much smaller for the corrected measurements. It is also noted that both corrected and uncorrected measurements deviate from the theoretical profile with a few millimetres, probably this is due to the allowed tolerance in the production process (see, *e.g.* Clemens, 2001).

This can also be observed in Figure 4.8 for the 89 years old egg-shaped pipe. Without correction there are significant differences (loss of wall thickness) at the invert of the pipe, which was not visually observed, while the effect of crown corrosion is exaggerated to have a maximum value of 20 mm. After correction (lower chart in Figure 4.8), there is no loss of wall thickness at the invert while this reaches a maximum of 15 mm at the top due to crown corrosion. It is also noticeable that a large area at the crown shows significant less loss of wall thickness after correction. It is also observed that at 200 mm along the perimeter of the pipe, along the length a difference of about 210 mm occurs, which is shifted to the right along the perimeter in the uncorrected measurement, while in the corrected measurements, this band is more or less parallel to the axis of the pipe.
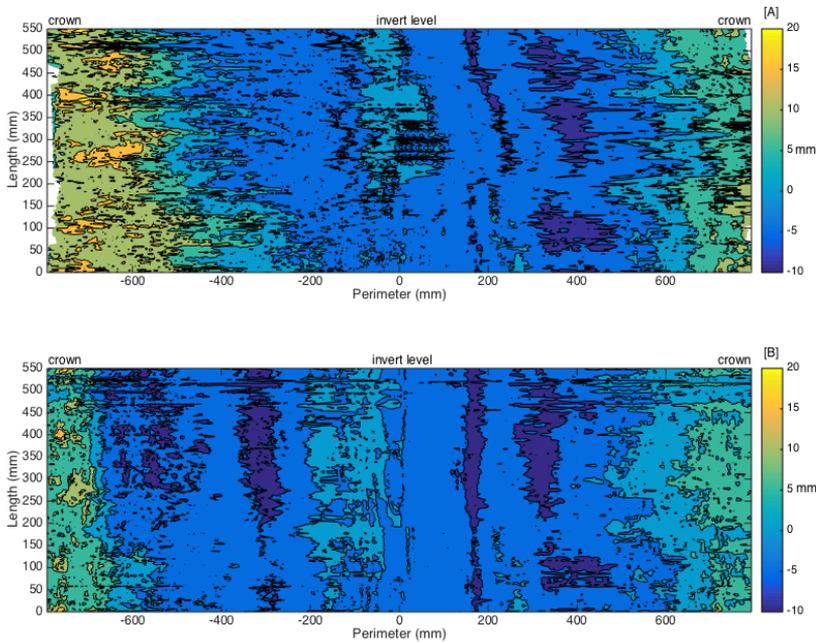
Figure 4.8: Difference between theoretical and measured geometry for the old pipe (P08). The upper chart shows the uncorrected result, and the lower chart shows the result after correction for position and orientation of the measuring platform. A] uncorrected; [B] corrected measurements.

Figure 4.10 (definition sketch is shown in Figure 4.9) illustrates the difference between the uncorrected and corrected profiles for one typical frame obtained from the measurements on the new pipe, while Figures 4.11 and Figure 4.12 show σ_x, σ_y and σ_z as a function of the perimeter for $\sigma_{misalignment} = 2.5 \times 10^{-5}$ radials (Figure 4.11) and $\sigma_{misalignment} = 8.3 \times 10^{-6}$ radials (Figure 4.12). $\sigma_{misalignment} = 2.5 \times 10^{-5}$ is the standard deviation determined for the alignment of the lasers (see Section 4.3.1), the value of 8.3×10^{-6} radials, being one-third of this value, is used to illustrate the sensitivity of the accuracy for the misalignment.
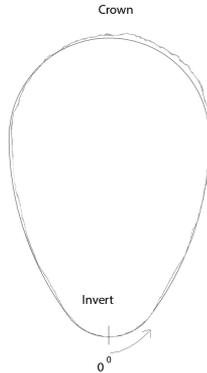
Figure 4.9: Definition sketch for the angles indicated in Figures 10-17, $0°$ is the invert level going counter-clockwise the crown is at $180°$.
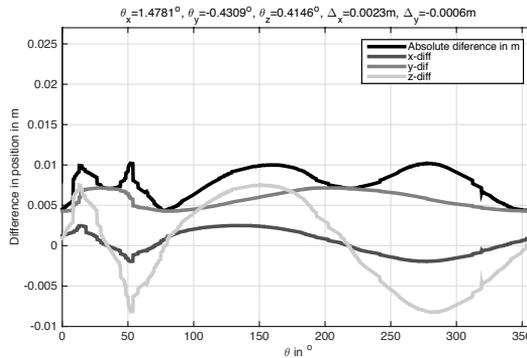
Figure 4.10: Difference between corrected and uncorrected profiles for one frame obtained from the new pipe.

Figure 4.13 shows σ_x, σ_y and σ_z for the uncorrected profile of the same frame. Figures 4.14-17 show the same information for a typical frame as obtained from the old pipe. As can be seen, the difference between corrected and uncorrected profiles as well as the accuracy of the measurements varies along the perimeter of the profile and is strongly influenced by the accuracy of the alignment of the lasers. Figures 4.18 and 4.19 present two typical examples of the relative contributions to the measuring uncertainty of the different sources for $\sigma_{misalignment} = 2.5 \times 10^{-5}$ radials and $\sigma_{misalignment} = 8.3 \times 10^{-6}$ radials, respectively, for the new pipe. As can be seen, the misalignment is dominant when $\sigma_{misalignment} = 2.5 \times 10^{-5}$ radials (60-90% of the uncertainty is caused by this factor, while this drops to 15-50% when $\sigma_{misalignment} = 8.3 \times 10^{-6}$ radials). A similar observation is made for the results for the old pipe shown in Figures 4.20 and 4.21.

Tables 4.3 and 4.4 summarise the results. A one-sided t-test with acceptance level $p = 0.95$ shows that for the new pipe only the differences in the z-direction between corrected and uncorrected profiles are significant, even if the alignment of the lasers is improved by a factor of three. For the old pipe, the observed differences are significant, with the exception of the z-direction. The results show clearly that results obtained from laser profiling have a tendency to overesti-
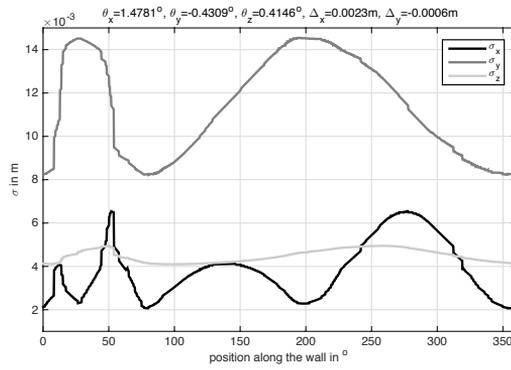
Figure 4.11: Standard deviation for the new pipe for one frame using $\sigma_{misalignment} = 2.5 \times 10^{-5}$ radials.
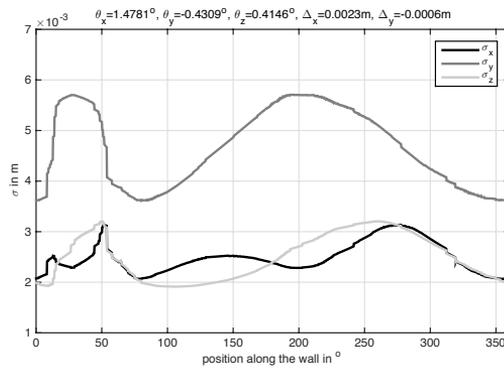
Figure 4.12: Standard deviation for the new pipe for one frame using $\sigma_{misalignment} = 8.3 \times 10^{-6}$ radials.
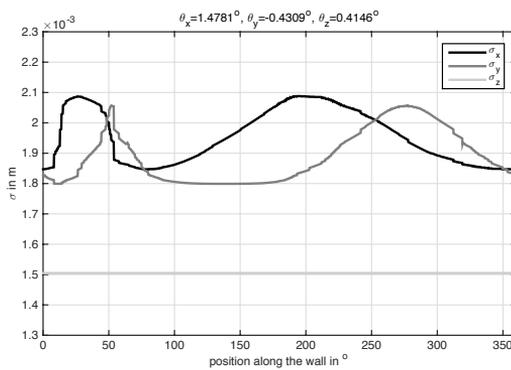
Figure 4.13: Standard deviation for the new pipe for one frame for the uncorrected profile.
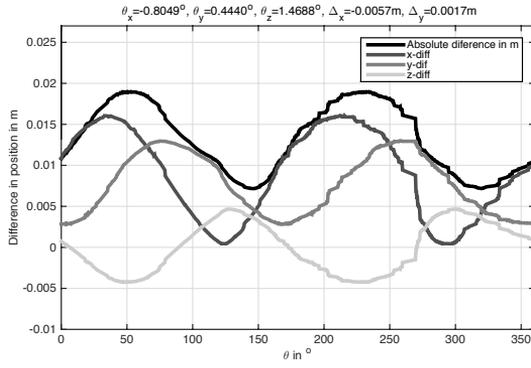
Figure 4.14: Difference between corrected and uncorrected profiles for one frame obtained from the old pipe.
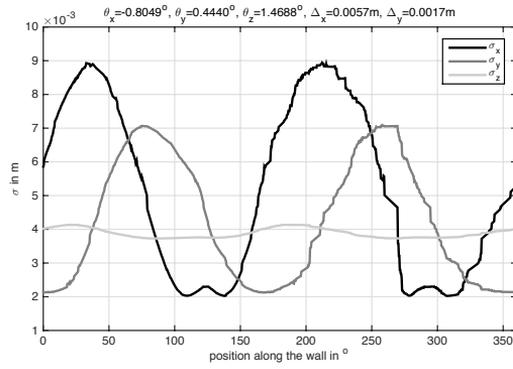
Figure 4.15: Standard deviation for the old pipe for one frame using $\sigma_{misalignment} = 2.5 \times 10^{-5}$ radials.
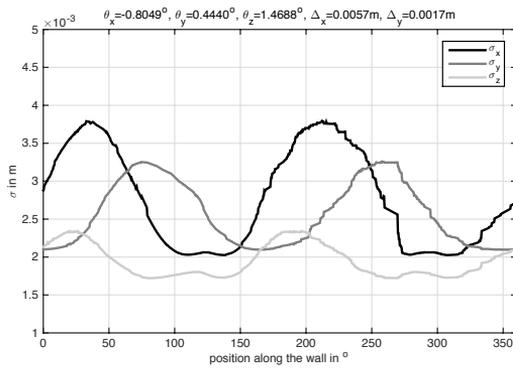
Figure 4.16: Standard deviation for the old pipe for one frame using $\sigma_{misalignment} = 8.3 \times 10^{-6}$ radials.
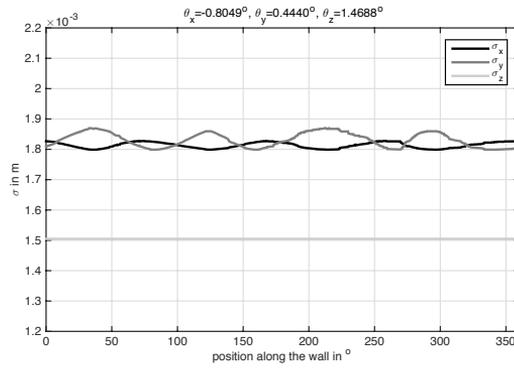
Figure 4.17: Standard deviation for the old pipe for one frame for the uncorrected profile.
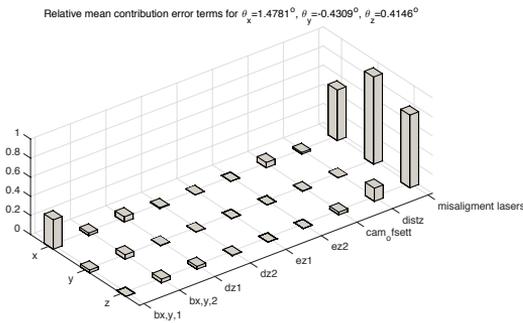
Figure 4.18: Relative contribution of the individual source of error to the overall measuring error in x, y and z positions for the new pipe with $\sigma_{misalignment} = 2.5 \times 10^{-5}$ radials.
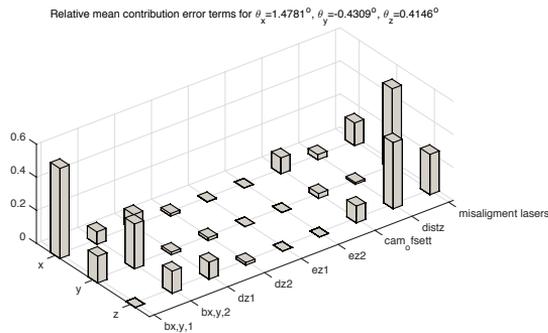
Figure 4.19: Relative contribution of the individual source of error to the overall measuring error in x, y and z positions for the new pipe with $\sigma_{misalignment} = 8.3 \times 10^{-6}$ radials.
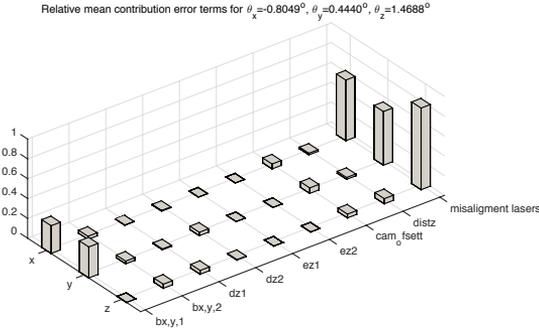
Figure 4.20: Relative contribution of the individual source of error to the overall measuring error in x, y and z positions for the old pipe with $\sigma_{misalignment} = 2.5 \times 10^{-5}$ radials.
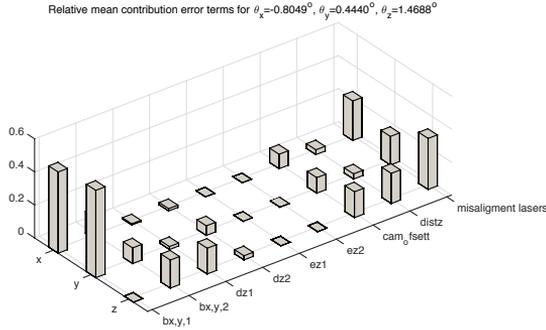
Figure 4.21: Relative contribution of the individual source of error to the overall measuring error in x, y and z positions for the old pipe with $\sigma_{misalignment} = 8.3 \times 10^{-6}$ radials.

mate loss of wall thickness if they are not corrected for position and orientation of the measuring set-up relative to the pipe. Underestimation will not occur, since any deviation of a projection perpendicular to the axis of the pipe will result in an increase in dimension of the profile recorded.

Table 4.3: Maximum deviation between corrected and uncorrected profile and the maximum standard deviation for the new pipe.

	Maximum deviation (in mm)	Maximum σ for the corrected profile with $\sigma_{misalignment} = 2.5 \times 10^{-5}$ radials (in mm)	Maximum σ for the corrected profile with $\sigma_{misalignment} = 8.3 \times 10^{-6}$ radials (in mm)	σ for the uncorrected profile (in mm)
X	4.9	6.4 (p = 0.78)	3.2 (p = 0.94)	1.8
Y	7.7	14.3 (p = 0.70)	5.7 (p = 0.88)	1.8
Z	10.0	4.9 (p = 0.97)•	3.2 (p = 0.99)•	1.5

Notes: Results marked with an asterisk show a significant difference between corrected and uncorrected result for which a one sided t-test with acceptance level p = 0.95 was used. The figures between brackets show the t-test significance level.

As an example, the observed differences between corrected measured and theoretical profiles for the new pipe at z = 23 mm are shown in Figure 4.22. As can be seen, a difference between measured corrected and theoretical profiles is visible (though well within the 95% confidence interval). Figure 4.23 displays the difference between measured corrected and theoretical profiles

Table 4.4: Maximum deviation between corrected and uncorrected profile and the maximum standard deviation for the old pipe.

	Maximum deviation (in mm)	Maximum σ for the corrected profile with $\sigma_{misalignment} = 2.5 \times 10^{-5}$ radials (in mm)	Maximum σ for the corrected profile with $\sigma_{misalignment} = 8.3 \times 10^{-6}$ radials (in mm)	σ for the uncorrected profile (in mm)
X	15.9	8.9 (p = 0.96)•	3.7 (p = 1.00)•	1.8
Y	12.8	7.0 (p = 0.96)•	3.2 (p = 1.00)•	1.8
Z	1.2	4.1 (p = 0.60)	2.3 (p = 0.66)	1.5

Notes: Results marked with an asterisk show a significant difference between corrected and uncorrected result for which a one sided t-test with acceptance level p = 0.95 was used. The figures between brackets show the t-test significance level.

for the old pipe at $z = 300$ mm. At the crown, there is a loss of wall thickness up to 10-14 mm, while at the bottom there is a difference of about 0-6 mm.
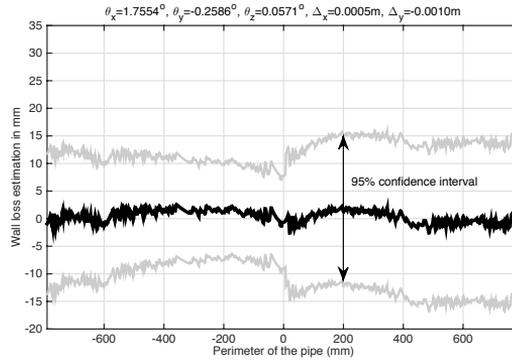
Figure 4.22: Difference between corrected measured and theoretical profiles for the new pipe.
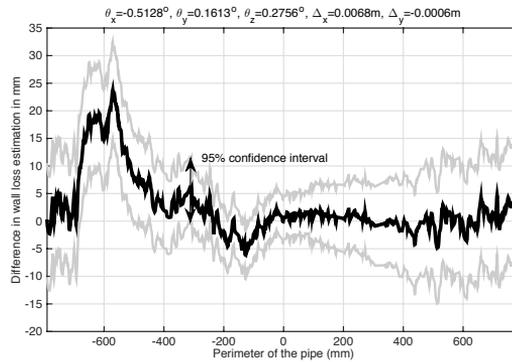
Figure 4.23: Difference between corrected measured and theoretical profiles for the old pipe.

Figures 4.24 and 4.25 present for the old and new pipe, respectively, the difference between uncorrected and theoretical profiles. As can be seen, the systematic differences are significant in both cases. For the old pipe, it is noticed that the maximum loss of wall thickness is larger in the uncorrected profile (18 mm) than in the corrected profile (14 mm). These figures only serve as an example. The 95% confidence interval in Figures 4.22, 4.23, 4.24 and 4.25 is based on the

standard uncertainty in the x and y directions: $\sigma_{wall\ loss} = \sqrt{\sigma_x^2 + \sigma_y^2}$, assuming that the uncertainties in the x and y directions are mutually independent. It has to be mentioned that this is the lower limit for $\sigma_{wall\ loss}$, when assuming a correlation of 1, the upper bound is defined as: $\sigma_{wall\ loss} = \sigma_x + \sigma_y$.
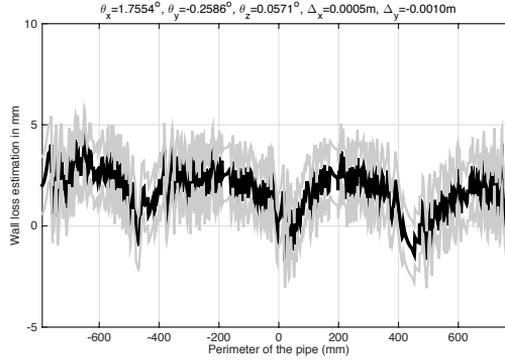
Figure 4.24: Difference between theoretical and uncorrected profiles for the new pipe.
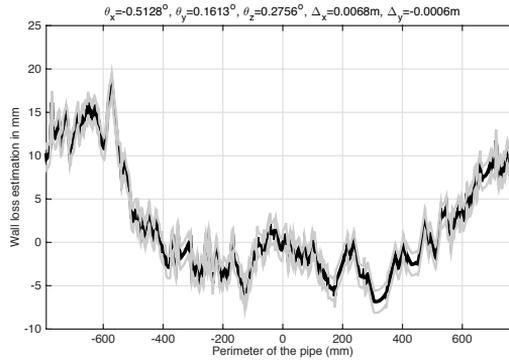
Figure 4.25: Difference between uncorrected and theoretical profiles for the old pipe.

4.5   DISCUSSION OF THE RESULTS

Using laser profiling techniques it is possible to obtain information on the 3D geometry of a pipe. The obtainable uncertainty in the result is quantified and depends largely on the uncertainty of the laser distance measurements and the alignment of the reference coordinate system defined by three parallel lasers. Using relatively simple instruments, statistically significant differences between corrected and uncorrected profiles in the x, y and z directions are obtained under laboratory circumstances. It has to be noted that the covered lengths in the experiments were relatively small, 17 and 55 cm for the new and old pipe, respectively. This results in relatively small values for shifts in the x and y directions. It is anticipated that, when longer stretches are measured, these shifts will be significantly higher, resulting in larger systematic differences between corrected and uncorrected profiles. It has been shown that, using the corrections as de-

scribed in this article, compensation for systematic errors due to orientation and position of the measuring platform is possible but at a price of an increased 95% confidence interval compared to uncorrected measurements. In the simple set-up and the example shown, the corrections are not significant for the whole range of measurements performed. In the laboratory experiments, relatively simple and cheap instruments (as applied in practice) are used in order to investigate the practically feasible uncertainty. It is stressed that, when using high end instrumentation, a far better accuracy is obtainable. The challenge, however, is to develop a measuring system that is applicable under practical circumstances and therefore has to be robust and economically feasible. To this end, the main issues to work on are a more accurate distance measurement (see, *e.g.* Minoshima & Matsumoto, 2000) and the exact alignment of the three parallel lasers, or the implementation of another manner to measure the orientation and position of cam_{FRONT}.

As it has been shown, there are three main contributing sources of uncertainties, given in descending order: the misalignment of the lasers, the image quality of the two cameras and the distance measurement. In laboratory circumstances, the alignment of the lasers is feasible to within 2.5×10^{-5} radials. For obtaining a system that is also applicable in practice, especially this issue seems to be quite a challenge and subject to further development. It is anticipated that for practical applications, the measurement of the orientation of the camera might be done using optical gyroscopes, although their main disadvantage is still their high costs.

Typically the price of optical gyroscopes is 10 times higher than the price of laser distance meters. In the measuring set-up as presented here, the achievable accuracy in the orientation of the measuring platform is in the order of magnitude of 7×10^{-4} radials. Optical gyroscopes achieve an accuracy in angle measurement in the order of magnitude of 10^{-7} radials (see, *e.g.* Titterton & Weston, 2004). Applying such a device will result in an overall uncertainty (95% confidence interval) of ± 3-4 mm, the accuracy given by Kirkham *et al.*, (2000) while neglecting misalignment and positioning issues. Apart from realising a decrease in uncertainty, application of optical gyroscopes also allows for application in pipes that have bends; using the set-up as presented in this article the measuring device must be visible for stationary lasers.

Application of more accurate and sensitive video equipment is relatively simple to achieve given the rapid development of affordable video equipment. It is, however, questionable whether a more accurate camera is the key issue here, since the scatter in the light intensity on the sensor is also determined by the diffusion of the reflected laser light from the pipe wall, which cannot be totally controlled. Certainly, the sensor area and the dimensions of the pixels become more important when working with large sewer profiles. Possibly the application of laser light with a shorter wavelength (here a red laser with a wavelength range of 635-670 nm was applied) will result in an increase of accuracy since the divergence of a laser beam is less at shorter wavelengths (see, *e.g.* Wright *et al.*, 1992).

A disadvantage of the presented set-up is that, when sewers show significant curves, the three laser points may be projected outside the area of the reflection board. In such a case, the method will not work, unless the specific circumstances allow for the stationary lasers to be moved into the sewer. In such a case, a piece-wise approach is possible. For very big sewers, the dimensions of the set-up have to be adapted. For instance, the distance between the front camera and the laser profiler and the field of view of the front camera should be such that the laser projection on the pipe wall is completely visible. Furthermore, in order to achieve the accuracy sought for, the mutual distance between the three stationary lasers should be as large as possible.

Apart from obtaining the 3D inner geometry of a pipe using the proposed technique, it has been suggested by Duran *et al.*, (2007) that using pattern recognition, defects such as cracks, surface damage, intrusion of house and gully pot connections can be detected. Using these techniques in combination with the technique presented in this article, it may become feasible to obtain an efficient method to collect data on the condition of pipes using just one apparatus.

4.6   CONCLUSIONS AND RECOMMENDATIONS

Laser profiling has been shown to potentially be a technique that allows to measure the interior geometry accurately enough to be able to quantify the interior geometry, provided that the position and alignment of the camera and laser are adequately accounted for. Laser profiler results that are not corrected are subject to unknown, and potentially very large, errors, which systematically overestimate wall losses.

The accuracy of the experimental set-up is mainly determined by the uncertainty of the distance measurement and the alignment of the three lasers used to quantify the position and orientation of the camera and the laser sheet. Applying more accurate laser distance-measuring techniques easily solves the former; the latter is, certainly in practical circumstances, a challenge. Improving the alignment of these lasers, or introducing another method for measuring the orientation of the mobile platform allows for an accuracy level leading to an anticipated 95% confidence interval of about 4-5 mm in profiles up to 600 mm in dimension, yielding significant differences between corrected and uncorrected profiles.

Once the 3D geometry is obtained, this can serve as an input for FEM analysis on the structural strength and stability (see, *e.g.* de Borst *et al.*, 2012). Certainly, the external profile and material properties have to be known for this, in most cases, however, the former can be obtained either from documentation of the manufacturer, whereas the material properties can be determined from analysis of drill cores. Future developments will focus on the following:

- Alternative methods, *e.g.* optical gyroscopes, for determining the orientation.
- More accurate laser distance meters.
- Construction of a low-cost device that can operate in practical applications.
- Effects on the overall uncertainty using lasers with smaller wave lengths.
- Optimisation of the post-processing software.

5

STRUCTURAL STRENGTH AND MATERIAL PROPERTIES OF DETERIORATED CONCRETE SEWER PIPES

One important parameter related to the structural condition is the wall thickness, which can be measured directly by *e.g.* core sampling, but also estimated indirectly by calculating the wall losses based on a measurement of the interior shape of the pipe. In Chapter 4 the laser profilers are shown to be capable of measuring the pipe interior, with a high accuracy, which is sufficient to be able to detect and quantify wall losses. This provides information about the geometry of deteriorated concrete sewer pipes. However, based on this information alone it is not possible to derive the remaining strength of the concrete pipes. In this chapter the design of a new laboratory set-up for evaluating the structural response of buried and degraded sewer pipes is described. Furthermore, a better understanding of the structural behaviour of concrete pipes was attained, thus providing more information needed for proper decision making.

The first section of this chapter presents the necessity of understanding the structural behaviour of deteriorated sewer pipes. In the second section of the chapter the adopted experimental boundary conditions, test set-up design and the experimental protocol are presented. The third section discusses methods for the structural strength testing of concrete sewer pipes, material testing retrieved from core samples and the relation between them, followed by sampling strategies for core sampling.

5.1 INTRODUCTION

The structural behaviour of buried concrete pipes is fairly well understood (see, *e.g.* Kang *et al.*, 2007; Kim *et al.*, 2010; Krizek & McQuade, 1978; Trautmann & O'Rourke, 1985), provided that information is available on the soil properties, pipe geometry and material properties. The pipe geometry, such as interior shape and related to this the estimated remaining wall thickness, can be measured by employing a laser-based profiler coupled to a closed-circuit television camera (CCTV) (Clemens *et al.*, 2015; Duran *et al.*, 2003). The material properties are typically measured by employing core sampling. Typically, a single core sample is taken from the crown of the sewer. However, Oualit *et al.*, (2012) and Stanic *et al.*, (2013a) have demonstrated that material properties may vary with the location in the pipe at crown, invert and side positions and that core sampling is associated with significant uncertainties.

In literature, some attempts to study the behaviour of buried pipes under laboratory conditions have been reported so far (Brachman *et al.*, 2000; Trautmann & O'Rourke, 1985). However, to the knowledge of the authors no attempt to evaluate the structural response of deteriorated concrete sewer pipes under laboratory conditions has been reported. Furthermore, core samples can be exposed to a range of tests, ranging from general material properties such as density and water absorption to material strength properties, such as splitting tensile strength or crushing strength. It is unclear which material tests on core samples give the most representative results when compared with the 'real' structural strength of concrete sewer pipes. A reliable prediction of the moment of pipe collapse (life-cycle of the pipe) is critical for the optimization of the inspection and maintenance of sewer structures.

This chapter is based on: Stanić, N., Langeveld, J. G., Salet, T., & Clemens, F. H. L. R. (2015). Relating the structural strength of concrete sewer pipes and material properties retrieved from core samples. *Structure and Infrastructure Engineering*: under review.

5.2   MATERIALS AND METHODS

The study was conducted on excavated sewer pipes that were scheduled for replacement according to the municipal sewer rehabilitation plans of The Hague and Breda. Prior to excavation visual inspections were performed to determine the condition of the inner surface of the sewer i.e. surface damage by internal chemical (corrosion) or mechanical action (BAF). The registration of defects was done according to the visual inspection coding Standard EN 13508-2, while the Standard NEN 3399 was used for condition assessment (European Committee for Standardization, 2003; Nederlands Normalisatie Instituut, 2004a).

The pipes studied here have been in service in combined sewer systems; they are egg-shaped with dimensions of 400/600 mm, 1m long and made of concrete. The sewer in The Hague (P08 and P10) was located in a domestic housing area around old dunes. In this area the groundwater is below the sewer invert level (Gemeente Den Haag 2011). The area in Breda (P02 and P06) used to be partly industrial and partly domestic. As a consequence, the Breda sewer was under a constant high traffic load for approximately 35 years. In this area, the groundwater is above the sewer crown level and the surrounding soil is a combination of peat, clay and sand (Oranjewoud 2009). As a reference, a new concrete sewer pipe (P01) egg-shaped with dimensions of 400/600 mm, from De Hamer factory, was used to validate the experimental results. The new pipe was 2 m long, being shortened to 0.85 m length to allow testing in the same test facility. The quality and the shape of the new pipe meets the requirements required by the Netherlands and European standards NEN 7126, EN 1916 (European Committee for Standardization, 2002; Nederlands Normalisatie Instituut, 2004c). A detailed characteristic of each pipe is shown in Table 5.1.

Table 5.1: Characteristics of studied sewer pipes.

No.	Origin	Service life	Surface damage class (BAF)	BAF class description
P01	De Hamer factory	new	-	
P08	The Hague	1924-2013	4	Missing aggregates or reinforcement
P10	The Hague	1924-2013	4	outside the surface protrudes
P02	Breda	1952-2013	3	Aggregates that protrude beyond the
P06	Breda	1952-2013	3	surface or visible reinforcement

5.2.1   *Experimental set-up pipe structural strength*

Boundary conditions. The first step considered in the design of the laboratory set-up involved simplification of boundary conditions experienced by an underground pipe. The structural performance of the pipe depends on both the soil and pipe stiffness and the resulting soil-structure interaction. A mechanical load on the pipes causes tensions having a vertical component F_v arising from the weight of the overlying materials above the pipe and a horizontal component F_h associated with the restraint against lateral soil movement within the embankment.

In the set-up design hypothetical soil properties were assumed (Young's modulus E = 80 MPa, Poisson's ratio $\nu = 0.25$, angle of internal friction $\phi = 40°$, angle of dilatancy $\psi = \phi/4$, cohesion c = 0, and unit weight $\gamma = 18$ kN/m^3) (Brachman *et al.*, 2000). Further, horizontal stresses are expressed as $K \cdot F_v$, where $K = \nu/(1 - \nu) = 0.33$ is the coefficient of lateral earth pressure. This is a laboratory idealization of field conditions. The applied experiment principle is shown in Figure 5.1 (left).

Test set-up design. The experimental set-up (Figure 5.1, right) consists of a test cell (steel frame/beams) and a concrete, egg-shaped sewer pipe. Applying a uniformly distributed pressure at the crown of the pipe may reasonably represent the vertical stress from the weight of the overburden material. As a reaction vertical stresses are present at the invert level of the pipe. Horizontal stresses could be simulated in a similar manner by applying lateral pressures equivalent to the

horizontal stresses generated in the field. A system of oil pressure jacks and steel beams has been used to deliver stress on the pipe during the tests. In order to achieve a uniform distribution of stress, plaster moulds of pipe and soft boards were attached to the steel beams. The size of the load bearing plates is 1.5 times the pipe thickness. The tests were carried out at a loading rate of 10 kN/min. Sewer pipes were loaded in the set-up till the point of complete loss of carrying capacity - collapse of the pipe. Vertical and horizontal loads were measured together with their front and back vertical/horizontal displacements.
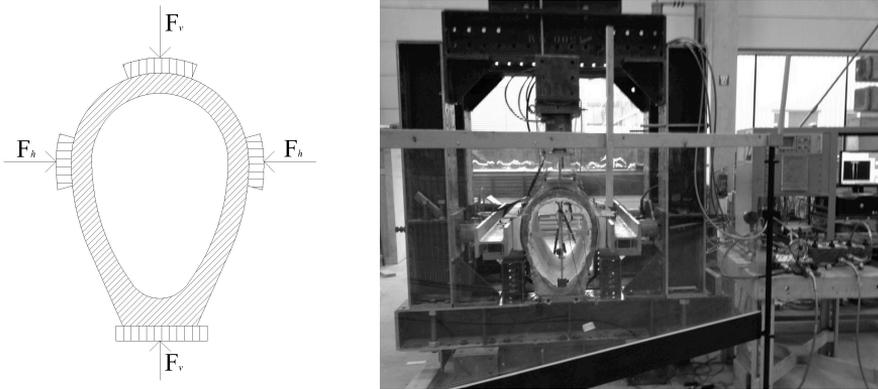
Figure 5.1: Schematic diagram of the adopted experiment principle (left) and actual experimental set-up (right).

5.2.2 *Pipe material testing methods*

In order to determine the material properties of the pipes core sampling was applied. Core samples, however, provide information on the material properties of a few locations only (Stanić *et al.*, 2013a). Therefore, numerous samples (6 samples from the new pipe and 20 samples from each individual deteriorated pipe) were taken in order to obtain data on the material properties of the whole pipe. According to Standard EN 12390-1 the nominal size of the cylinder *i.e.* height-diameter ratio should be 2:1 (European Committee for Standardization, 2012). The nominal wall thickness (height) of the new pipe was ±70 mm. Consequently, this ration can not be achieved in practise otherwise core diameter would be in the order of the maximum aggregate size which is not according to standard ISO1920-6 (International Organization for Standardization, 2004). However, Neville (1995) noted that the height-diameter ration could be lower but not lower then 1; hence making the results unreliable. Consequently, drilled cylinders are also ±70 mm in order to keep height diameter ratio equal, which is a minimum test requirement. Furthermore, by visual inspection of the core samples Maximum Aggregate Size (MAS) was estimated.

Compressive strength, density and water absorption. Compressive strength testing was conducted according to standards EN 12504-1, EN 12390-3 and EN 12390-7 (European Committee for Standardization, 2009a; b; e). If the core height diameter ratio was too small (caused by deterioration of the pipe) the real compressive strength was calculated according to CUR 74 (Civieltechnisch Centrum Uitvoering Research en Regelgeving, 2000). In some cases no value is calculated because the height was too small and the ratio fell out of the scope of CUR 74. Before conducting compressive strength tests the samples were subjected to a water absorption and a density test. Absorption tests are conducted according to EN 13369 (European Committee for Standardization, 2013). After completion of the water absorption tests the specimens were placed in a climate chamber for a few days (20°C, relative humidity (RH) 95%).

Splitting tensile strength and carbonation depth. Tests were conducted according to standards EN 12390-6 (European Committee for Standardization, 2009d). The test specimens used for the tensile strength were also used for the determination of the carbonation depth. For testing both contact lengths were measured and the average length was used to calculate the splitting tensile strength. Further, the carbonation depth was quantified on the leftover samples of the splitting tensile tests. Tests were conducted according to RILEM CPC-18 (1988) by spraying phenolphthalein and measuring the carbonation depth at two point in the section at the inner-side and the outer-side of the pipes. If the carbonation front was irregular another measurement point was taken.

Bending tensile strength. The four-point flexural tests (Figure 5.2) were carried out on rectangular samples (with dimension of 105 mm x 62-75 mm x 480 mm) taken from the upper and lower part of broken pieces of the pipes in order to quantify the ability of the concrete to resist deformation under load - EN 12390-5 (European Committee for Standardization, 2009c). The specimens were positioned in the middle of the rollers. In order to achieve a uniform distribution of stresses, steel plates and soft board roles were placed between roller and sample, if necessary with some plaster for correction. The four-point loading flexural tests were carried out at a loading rate of 0.5 mm/min. The bending (flexural) strength of both outer and inner side of the pipe was determined.

Figure 5.2: Test set-up used for four-point loading flexural tests.

PFM microscopy. As Elsen (2006, p. 1421) has stated, 'PFM (Piezo Response Microscopy) is used as an important tool for diagnosing the degradation mechanism'. For the determination of the water to cement ratio in the pipes optical fluorescence microscopy was used. For the test drill core from the invert and crown region of deteriorated pipes samples were taken (12 in total) to make the thin sections. The specimens were vacuum impregnated which makes determination by fluorescence microscopy possible. When the samples are exposed to fluorescence light all voids, pores and cracks become highlighted. The brightness of the sample gives indication of the porosity and thereby the water to cement ratio. This brightness was compared with reference samples with a known water to cement ratio.

5.3   RESULTS AND DISCUSSION

5.3.1   *Pipe structural strength*

For all pipes cracks appeared at the same location suggesting that the distribution of stresses through the pipes during the tests was the same. The first crack always appeared at the pipe invert level, followed by cracks at the pipe crown area and one on each side (Figure 5.3). CCTV footage in practice hardly revel the presence of the cracks at the invert level probably due to the fact that it cannot be recognised because of the presence of water, debris and/or sediments.

Figure 5.4 shows load-displacement response for the studied pipes. The results show clearly the regions of crack formation and points of the pipe collapse. Major cracks on the new pipe

appeared at the vertical load, F_v = 280 kN. The major cracks on the 61 and 89 year old pipes appeared at around 25% and around 55% smaller load (Figure 5.4). With an increase of the load, however, the pipes resisted collapse due to the combination of vertical and horizontal loads.

Test results showed that the complete loss of carrying capacity for the new pipe was at 330 kN. Also, results showed that the 61 year old pipes could withstand almost the same amount of load, F_v = 315 kN and F_v = 290 kN. In contrast, the 89 year old pipes could withstand a load up to 185 kN and 162 kN (around 40% less stress). This implies that pipes, which are considered old (61 year old), can withstand similar loads as a new pipe before total collapse takes place. Furthermore, from the results it can be seen that the first cracks occurred with displacement of about 0.6 mm, and that the pipes reach the point of collapse with displacements between 13 and 19 mm.

a. F_v = 130.1 kN   b. F_v = 145.9 kN

c. F_v = 165.8 kN   d. F_v = 181.5 kN
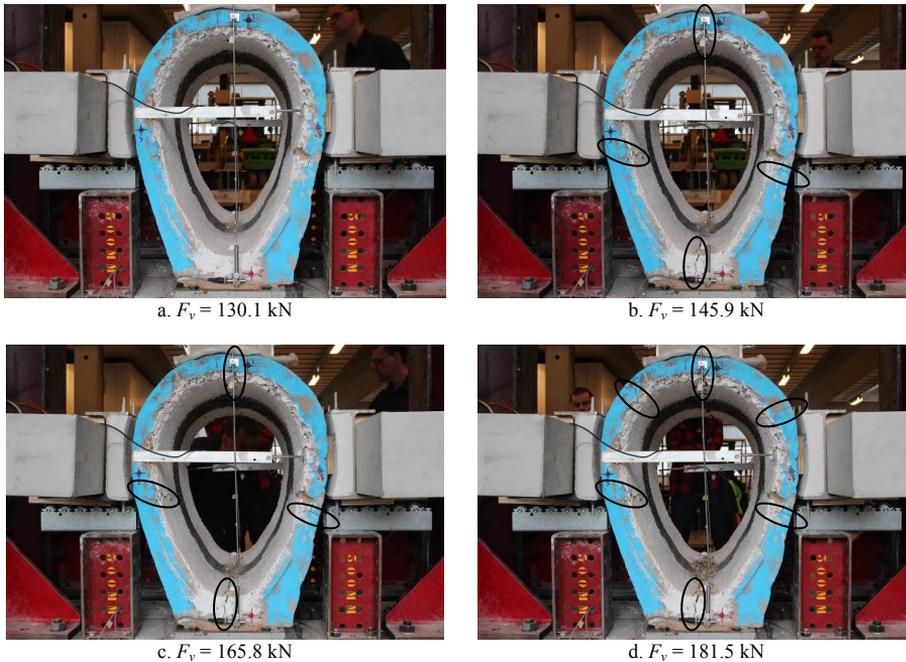
Figure 5.3: Successive stages in the test of a sewer pipe (P08) from Municipality of The Hague during the experiment.

The test method for the crushing strength of new concrete pipes is defined by standards NEN 7126 and EN 1916 (European Committee for Standardization, 2002; Nederlands Normalisatie Instituut, 2004c). For egg-shaped pipes with a flat base, the uniaxial load shall be applied through one top bearer and they shall be supported on two bottom bearers placed with their centres at a distance equal to 0.3 times the internal diameter or width. De Hamer concrete factory performs these quality check test regularly. The average value, obtained from the factory, was 131 kN/m (σ = 1.87 kN/m) for the pipe crushing strength. This crushing strength is about 60% smaller than the experimental set-up recorded crushing strength. This result was to be expected, as the horizontal support in the experiments has a strong impact on the strength of the pipe/soil construction. The results shows that the quality-check test can be regarded only as the material quality check for the whole pipe and not as the pipe crushing strength.
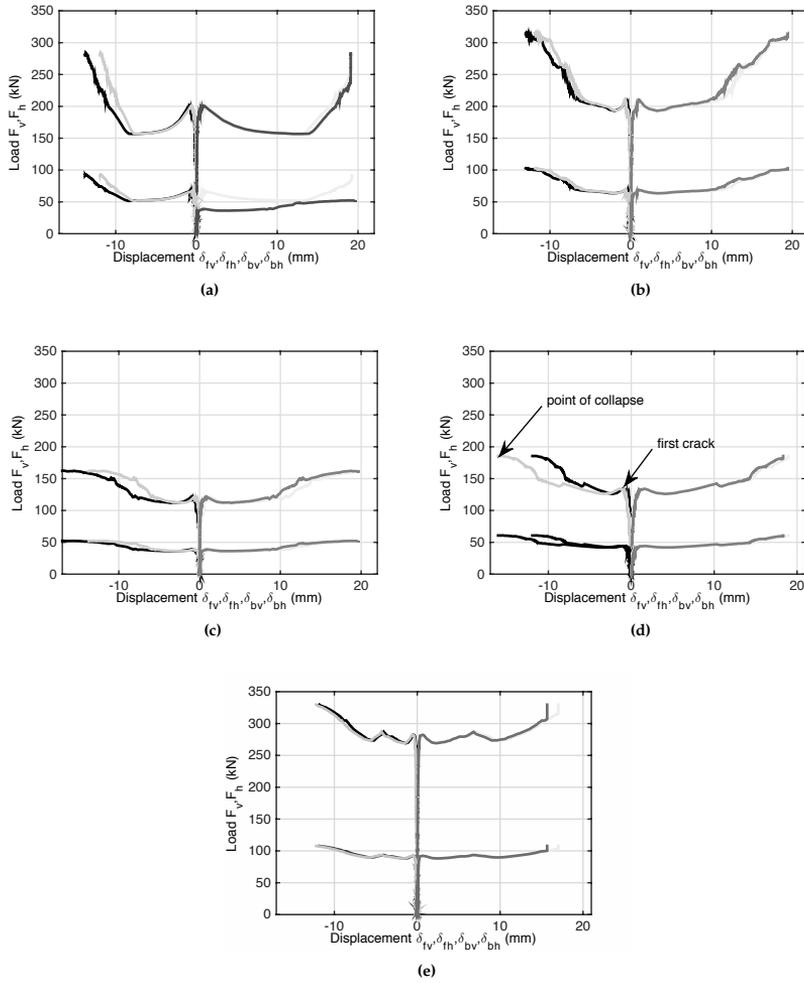
Figure 5.4: Force-displacement response for: (a,b) the 61 year old sewer pipes - P02, P06; (c,d) the 89 year old sewer pipes - P08, P10; (e) the new sewer pipe - P01. (Legend: F_v - vertical force; F_h - horizontal force; δ_{fv} - front vertical displacement; δ_{fh} - front horizontal displacement; δ_{bv} - back vertical displacement; δ_{bh} - back horizontal displacement).

5.3.2   *Pipe material testing methods*

The results of the splitting tensile strength, density and water absorption test show that the difference between measured values (maximum and minimum) increases with decrease of the concrete quality, being the highest for the cores from the Municipality of The Hague (Table 5.1 and 5.2). However, the results of compressive strength test do not show this trend. This is probably due to the effect of MAS. MAS for the pipes P02 and P06 was 16 mm and for P08 P10 was 32 mm. The relative strength values of cores gradually decreased with the increase in maximum size of the aggregate. This becomes more apparent for the smaller diameter cores (<100 mm), which is in this case (Tuncan *et al.*, 2008). The ratio of core diameter to the maximum aggregate size

should generally be greater than 3 (International Organization for Standardization, 2004). This was fulfilled for the pipes P01, P02 and P06. However, this was not fulfilled for the cores from the pipes P08 and P10. This may (partially) explain the variability in the results.

The results of the material tests are compared with the pipe structural strength in the next section. This section describes in some detail the results of the carbonation depth and the four-point flexural tests.

Figures 5.5 and 5.6 show box plots for the carbonation depth for the outside and the inside of drill core samples for the old pipes. As can be seen there is large variability. The ranges for the crown and the lateral locations are almost equal, while the carbonation depth at the inside invert location is significantly less that at the crown and the lateral locations. This was to be expected and points at the occurrence of the classic process crown deterioration (see, *e.g.* O'Connell *et al.*, 2010). On the other hand, chemical attack from the outside was also occurring and is almost identical for all three regions (Figure 5.6). Soil surrounding pipes was probably acidic thus attacking concrete possibly combined with the effects of acidic groundwater (in case of Breda, pipes P02 and P06) (Hobbs, 2001). Although the (bio-)chemical attack at the outside caused less damage than at the inside, the material deterioration is considerable, thus confirming the relevance of exterior damage (Oualit *et al.*, 2012).
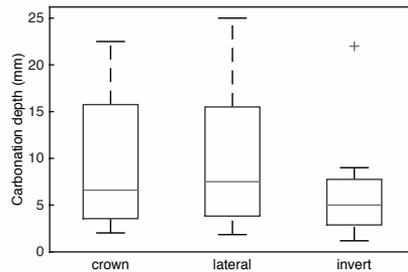
Figure 5.5: Boxplot for the carbonation depths at the inside for pipes P02, P06, P08 and P10; discriminating between crown, lateral and invert positions. On each box, the central mark is the median, the edges of the box are the 25th and 75th percentiles, the whiskers extend to the most extreme data points not considered outliers (approximately $\pm 2.7\sigma$), and outliers are plotted individually.
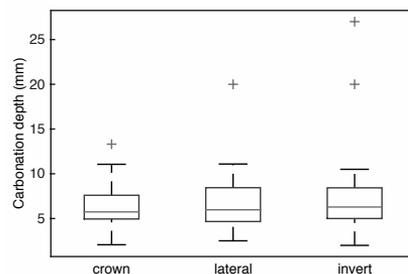
Figure 5.6: Boxplot for the carbonation depths at the outside for pipes P02, P06, P08 and P10; discriminating between crown, lateral and invert positions. On each box, the central mark is the median, the edges of the box are the 25th and 75th percentiles, the whiskers extend to the most extreme data points not considered outliers (approximately $\pm 2.7\sigma$), and outliers are plotted individually.

The four-point flexural tests were carried out in order to quantify the ability of the concrete to resist deformation under load. Results show a high variability between samples per individual

pipe and between samples between pipes (Figure 5.7). The variability may be partly due to the fact that the tested beams were not completely rectangular due to the shape of the pipes. In addition to the irregular shaped beams, the 61 and 89 old pipes apparently did not deteriorate uniformly over the pipe length and circumference. Furthermore, the initial quality of the concrete is most likely not the same for the studied sewer pipes. However, this cannot be tested as there is no recorded information on the initial quality of the studied old concrete sewer pipes.
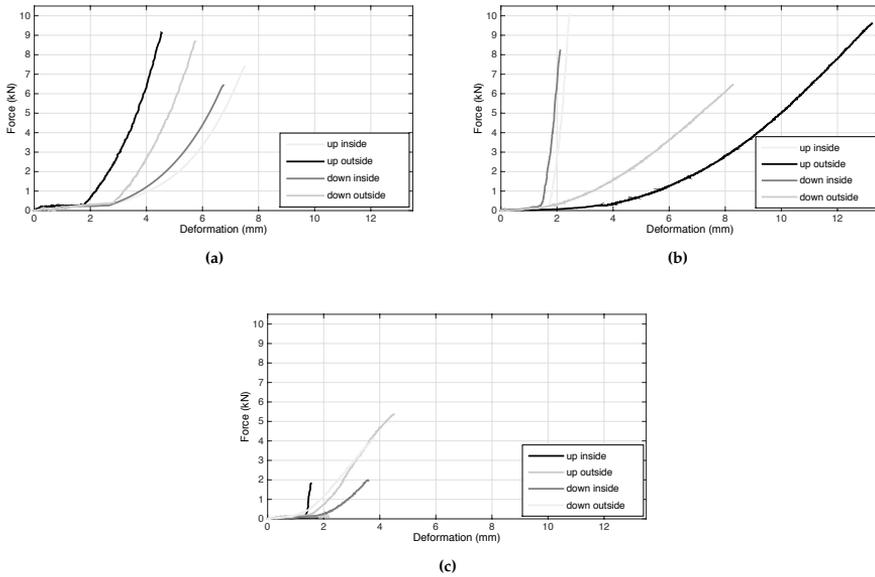
Figure 5.7: The four-pint flexural test force-deformation response for; (a) the new sewer pipe - P01; (b) the 60 year old sewer pipe - P02; (c) the 90 year old sewer pipe - P08.

PFM experimental results for porosity were out of the apparatus measuring range, therefore it was not possible to determine the relevant material property of water to cement ratio. Also, along the Interfacial Transition Zone (ITZ) the concrete was porous (Figure 5.8). At the surface of the thin section some very small vertical cracks were observed.
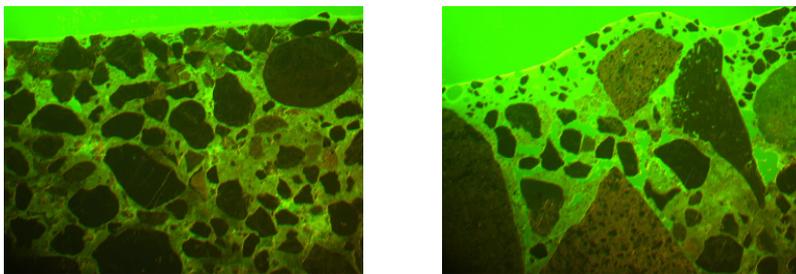
Figure 5.8: Examples of the studied thin section under the fluorescence light (P02 and P06).

Generally deterioration in concrete sewer pipes only occurs at the inside due to biological produced acid (see, *e.g.* Pomeroy & Parkthurst, 1977; Bielecki & Schremmer, 1987); in literature

there are cases described that show that sulphur related corrosion does occur due to other mechanisms (see, e.g. Oualit *et al.*, 2012). Overall, there are multiple (bio)chemical processes that may contribute to the structural deterioration; and it is difficult to quantify them all. For the pipes P02, P06, P08 and P10 the presence of ettringite, an indication of sulphate attack, was investigated using PFM. Ettringite was found in all samples (Figure 5.9). When looking at the sections with polarized light, over the whole thin section samples (from top and bottom) large amounts of ettringite were found; however no large cracks were detected. Furthermore, the very small cracks, which can be seen under fluorescent light, were not observed under polarized light. Thus suggesting that no link can be found between the amounts of ettringite and presence of the small cracks.
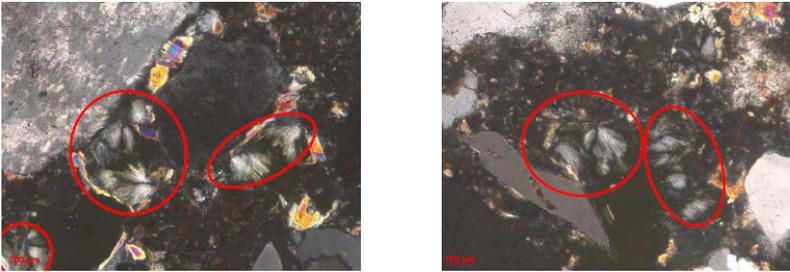
Figure 5.9: Examples of the studied thin sections under the polarized light with the highlighted ettringite (P06 and P02).

The formation of ettringite in hardened concrete in relation to concrete deterioration is the result of complex long-term processes in which the concrete composition, technological factors during concrete production, and the effects of the environment are important (Stark & Bollmann, 1999). Moreover, the pipes from Municipalities of Breda and The Hague (P02, P06, P08 and P10 respectively) were produced *in situ* and installed. In conclusion, they were made in a non-controlled environment, using water of unknown quality (possible presence of sulphate) which could also explain the presence of ettringite in the concrete. As Stark and Bollmann (1999, p. 21) stated, 'It cannot be excluded that ettringite is often not involved in the damage mechanism and thus only a consequence of the microstructure damage caused by other processes'.

There is no clear division in damaged or undamaged parts of the concrete. Visually some colouring and deterioration was observed but overall there is no real deterioration (cracks or loss of coherence) visible under the microscope. This means there is no damaged layer present and therefore no thickness of the possibly damaged layer can be determined. PFM experimental results could therefore not clearly distinguish the degradation mechanism. However, the results imply that material degradation of the sewer pipes from both Breda and The Hague grossly occurred in the same manner, although the pipes originate from different environments with respect to soil properties and groundwater levels.

5.3.3 *Relation between material properties and structural strength*

The relation between the data obtained from the sample tests and the force applied ($F_{v,max}$) on the pipes at the moment the first crack appeared in the pipe crack experiments are shown in Figures 5.10-17. In the graphs a distinction is made between minimal, maximum and mean values of the materials properties per pipe, from these graphs the following observations are made:

- With respect to carbonation depth, the sum of the inner and outer carbonation show a better correlation with $F_{v,max}$ than the values obtained for the inside wall alone. Further it can be seen that the mean values ($R^2 = 0.98$) correlate slightly better with $F_{v,max}$ than the

maximum values observed (R^2 = 0.92). (Figure 5.10 and 5.11). With respect to carbonation depth, the mean value is therefore the most appropriate parameter.

- With tensile splitting (Figure 5.12) the best correlation with $F_{v,max}$ is obtained for the minimum values found for the tensile splitting strength with an R^2 of 0.96. The correlation with the mean splitting tensile strength, with an R^2 of 0.83 is still acceptable.

- With respect to tensile bending strength (Figure 5.13), the values for the tensile bending strength show very low correlations for the minimum, mean and maximum. Tensile bending strength is therefore not a very suitable parameter to assess the material properties.

- Compressive strength seems to have no significant with $F_{v,max}$ (Figure 5.14) and is therefore also not a suitable parameter to assess pipe strength.

- The material properties water absorption and density (Figure 5.15 and 5.16) show only a significant correlation (R^2 = 0.89) for the minimum values found for the material density, with respect to water absorption only a very weak correlation (R^2 = 0.35) between the maximum values and $F_{v,max}$ was found.
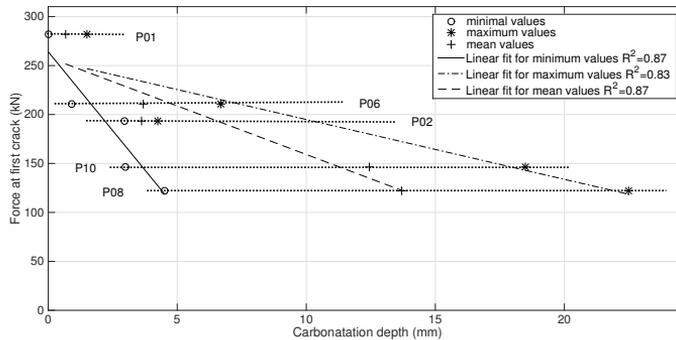
Figure 5.10: Relation between force at the first crack and carbonation depth at the inner wall of the pipes.

The minimal tensile splitting strength apparently gives the best information with respect to the material's properties, while the carbonation depth gives the best information with respect to the geometry. The latter is illustrated when the remaining thickness of the healthy material is taken as a parameter. The thickness of the healthy material is defined by the measured wall thickness minus the values found for the carbonation depth on the in- and outside of the pipe. Figure 5.17 shows the results. Indeed, the mean and maximum values of the remaining healthy material have respectively a R^2 of 0.90 and 0.93 with the force applied when the first crack appeared.

It should be noted that carbonation is a disadvantage in reinforced concrete, while on the other hand may have an advantage in non-reinforced concrete. Carbonation is indicator of pipe aging; with age material quality deteriorates. Consequently, the term 'healthy material' is regarded as the material that is not affected by a degradation process(es).

Furthermore it is observed that the material characteristics of the new pipe (P01) are more homogeneous than of the old pipes for most parameters, apart from compressive strength and tensile bending strength. It is also these two parameters that show the least correlation with the force at the appearance of the first crack. Apparently, the homogeneity of the material decreases with age and, as a consequence, the number of samples required increases for older, more deteriorated pipes, which has significant consequences for the reliability of core sampling. Additionally, the dimensions of the drill core together with effect of MAS may explain a part of the variability. This conclusion was drawn although the initial quality of the concrete for all tested pipe is not
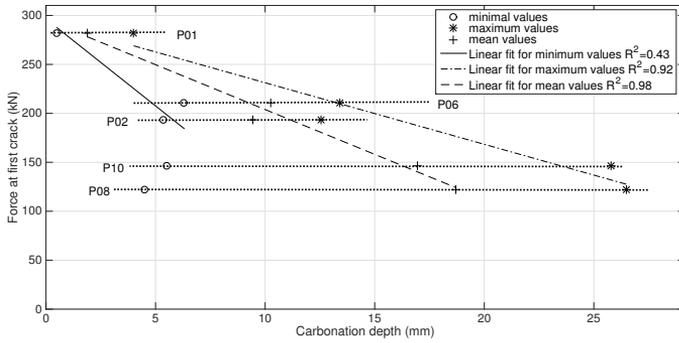
Figure 5.11: Relation between force at the first crack and the carbonation depth at the in- and outside wall of the pipes.
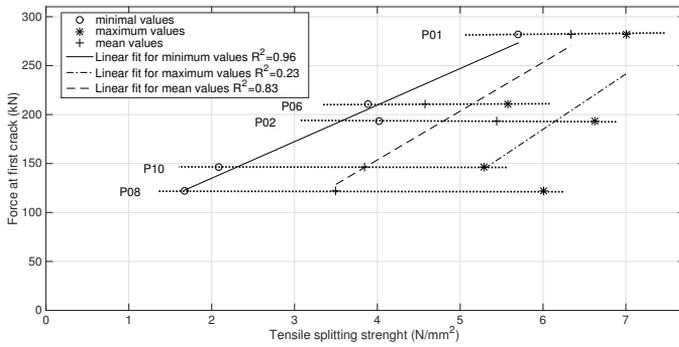
Figure 5.12: Relation between force at the first crack and the tensile splitting strength.
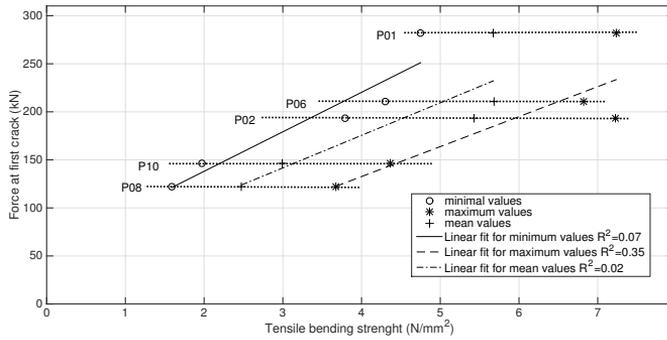
Figure 5.13: Relation between force at the first crack and the tensile bending strength.
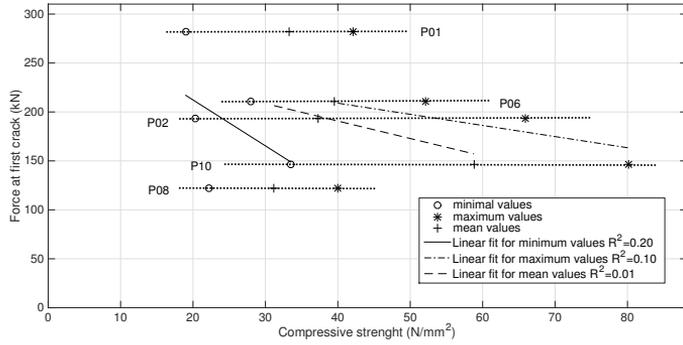
Figure 5.14: Relation between force at the first crack and the compressive strength.
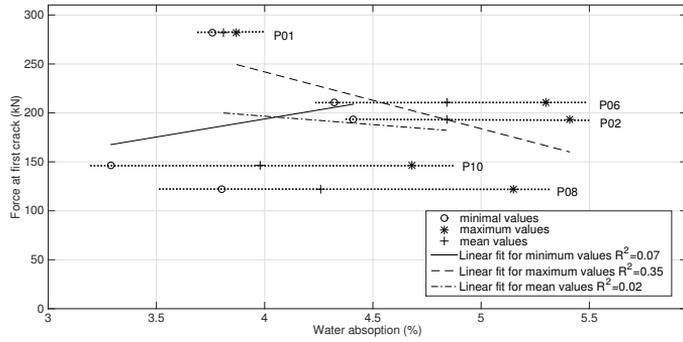
Figure 5.15: Relation between force at the first crack and the water absorption.
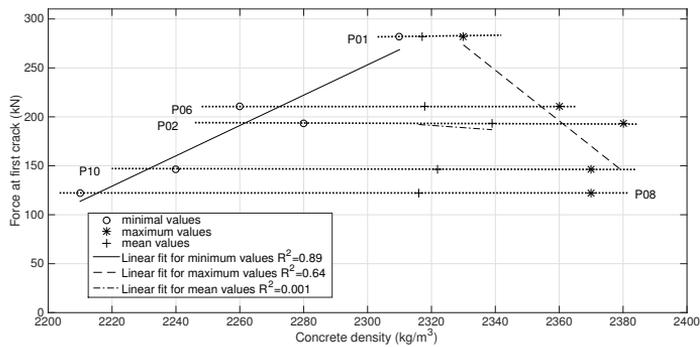
Figure 5.16: Relation between force at the first crack and the density of the concrete.
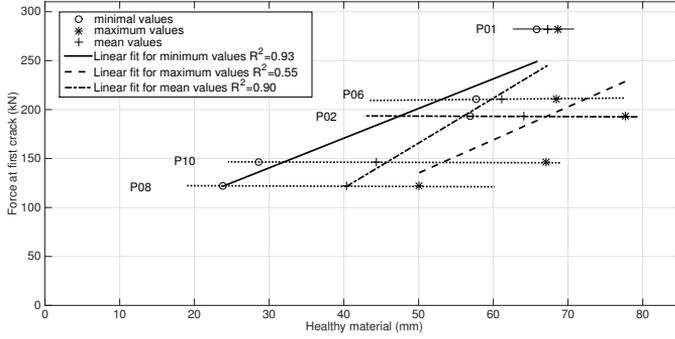
Figure 5.17: Relation between thickness of the remaining healthy material and force at the first crack.

known. The conclusion is based on the assumption that concrete (in a similar environment) over the long period of time has a tendency to deteriorate in the same manner.

Due to the inability to access independent samples to do rigorous cross-validation PRESS-related statistics were used. Holiday *et al.,* (1995) recommended the use of the PRESS approach for cross-validation of regression models when having small datasets, as well as a means of dealing with the problems of data-splitting. This is a method based on the jackknife technique. The idea is to fit the model without the ith observation x_i and use this fitted model to predict the response $\hat{y}_{(i)}$, at x_i. The PRESS residuals are defined as $e_{(i)} = \underline{y}_i - \hat{y}_{(i)}$. The process is repeated for all n observations. The PRESS statistic is computed as:

$$PRESS = \sum_{i=1}^{n} e_{(i)}^2 \tag{5.1}$$

Once determined, the PRESS statistic was used to calculate a predicted R^2 (R^2_{PRESS}) using the following formula: $R^2_{PRESS} = 1 - (PRESS/TSS)$, where TSS it the total sum of squares for the original regression equation (Myers, 1990). The smaller the difference between the two values for coefficient of determination, the more stable the model for prediction. For the given R^2 values the best R^2 predicticions (R^2_{PRESS}) were obtained for the minimal tensile splitting strength (R^2_{PRESS} = 0.92) and for the mean carbonation depth (R^2_{PRESS} = 0.96). Differences in values are small *i.e.* a decrease of 0.04 and 0.02 from R^2 for their prediction model, respectively. Overall, these models appear to be stable, hence they can be regarded as representative.

5.3.4 *Sampling strategies for core sampling*

For older concrete pipes, a rather large variability in the material characteristics result from the analysis. Furthermore, it was shown that the relation between material characteristics and pipe failure strength is relatively strong for maximum and mean values of carbonation depth (R^2 = 0.92 and R^2 = 0.98), minimum and mean values of 'healthy material' (R^2 = 0.93 and R^2 = 0.90), minimum values for density (R^2 = 0.89) and minimum values for tensile splitting strength (R^2 = 0.96). This implies that when deciding on the number of samples to be analysed this variability has to be taken into account.

Assuming a normal distribution and using the experimental results as a first estimate for the mean and the standard deviation, the following calculations can be made for the estimate of the

sample size as a function of the reliability; with respect to the mean, the sampling size can be estimated by Louangrath (2014):

$$n_s \geqslant \left[\frac{Z_{\alpha/2} s}{E} \right]^2 \tag{5.2}$$

where E is the allowed difference between the estimated mean value and the 'true' value and $Z_{\alpha/2}$ defines the confidence interval (e.g. $\alpha = 0.05$ defines the 95% confidence interval).

With $\alpha = 0.05$, E is 10% of the initial estimated mean value for carbonation depth and tensile splitting strength and E = 5% for density, formula (5.2) shows that for new pipes one core sample is sufficient to estimate the remaining thickness of healthy material, but at least 7 samples are needed to determine the tensile splitting strength. For older pipes, with lower initial mean values and higher standard deviations, the number of samples for the thickness of heathy material ranges between 2 and 24 samples and for tensile splitting strength between 11 and 112 samples.

Table 5.2: Calculated sample size required for a 95% reliability.

Pipe	Parameter	Initial estimate for the mean value	Initial estimate for the standard deviation	Sample size for the mean values. Based on Eq. (5.2)
P01	Remaining healthy material	67.3 mm	2.05 mm	1
	Density	2317 kg/m^3	11.5 kg/m^3	1
	Tensile splitting strength	6.34 N/m^2	0.86 N/m^2	7
P02	Remaining healthy material	64 mm	5.4 mm	3
	Density	2339 kg/m^3	28.46 kg/m^3	1
	Tensile splitting strength	5.44 N/m^2	0.90 N/m^2	11
P06	Remaining healthy material	61 mm	3.4 mm	2
	Density	2318 kg/m^3	30.48 kg/m^3	1
	Tensile splitting strength	4.58 N/m^2	0.53 N/m^2	6
P08	Remaining healthy material	40.3 mm	8.9 mm43	19
	Density	2316 kg/m^3	25 kg/m^3	1
	Tensile splitting strength	3.5 N/m^2	1.32 N/m^2	55
P10	Remaining healthy material	44.3 mm	11.0 mm	24
	Density	2322 kg/m^3	41.04 kg/m^3	1
	Tensile splitting strength	3.85 N/m^2	2.08 N/m^2	112

Especially with respect to the parameter tensile splitting strength, for which the minimum value is more relevant than the mean value, the number of samples to be taken is also defined with the certainty with which the variance of the parameter has to be known. The confidence interval for the variance σ^2 is given by:

$$\frac{(n_s - 1)s^2}{\chi^{2(\alpha/2)}_{n_s - 1}} \leqslant \sigma^2 \leqslant \frac{(n_s - 1)s^2}{\chi^{2(1-\alpha/2)}_{n_s - 1}} \tag{5.3}$$

in which $\frac{(n_s-1)s^2}{\chi^{2(\beta)}_{n_s-1}}$ is the β quantile for chi-squared distribution with n_s-1 degrees of freedom, n_s is the sample size, s is the estimate for the standard deviation. If the interval is set to a certain minimal acceptable length; γs^2 then the sampling size is defined by:

$$\left(\frac{(n_s - 1)s^2}{\chi^{2(\alpha/2)}_{n_s - 1}} - \frac{(n_s - 1)s^2}{\chi^{2(1-\alpha/2)}_{n_s - 1}} \right) < \gamma s^2 \rightarrow \left(\frac{(n_s - 1)}{\chi^{2(\alpha/2)}_{n_s - 1}} - \frac{(n_s - 1)}{\chi^{2(1-\alpha/2)}_{n_s - 1}} \right) < \gamma \tag{5.4}$$
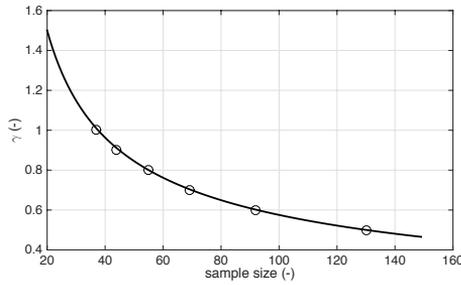
Figure 5.18: Relation between relative confidence interval and sample size.

Figure 5.18 shows the relation between the sampling size and the relative confidence interval γ for σ^2, as can be seen that in order to obtain a value for γ smaller than 0.5, a sample size of at least 131 has to be chosen. Even for $\gamma = 1$, the sample size should be at least 38.

It is clear that, in order to obtain reliable data, a number of samples have to be taken and that this number is highly variable. For instance, the pipes P02 and P06 on one hand and P08 and P10 were located in the same stretch of sewer and show significant different results. From the pipes analysed in this study the number of samples to be taken seem to increase with age (P01 = 0 years of service, P02 and P06 have seen 61 year of service, P08 and P10 have seen 89 years of service). The number of samples indicated is prohibitive in two ways: costs and the fact that after taking that many samples the conclusion would be 'The operation was successfull, a pity the patient died'. As a consequence, the parameter remaining healthy concrete material is clearly to be preferred over the parameter tensile splitting strength.

5.4   CONCLUSIONS AND OUTLOOK

Sewer systems deteriorate due to aging, overloading, misuse and mismanagement. The challenge for sewer asset management is to be able to estimate a safety margin for the collapse of pipes. Further, the presence of cracks does not imply that the pipe collapses. Cracked pipes could still withstand a reasonable additional load. Different factors, like road conditions, traffic load and especially local soil conditions may influence the sewer's lifespan. It is disputable to regard pipe age and CCTV as main and sufficient information sources in deciding upon sewer system renewal.

Core sampling is a destructive technique that is generally accepted for determining the material properties of concrete sewer pipes. The results show that concrete deteriorates non-uniformly in space and time; while deviations between results increases with worsening of conditions of studied pipe. In addition, PFM experimental results show that it is difficult to distinguish the degradation mechanism, due to the influence of numerous factors starting from the production stage to the end of pipe service life. Furthermore, based on the comparison of the results of controlled lab pipe cracking experiments and core sampling results of the pipe material, the following conclusions can be drawn:

- The minimal tensile splitting strength gives the best information with respect to the material's properties, with the mean tensile splitting strength as a reasonable alternative.
- The mean carbonation depth (*i.e.* loss of 'healthy' wall thickness) gives the best information with respect to the geometry.
- For severely deteriorated pipes the required number of core samples increases to a prohibitively high level. For these very deteriorated pipes other, non-destructive techniques should be developed as an alternative.

For sewer rehabilitation decisions, it is necessary to be able to calculate the remaining strength of the soil-pipe construction environment for deteriorated pipes. Further research will concentrate on simulations with a Finite Element Method (FEM), with the pipe geometry data provided by a laser profiling and material properties by core sampling. In addition, the results of this chapter will be used for future development of inspection strategies using core sampling.

Part II

HYDRAULIC CONDITIONS

6

ESTIMATION OF HYDRAULIC ROUGHNESS OF CONCRETE SEWER PIPES BY LASER SCANNING

In Part I - Methods for assessing structural performance of sewers was presented and discussed. Further, in order to determine whether or not a given pipe has an adequate hydraulic capacity it is important to know the actual status of the asset - pipes, such as wall roughness and thus hydraulic roughness. Wall roughness has a direct influence on the hydraulic performance of a sewer system; hence it needs to be quantified. In this chapter the testing method for assessing hydraulic performance by laser scanning is presented.

In the first section of the chapter the relevance of knowing the hydraulic roughness of concrete sewer pipes is discussed. The second section presents the material and methods applied, while in the third section the processing of data and the principle of estimating hydraulic friction loss coefficients from measured wall roughness are described. A spatial interpolation uncertainty analysis during data processing is also presented. The fourth section presents and discusses the results, finally concluding that a low-resolution laser scan is able to measure physical roughness and consequently the hydraulic roughness.

6.1 INTRODUCTION

For the purpose of the sewer system design, numerical models are used to reproduce the flow and pollution transport pattern in the sewer. User-specified parameters (*e.g.* hydraulic resistance, pipe diameter, local head loss coefficients *etc.*) are essential to the correctness of the hydraulic simulations made by performing software's. The hydraulic resistance *i.e.* friction resistance of pipes is one of many essential factors that needs to be known in transportation of liquids. In order to assess the friction resistance, it is necessary to know the pipe hydraulic roughness. Straub and Morris (1950) quantified the hydraulic roughness of new concrete pipes. Overall, the hydraulic resistance of new sewer pipes is fairly well understood (see, *e.g.* Ackers, 1961; Ackers *et al.*, 1964).

In practise there is a lack of reliable information on the actual hydraulic roughness of aged pipes; the roughness will change over time due to *e.g.* corrosion processes, joint eccentricity, protruding objects and subsidence (Bennis *et al.*, 2003), *etc.* Increased hydraulic roughness, due to aging of the pipe material, reduces the flow capacity of the pipe, resulting in decreasing systems' hydraulic performance (Bennis *et al.*, 2003). Furthermore, sewer repairs, like sewer relining, alter the hydraulic resistance mainly due to a decrease in diameter and, depending on the material used, the hydraulic roughness. Consequently, it is important to know the actual status of the asset - pipes, such as hydraulic roughness and the exact interior geometry in order to determine whether or not a given pipe has adequate hydraulic capacity. All in all, it is imperative to possess appropriate information of appropriate quality in order to move to a more rational sewer management decision process (Stanić *et al.*, 2014a).

In literature, some attempts to this end are reported. For instance, Romanova *et al.*, (2011) developed a novel, non-invasive and *in situ* acoustic method and instrumentation to measure the water surface pattern and hence determine the resistance and then the pipe wall roughness. Romanova *et al.*, (2011), however, does not measure the actual wall roughness and above all suggests further research. For example, the presence of the sediments or other objects can also induce the formation of patterns at the surface; hence it is hard to state that the actual roughness

---

is always measured using this method. Therefore, it is necessary to define methods that enable the collection of this information.

Pegram and Pennington (1996) have developed a method for the *in situ* determination of hydraulic friction loss coefficients of bored tunnels, using high accurate laser scan measurements. There is potential in applying this methodology in order to obtain an accurate estimation for the hydraulic condition of sewer pipes; *i.e.* quantifying physical (wall) roughness, quantifying the attached and/or settled deposits roughness.

In this chapter, the potential and uncertainties of laser scanning methods for an accurate, non-invasive and non-intrusive assessment of the hydraulic roughness of concrete sewer pipes is demonstrated and discussed. The studied concrete sample surfaces were reconstructed by using a geostatistical interpolation technique of kriging on scanned raw-sample-data to estimate the physical roughness - Nikuradse's (1933) equivalent sand-grain roughness k_s and consequently the hydraulic roughness - Manning's coefficient n. In order to identify the minimum scanning resolution required to obtain an accurate estimate of the hydraulic roughness sensitivity analysis is performed.

6.2 MATERIALS AND METHODS

6.2.1 *Materials*

The study was conducted on excavated sewer pipes that were scheduled for replacement according to the municipal sewer rehabilitation plans of The Hague and Breda (two pipes from each municipality). The concrete egg-shaped pipes (400/600 mm, 1m long) used in this project have been in service in combined sewer systems. The sewer in The Hague, in operation between 1924 and 2013 was located in a domestic housing area around old dunes. The area in Breda used to be partly industrial and partly domestic and the sewer was in operation between 1952 and 2013. As a reference, a new pipe (of the same material, shape and size) from De Hamer factory, was used to validate known wall roughness of the new pipes (further details can be found in Stanić *et al.*, (2014b)).

A high accuracy Nikon LC60Dx digital line scanner was used for acquiring the raw data. The Nikon LC60Dx multi-stylus test accuracy is 9 μm (according to manufacturer specifications), which represents the 95% uncertainty interval of the scanner ($\pm 2\sigma$) and represents the measuring uncertainty σ_m. The multi-stylus test (comparable to ISO 10360-5 (2010)) determines the level of measurement uncertainty when measuring location using multiple probe head positions. The LC60Dx laser scanner offers an adequate productivity with its 60 mm stripe width and scanning rate of 75 stripes per second thus attaining a scanning rate of 75,000 points per second (a stripe distance of 0.1 mm and a point distance of 0.06 mm). Further, the laser scanner possesses Enhanced Sensor Performance capability allowing effortless scanning of varying or hard-to-scan surface materials. Moreover, it features a filter to avoid capturing of scattered reflection points.

6.2.2 *Method validation*

For the purpose of validation of the Pegram and Pennington (1996) methodology, the physical roughness (k_s) was measured on a 5×10 cm size sample, made from 5-8 mm diameter gravel (mean roughness is 5.5 mm). The measured validation sample (Figure 6.1) represents the actual hydraulically rough field conditions of a floodplain (details are presented in Ali and Uijttewaal (2012)), for which the friction factor is already determined from hydraulic measurements in an hydraulic laboratory.
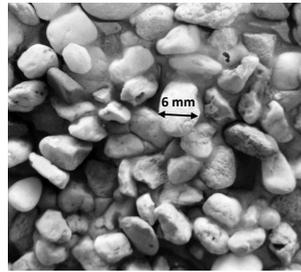
Figure 6.1: Photo of the validation sample used by Ali and Uijttewaal (2012).
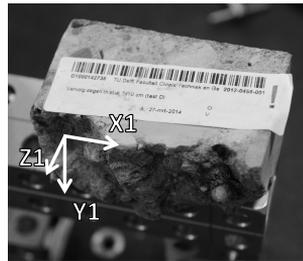
Figure 6.2: Photo of the sample from The Hague pipe - Po8 (X1 and Y1 define the position of elevation Z1).

6.2.3 *Experimental method*

Samples of 5×10 cm were carefully sawn-out, with minimum damage, using a diamond saw in the concrete laboratory of BAS Research & Technology. They samples were taken from the invert, lateral and crown region of each excavated pipe (example in Figure 6.2). Only one sample was taken from the new concrete sewer pipe. Strips of sample surfaces were scanned, with a high accuracy Nikon LC60Dx digital line scanner, at regular intervals of 0.1 mm and an average point distance of 0.01 mm (a higher point density from usual practice). Figure 6.3 shows the schematic diagram of the methodology.
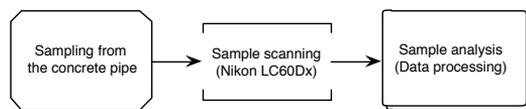
Figure 6.3: The schematic diagram of the experimental protocol.

6.3 DATA PROCESSING

This section describes the processing of samples of raw-scan-data (X1, Y1, Z1) carried out in the study. Two sets of analysis were carried out in parallel, (*i*) on the validation sample and (*ii*) on the samples from deteriorated sewer pipes. Figure 6.4 describes the applied data processing protocol.
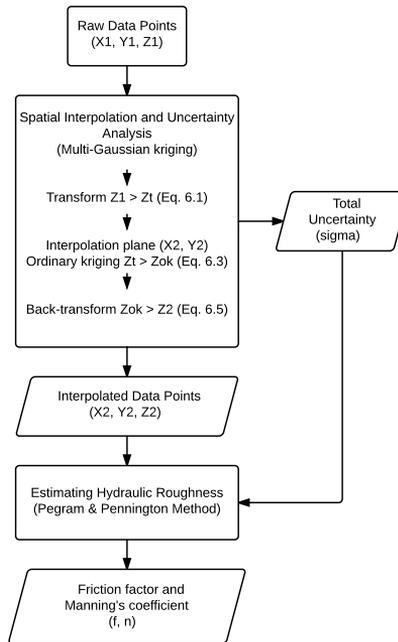
Figure 6.4: Data processing flow chart.

After all three samples roughnesses (from invert, lateral and crown region) were quantified, an estimate of a single roughness value for the whole sewer pipe was obtained by Horton-Einstein (1934) equation. Furthermore, in order to determine the minimal scanning resolution required to obtain useful results analysis was repeated on the validation sample with decreased spatial resolution (sensitivity analysis).

6.3.1 *Spatial Interpolation*

Due to an unevenly deteriorated pipe surface, laser light was scattered resulting in a non-uniform distribution in space. For the purpose of further analysis, however, it is necessary to have equidistant series of points in space. Therefore, the raw data had to be interpolated. A 'kriging' method was applied in spatial interpolation from point measurement to continuous surfaces. The term kriging was introduced in 1950s by Daniel Krige (1951) and refers to a group of geostatistical interpolation methods. It is a process of a theoretical weighted moving average where the prediction at unobserved location is a linear combination of observations nearby. Further, due to the size of data sets (around 700,000 points per sample) data was analysed in subsets. Sample edges were excluded from analysis to avoid over estimating of the physical roughness. Few of the sample elevations ($Z1$-data) follow the normal distribution (Figure 6.5). While, all the sample subsets elevation ($Z1$-data) deviates from the normal distribution (Figure 6.6). Nevertheless, the kriging method is based on Gaussian statistics; assuming that the data follows the Gaussian distribution. Consequently, to symmetrize the distribution of data and to analyse it the Multi-Gaussian kriging (MG) was applied (Deutsch & Journel, 1998). In this study, the post-processing was done in open-source R programming language, which has well-developed procedures (packages) for a spatial statistical analysis (Bivand *et al.*, 2008; Hengl, 2007).
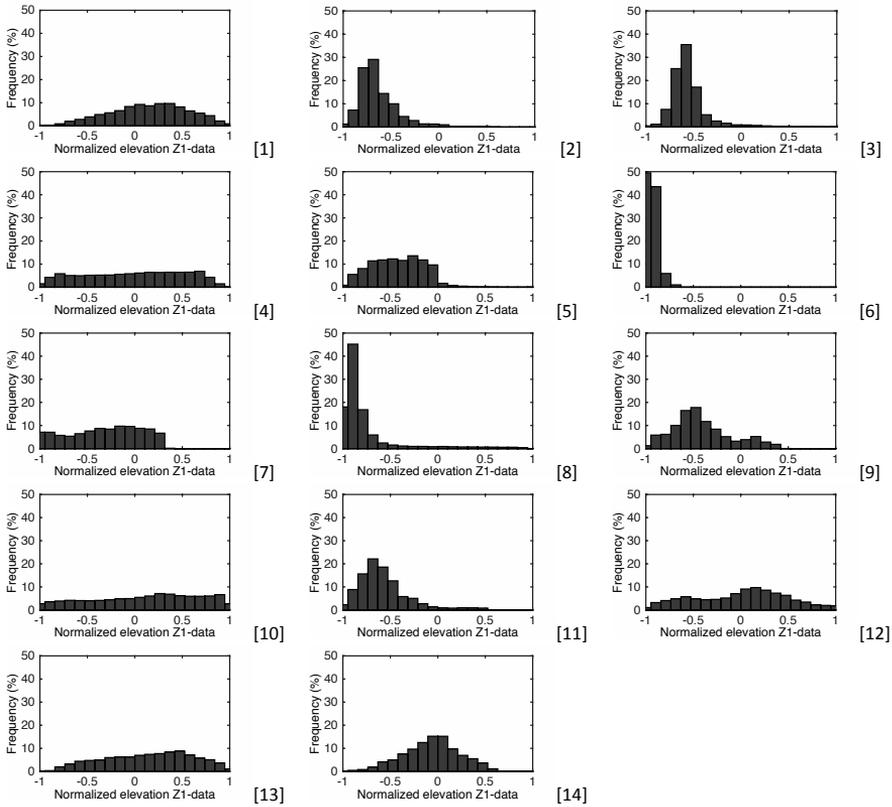
Figure 6.5: Histogram of elevation of sample: [1, 2, 3] Breda pipe - P02 (invert, lateral and crown); [4, 5, 6] Breda pipe - P06 (invert, lateral and crown); [7, 8, 9] The Hague pipe - P08 (invert, lateral and crown); [10, 11, 12] The Hague pipe - P10 (invert, lateral and crown); [13] new pipe - P01; [14] validation sample.
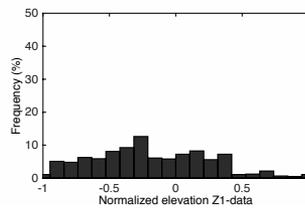
Figure 6.6: Example of the histogram of elevation for one subset of the validation sample (Fig. 6.5 [14]).

The MG starts with a normal-score transformation of the original $Z1$-data into Zt-values, because prediction performances are usually better if data does not display a strong skewness. Normal-score transform is a graphical transform that can normalize any non-Gaussian data (Eq. 6.1) (Deutsch & Journel, 1998).

$$Zt(u) = G^{-1}[F(Z1(u))] \qquad (6.1)$$

where $Z1(u)$ and $Zt(u)$ are measurement and its normal-score transformation at location u; F is cumulative distribution of $Z1$ and G is cumulative Gaussian distribution.

Once the transformation has been performed, the spatial variation of Zt-values can be quantified using so-called semivariance. The experimental semivariogram for a given lag vector h is estimated as:

$$\hat{\gamma}(h) = \frac{1}{2N(h)} \sum_{\alpha=1}^{N(h)} [Zt(u_\alpha) - Zt(u_\alpha + h)]^2 \qquad (6.2)$$

where $\hat{\gamma}(h)$ is semivariance, $N(h)$ is number of data pairs for given distance, and $Zt(u_\alpha)$ and $Zt(u_\alpha + h)$ are measurement at location u_α and at location $u_\alpha + h$.

When presenting the semivariogram, implicit assumptions of stationarity and isotropy were made. The semivariogram model was fitted to the experimental semivariogram using weighted least squares fit - $N/\{\hat{\gamma}(h)\}^2$, furthermore providing the input parameters for further kriging analysis (example in Figure 6.7).
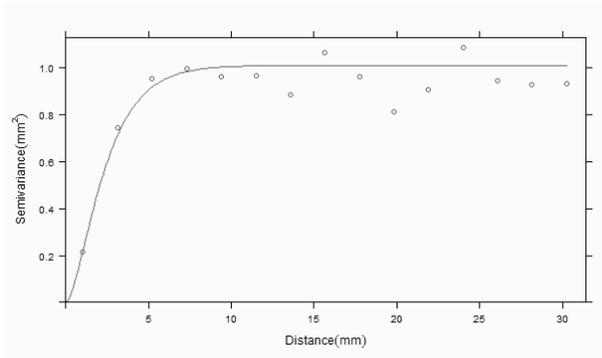
Figure 6.7: Semivariogram of the section of the sample from The Hague - P08. The circles represent the experimental semivariogram, and the black line indicates the fitted semivariogram model.

Ordinary kriging (OK) was applied to predict $\hat{Z}_{OK}(u)$ at unobserved location u using observation u_α as follows (Matheron, 1971):

$$\hat{Z}_{OK}(u) = \sum_{\alpha=1}^{n(u)} \lambda_\alpha(u) \cdot Zt(u_\alpha) \qquad (6.3)$$

The OK weights λ_α, are chosen such that $\sigma_E^2(u) = E\left[(\hat{y}(u) - y(u))^2\right]$ is as small as possible, under the unbiased condition $\sum_{\alpha/\beta=1}^{n(u)} \lambda_\beta = 1$.

Kriging, as statistical method, makes some assumptions; this particularly refers to the stationary one. A cross-validation prior to the OK was performed to ensure that assumption can be done. Due to high point density (around 700,000 points per sample) given OK estimation was carried out at each sample location using the 24 nearest neighbouring points (subjective choice), where nearest is defined by the distance of the spatial locations. The results of the cross-validation are given by standardised errors (Z-score) (Isaaks & Srivastava, 1989). The standardised errors Zt_{score}, were computed at each location (Eq. 6.4):

$$Zt_{score}(u) = \frac{\hat{Z}t(u) - Zt(u)}{\sigma_{OK}(u)} \tag{6.4}$$

where $Zt(u)$ is the best linear prediction based on observation $\hat{Z}t(u)$ and $\sigma_{OK}(u)$ is the corresponding OK prediction standard deviation.

If the mean value of Zt_{score} (Eq. 6.4) is close to zero and the normalised standard deviation is close to 1 the quality of information on local accuracy and of model is satisfied (Isaaks & Srivastava, 1989).

The OK results were back-transformed to produce the final original spatial distribution map (Deutsch & Journel, 1998). A back-transformation $Z2$ (Eq. 5) is achieved by applying the inverse of the normal score transform introduced in equation (6.1).

$$Z2(u) = F^{-1}\left[G(Zt(u))\right] \tag{6.5}$$

The back-transformation of the normal-score estimate $\hat{Z}_{OK}(u)$ is sensitive to errors in the interpolation process, especially when extrapolating for small and large value; therefore, the conditional distribution of the normal variable at any un-sampled location was simulated and back-transformed to the original $Z2$-value (Wu *et al.*, 2006).

Overall, the ordinary MG approach is straightforward and provides an unbiased estimation (Emery, 2006); and is theoretically less accurate than the conditional methods (*e.g.* indicator kriging). However, if the data are abundant, the results obtained with ordinary kriging are almost identical to results obtained with simple kriging, hence the results from ordinary MG are close to the optimal conditional expectation (Goovaerts, 1997).

6.3.2   *Spatial uncertainty analysis*

Insight in total elevation $Z2$ uncertainty and its propagation through space is crucial for further estimation of the hydraulic roughness. For the purpose of generating best predictions of the elevations MG is used. For the purpose of the uncertainty propagation analysis Monte Carlo method is more appropriate; the stochastic spatial simulations, using a conditional sequential Gaussian simulation, generate a multiple possible realities; where any of the simulated realities could be the true one (Goovaerts, 1997).
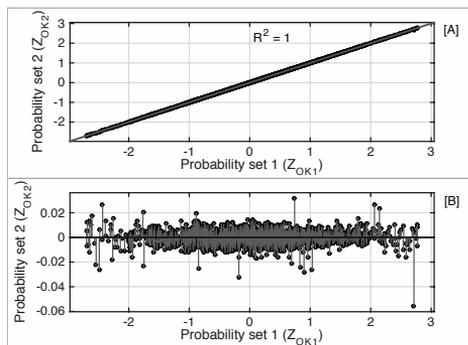
Figure 6.8: The probabilities of two independent Monte Carlo analyses: [A] scatter plot; [B] residual plot.

An empirical approach was used, based on an estimate of the coefficient of determination R^2, to analyse whether the number of Monte Carlo runs was sufficient to produce stable results

(Beekhuizen *et al.*, 2011; Oksanen & Sarjakoski, 2005). This was done by repeating the Monte Carlo uncertainty propagation analysis and by plotting the results from the first against those of the second analysis (Z_{OK1} vs. Z_{OK2}). When there are infinite numbers of Monte Carlo runs, the first and second analysis will possess high linear correlation ($R^2 = 1$). For finite number of runs the magnitude of the deviation may be visually inspected to verify whether the Monte Carlo results were sufficiently stable. The number of simulations was determined when a strong relationship between the two sets is established. For this study 500 runs were adoptedfrom, based on a subjective judgment; and a strong relationship is confirmed by the R^2 of the data sets of above 0.995 (example in Figure 6.8). The results of the 500 Z_{OK} runs were back-transformed to obtain the Z2. Finally, the spatial uncertainty σ_i, was quantified as the standard deviation of the Monte Carlo simulations.

6.3.3   *Estimation of the hydraulic roughness*

For this study the method proposed by Pegram and Pennington (1996) for linking hydraulic roughness to measured physical roughness of an irregular surface was adopted. In this analysis, Nikuradse's equivalent sand-grain roughness is assumed to be equal to the so-called mean range height of each roughness profile (X2, Z2-data). The mean range height is calculated by averaging the differences between maxima and minima within intervals of the centroidal wavelength of the profile. The Pegram and Pennington method is described hereafter.

A digital signal processing concept, the power spectrum, was used to analyse the raw physical roughness data and obtain a measure of an average, or representative, wavelength associated with the roughness. The power spectrum shows how the variance of the data is distributed over the frequency. The sample spectrum, for each of the data sets obtained, was calculated to determine the dominant frequencies and hence wavelengths. The sample spectrum $C_{xx}(\phi)$ for discrete cases is given by (Eq. 6.6)

$$C_{xx}(\phi) = \frac{\triangle}{N} \left| \sum_{t=-N}^{N-1} x_t e^{-i2\pi\phi t\triangle} \right|^2 \tag{6.6}$$

The logarithm of power spectrum is plotted against frequency - log spectrum, because the confidence interval remains constant on a logarithmic scale. The value of the total uncertainty σ_{tot} (Eq. 6.7) at the interpolated point is regarded as a Gaussian white noise. The noise is on average a constant value equal to the variance of the original signal.

Kriging is a statistical technique that quantifies the *error variance* at each point and thus its square root is the *standard error*. Consequently, the total uncertainty σ_{tot}, at the interpolated point is defined as:

$$\sigma_{tot} = \sqrt{\sigma_m^2 + \sigma_{in}^2} \tag{6.7}$$

where σ_{in} is spatial interpolation uncertainty obtained during kriging statistical analysis and σ_m is the measuring error under the assumption the two sources of uncertainty are mutually independent. The Gaussian white noise is plotted over the power and values greater than the white noise may be regarded as significantly different from white noise and thus representative for the further statistical analysis. Figure 6.9 shows the maximum sampling frequency that yields information of interest.

In order to determine the maximum sampling frequency that yields information of interest and avoid small variation within power density spectrum, the following smoothing technique was applied:
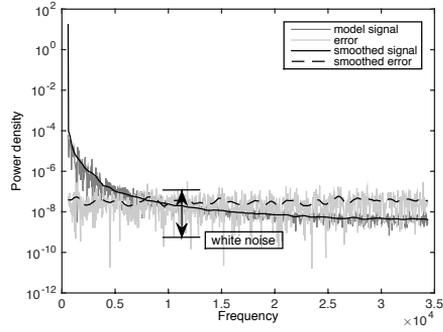
Figure 6.9: Example of power density spectrum.

$$C_{xx}(\phi_i) = \sum_{m=-h}^{h} \kappa(\phi_{i+m}, \phi_i) \cdot C_{xx}(\phi_{i+m}) \tag{6.8}$$

The kernel κ applied here was proposed by Hamilton (1994):

$$\kappa(\phi_{i+m}, \phi_i) = \frac{h+1-|m|}{(h+1)^2} \tag{6.9}$$

The kernel indicates how much weight is given to each frequency in the bandwidth h. A bandwidth of 15 frequencies was applied, based on the subjective judgment, which yielded a fairly smooth spectrum (see Figure 6.9).

In order to find the longitudinal spacing representative of the roughness, Pegram and Pennington (1996) developed the idea of the centroidal frequency, ϕ_c, which is found by calculating the centroid from the spectrum:

$$\phi_c = \frac{1}{\sigma^2} \int_0^{1/2} \phi C_{xx}(\phi) d\phi \tag{6.10}$$

where σ^2 is the variance of the data. In principle, a power spectrum gives the distribution of variance within the series with frequency.

This yields the centroidal wavelength, λ_c the representative interval between roughness projections of a rough surface *i.e.* (Eq. 6.10):

$$\lambda_c = \frac{1}{\phi_c} \tag{6.11}$$

The mean range height h_λ is calculated by averaging the differences between maxima and minima within intervals of the length - representative wavelength (Eq. 6.12-13).

That is, for a roughness profile *x(t)*, where $0 \leqslant t \leqslant T$ (T is number of points in the profile)

$$r_i = max\,[x_i, x_{i+\lambda_c}] - min\,[x_i, x_{i+\lambda_c}], 1 \leqslant i \leqslant T - \lambda_c \tag{6.12}$$

and

$$h_\lambda = \frac{1}{T - \lambda_c} \sum_{i=1}^{T-\lambda_c} r_i \tag{6.13}$$

It is finally assumed that the mean range height is equal to the sand grain roughness

$$k_s = h_\lambda \tag{6.14}$$

When sand-grain roughness k_s is known the Darcy-Weisbach friction factor f can be determined using Colebrook-White:

$$\frac{1}{\sqrt{f}} = -2\log 10 \left(\frac{k_s}{3.71 D_h} + \frac{2.51}{Re\sqrt{f}} \right) \tag{6.15}$$

where Re is Reynolds number and D_h is hydraulic diameter.

For hydraulically rough or fully-developed flow at high Re equation (6.15) reduces to:

$$\frac{1}{\sqrt{f}} = -2\log 10 \left(\frac{k_s}{3.71 D_h} \right) \tag{6.16}$$

Consequently, for a sewer pipe flowing full at high Re, Manning's coefficient n and Darcy-Weisbach f are related by:

$$n = R_h^{\frac{1}{6}} \sqrt{\frac{f}{8g}} \tag{6.17}$$

where g is acceleration due to gravity and R_h is hydraulic radius.

Once the Manning's n is calculated for samples from the invert, lateral and crown region of excavated pipe the composite roughness is calculated. For the sewer pipe the following Horton-Einstein (1934) equation is used:

$$n_e = \left(\frac{\sum p_i n_i^{\frac{3}{2}}}{\sum p_i} \right)^{\frac{2}{3}} \tag{6.18}$$

where n_e is equivalent Manning's coefficient of the pipe, and p_i and n_i are wetted perimeter and Manning's coefficient in each region i, respectively.

6.4 RESULTS AND DISCUSSION

Results of the geostatistical interpolation technique of kriging can be seen in Figure 6.10. The interpolation was conducted on the subsets of 0.2 mm width due to the very large spatial data set. The sand-grain roughness was calculated using the statistical analysis of roughness as proposed by Pegram and Pennington (1996). The results of the mean sand-grain roughness and mean total uncertainty for the all samples are presented in Table 6.1. It can be seen from the Table 6.1 that calculated mean roughness of the validation sample is identical to the actual mean surface roughness of 5.5 mm. Further, the friction factor f was calculated from equation (6.16)
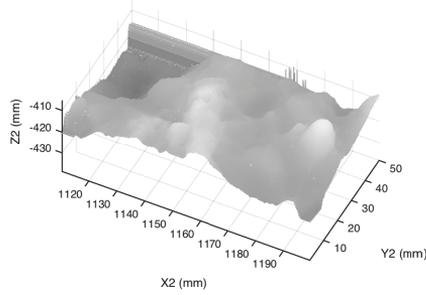
Figure 6.10: Results obtained by spatial interpolation of the sample from The Hague - P08. Photo of this sample can be seen in Figure 6.2.

Table 6.1: The mean sample sand-grain roughness and uncertainty.

Sample	k_s (mm)	σ_{tot} (mm)
Validation	5.33	1.06
New pipe	0.54	0.07
Breda (P02) pipe		
invert	0.53	0.13
lateral	1.48	0.05
crown	0.95	0.05
Breda (P06) pipe		
invert	0.54	0.03
lateral	0.94	0.04
crown	1.10	0.03
The Hague (P08) pipe		
invert	0.89	0.11
lateral	1.50	0.05
crown	9.93	0.32
The Hague (P10) pipe		
invert	0.76	0.09
lateral	1.44	0.06
crown	12.74	1.62

and compared with friction factor that was determined from hydraulic measurements of Ali and Uijttewaal (2012). The difference between these two friction factors is in order of 1.4% (within the uncertainty range), implying that the applied methodology is consistent with a proved method.

Results show that the local roughness varies with the location of the samples. The calculated values for the physical roughness of the samples from the invert region resemble the roughness value of the new pipe. The highest roughness values are found in the pipe crown region making this region important from the perspective of a pipe capacity. Probably due to sulphuric acid attack, carbonation and other deteriorate processes over the years, the pipes investigated show non-uniform deterioration, resulting in wide range of values for hydraulic roughness. Furthermore, the estimated total uncertainties are small for the calculated roughnesses. The value of the uncertainty depends on the surface characteristics. The higher the elevation deviation between the neighbouring points in space will generate higher uncertainty in the calculation.

In order to evaluate n Manning's coefficient for all the pipe samples equation (6.17) was used; while the Manning's coefficient of the whole pipe ne is estimated using equation (6.18). The sewer

Table 6.2: The sample Manning's n.

Sample	n	n_e
New pipe	0.0115	0.0114
Breda (P02) pipe		
invert	0.0120	
lateral	0.0129	0.0124
crown	0.0120	
Breda (P06) pipe		
invert	0.0109	
lateral	0.0122	0.0121
crown	0.0123	
The Hague (P08) pipe		
invert	0.0117	
lateral	0.0132	0.0149
crown	0.0177	
The Hague (P10) pipe		
invert	0.0114	
lateral	0.0135	0.0155
crown	0.0187	

pipe cross-section was divided in three regions to determine their hydraulic radiuses R_h (Figure 6.11). In Table 6.2 the results of the calculations are presented. Results show that the hydraulic roughness for the new pipe is in the expected range. Further, the results suggest that n_e for pipes of the same origin is in the same order of magnitude, thus implying that it may be possible to estimate the single Manning's coefficient for deteriorated concrete sewer. This is only valid under the assumption that the pipes have deteriorated in the same manner. In reality this is usually not the case. The value of n is affected not only by the friction factor but also by the hydraulic radius therefore by the pipe interior geometry. Information on the exact pipe interior geometry will contribute to a more accurate estimate of the hydraulic roughness.
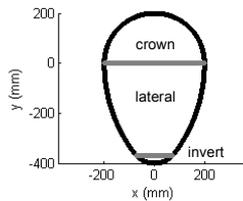
Figure 6.11: Regions of different roughness of deteriorated concrete sewer pipe.

Finally, the sensitivity analysis on the validation sample was carried out to determine the minimal scanning resolution required to obtain useful results by decreasing the spatial resolution c_i. The size of the data subsets remained the same and is 0.2 mm. Figure 6.12 shows the boxplot of the calculated sand-grain roughness over the validation sample cross-section. With a decrease of the spatial resolution - $c_i = V_f/V_i$, the individual roughness of subset deviation increases. A lack of data points leads to an underestimation of the median with increasing uncertainty. With averaging over the whole width that effect is diminished. While looking at the boxplot it can be noted that with decrease of resolution up to 5 times (from 0.01 mm to 0.05 mm) there is hardly any change of the median k_s values. With the subset width (SW) of 0.2 mm and a reduction of the point density of 100 times the limit of the application of this method is reached. Friction factors were calculated using mean sand-grain roughness k_s for the validation sample over the

cross-section. Also, the uncertainty was quantified. Figure 6.13 shows the results of the statistical analysis.
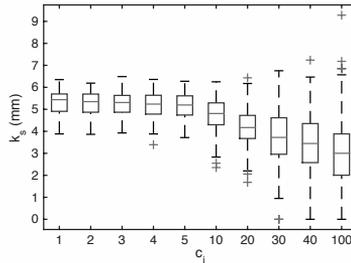
Figure 6.12: Boxplot of the calculated sand-grain roughness for the validation sample over the cross-section. On each box, the central mark is the median, the edges of the box are the 25th and 75th percentiles, the whiskers extend to the most extreme data points not considered outliers (approximately $\pm 2.7\sigma$), and outliers are plotted individually.
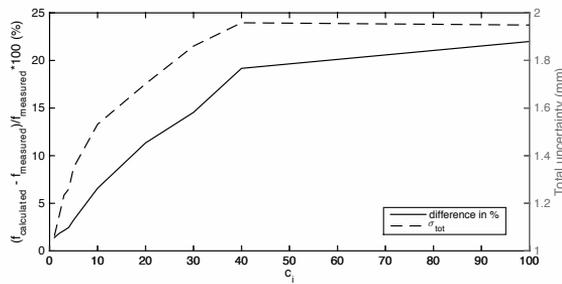
Figure 6.13: Effect of the decreased spatial resolution on the estimation of friction factor for the validation sample. The x-axis presents the decrease of spatial resolution. The left-hand y-axis presents the difference in % between the calculated and measured f and the right-hand y-axis is the total uncertainty of the calculated values.

The results suggest that a decrease of spatial resolution up to 7 times yields a friction factor that differs only 5% from the measured one. This refers to the case when the $SW = 0.2$ mm. The calculation uncertainty does not increase significantly with a decrease of spatial resolution. This can be explained from the fact that the behaviour of the variogram 'near the origin' stays the same with the change of resolution thus not altering significantly the kriging predictions (Cressie, 1988).

Further sensitivity analysis concentrated on studying the effect of the increase of the data subset width (Figure 6.14) on the estimation of friction factor when the spatial resolution is decreased 100 times. The obtained results suggest (Figure 6.15) that with an increase of the subset width ($SW > 1$ mm) the estimation of the friction factor inclines towards the measured one.

Table 6.3 shows the Manning's n obtained using full spatial resolution ($SW = 0.2$ mm) and using decreased resolution of 100 times ($SW = 2$ mm) for the first pipe from The Hague. It can be seen that ne equivalent Manning's of the pipe are identical. Overall, it is concluded that the lasers scanning techniques with a lower resolution, like laser profiling can be applied in practise for *in situ* measurement of the hydraulic roughness of deteriorated concrete sewer pipe.

When the studied sample resolution was reduced up to 200 and 400 times (distance between points 2 and 4 mm) it resembled the laser profiler conditions. The examples of this roughness
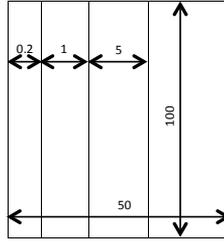
Figure 6.14: Sample size and subsets in mm.
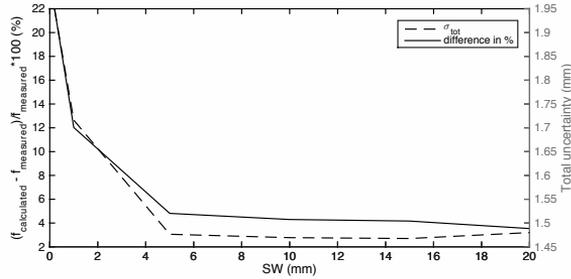
Figure 6.15: Effect of the increase of the data subset width on the estimation of friction factor for the validation sample. The x-axis presents the increase of the subset width. The left-hand y-axis presents the difference in % between the calculated and measured f and the right-hand y-axis is the total uncertainty of the calculated values.

Table 6.3: Manning's coefficients - full spatial resolution vs. decreased resolution.

The Hague (P08) pipe					
$c_i = 1$, $SW = 0.2$ mm			$c_i = 100$, $SW = 2$ mm		
sample	n	n_e	sample	n	n_e
invert	0.0117		invert	0.0116	
lateral	0.0132	0.0149	lateral	0.0132	0.0149
crown	0.0177		crown	0.0178	

analysis are given in Table 6.4. The results show that with an increase of the SW to 5 mm an almost identical n_e compared to the full resolution one was calculated. This confirms the capacity of the studied method for application in conjunction with a laser profiling technique to determine hydraulic roughness.

Table 6.4: Manning's n for the resolution resembling the resolution of the laser profiler.

The Hague (P08) pipe		
sample	n	n_e
invert ($c_i = 200$, $SW = 5$ mm)	0.0117	
lateral ($c_i = 200$, $SW = 5$ mm)	0.0133	0.0150
crown ($c_i = 400$, $SW = 5$ mm)	0.0179	

The largest part of the total uncertainty is associated with the measuring uncertainty. When the surfaces $k_s > 10$ mm, the interpolation uncertainties may increase significantly if the elevation between the neighbouring measured points is high. In conclusion, the measuring accuracy should

be, in this case, around 0.5 mm (at least 50% less than k_s) for the invert and lateral region ($k_s \leqslant$ 2 mm), otherwise it could be regarded that the results of the roughness are unreliable. In the case of the crown region ($k_s > 10$ mm) of the measuring uncertainty of 3 mm will not yield the results which are unreliable. Overall, it is important that the uncertainty of the analysis is limited ($\sigma_{tot} \leqslant k_s \cdot 30\%$) in the regions with higher roughness because they most affect the hydraulic resistance. In practise the initial estimation of the physical roughness can be obtained using a low-resolution laser scanning technique.

Knowing the friction factor f, the pipe hydraulic diameter D_h, length of the conduit L and the average flow velocity $\overline{v}$, the head loss h_f may be calculated using the Darcy-Weisbach head loss equation:

$$h_f = f \cdot \frac{L}{D_h} \cdot \frac{\overline{v}^2}{2g} \tag{6.19}$$

For example, if it is assumed that the sewer section (length between two manholes) is 60 m, the flow velocity is 1 m/s and different egg-shaped pipe dimensions then the hypothetical head losses can be calculated. In addition, if it is assumed that the full pipe flow, the equivalent friction factor f_e can be calculated from known n_e using equation (6.17). The obtained results (Table 6.5) show that the friction resistance increases with an increase of the roughness. However, with an increase of the hydraulic diameter roughness has a decreasing impact on the estimation of the head loss values. This can be clearly seen in the equation (6.19).

Table 6.5: Effect of the friction factor and the hydraulic diameter on the head loss.

Dimension (mm)	h_f (m)				
	New (P01) pipe	Breda (P02) pipe	Breda (P06) pipe	The Hague (P08) pipe	The Hague (P10) pipe
300/450	0.200	0.232	0.221	0.335	0.363
400/600	0.136	0.158	0.151	0.228	0.247
500/750	0.101	0.118	0.112	0.170	0.184
700/1050	0.065	0.075	0.071	0.108	0.117
1000/1500	0.040	0.047	0.044	0.067	0.073
1200/1800	0.031	0.037	0.035	0.053	0.057
1600/2400	0.021	0.025	0.024	0.036	0.039

6.5 CONCLUSIONS AND PERSPECTIVE

Laser scanning offers a new and challenging perspective for measuring structural characteristics of a sewer pipe, such as physical roughness. Information on hydraulic roughness will extend and improve the quality of existing system condition information on which rehabilitation and maintenance decisions can be based.

For the deteriorated concrete pipe surfaces a low-resolution laser scan is able to measure physical roughness and consequently the hydraulic one. The more sewer pipe surfaces are deteriorated, the more feasible the application of a lower resolution laser becomes. For highly deteriorated regions ($k_s > 6$ mm), which have the highest influence on the hydraulic resistance, it is essential to strive for a lower uncertainty ($\sigma_{tot} \leqslant k_s \cdot 30\%$) in the analysis. On the other hand, to avoid the unreliability of the results it should be strived for a maximum acceptable uncertainty $\sigma_{tot,max} \approx k_s \cdot 50\%$ for the regions with lower roughness. Overall, this gives an opportunity to the laser profiling as a technique for *in situ* determination of the hydraulic roughness of the sewer pipes. Laser profilers have shown to be capable of measuring the pipe interior and quantify wall losses, with a potentially high enough accuracy (see, *e.g.* Clemens *et al.*, 2015). The combination of the two methods, *i.e.* to use the laser profiler to determine the pipe interior geometry as well as to identify representative patches where roughness should be measured, is an opportunity to strengthen laser profiling as a method that may partially replace a CCTV inspection as a dominantly applied sewer investigation technique. Ergo, it will provide an input for the hydrodynamic

sewer models thus enabling an accurate estimation of actual hydraulic characteristics and thus may serve as a basis for a sewer asset management based on actual functionality.

It has to be acknowledged that the overall hydraulic losses of a stretch of sewer pipes is determined by more factors than just the wall roughness of the individual pipes; among others, protruding lateral connection, displaced joints, local losses at manholes can contribute significantly as well. Potentially laser scanning combined with pattern recognition may provide information on these factors as well. Future research will address these options.

7

A NEW SEWER PIPE INSPECTION TECHNOLOGY

In chapters 4-6 conclusions were drawn on the potential of the laser profiling for measuring structural characteristics (*e.g.* interior geometry, physical roughness) that provide information on the structural and hydraulic performance of the sewer pipes. This may be achieved by further improving the laser profiling technique (Prototype v1.0) presented in Chapter 4. In this chapter the design of the improved laser profiling technique is described in detail, thus providing relevant feedbacks on device accuracy, laser alignment and a synchronisation of acquisition systems. Furthermore, the results of a series of laboratory experiments using the laser-profiling device are presented.

In the first section of the chapter a detailed design and drawings of the measuring set-up are presented (Prototype v2.0), while in the second section the mathematics and protocols behind the issues of the sensor calibration and misalignment as well as the data processing method are presented. The third section presents the initial results in order to demonstrate the accuracy of the proposed apparatus. The fourth section presents the extensive experimental results and discusses the potential and limitation of the application, followed by the concluding remarks and recommendations for further improvements.

7.1 APPARATUS DESIGN

The main goal of the laser profiling technique is to inspect linear infrastructures (as sewers) along the reach; limited by the maximum distance measurable by the laser distance meters or by a new direction of the pipe. The apparatus was designed and built to determine the position of the device (x, y and z), rotation (pitch θ_x, yaw θ_y and roll θ_z) and to ensure high accuracy results. A left handed coordinate system is applied, while the rotation angles are defined following the Tait-Bryan formalism (Figure 7.1). To avoid the limitation of the cables in practical application (*i.e.* unexpected disconnection, cable length limitation, cleaning and damaging of the cables and connectors) the system (Prototype v2.0) was divided into two individual parts: a fixed one with laser probes and a moving one with the laser profiler and cameras (Figure 7.2).
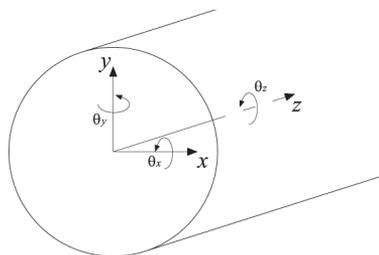
Figure 7.1: Left-handed coordinate system and definition of the Tait-Bryan angles.

This chapter is based on: Stanić, N., Lepot, M., Catieau, M., Langeveld, J. G., & Clemens, F. H. L. R. (2015). A new and collaborative technology for sewer pipe inspection (Part 1): design, calibrations, corrections and potential application of a laser profiler. *Automation in Construction*: under review.
Lepot, M., Stanić, N., & Clemens, F. H. L. R. (2015). A new and collaborative technology for sewer pipe inspection (Part 2): assessment of robustness and accuracy in laboratory. *Automation in Construction*: under review.
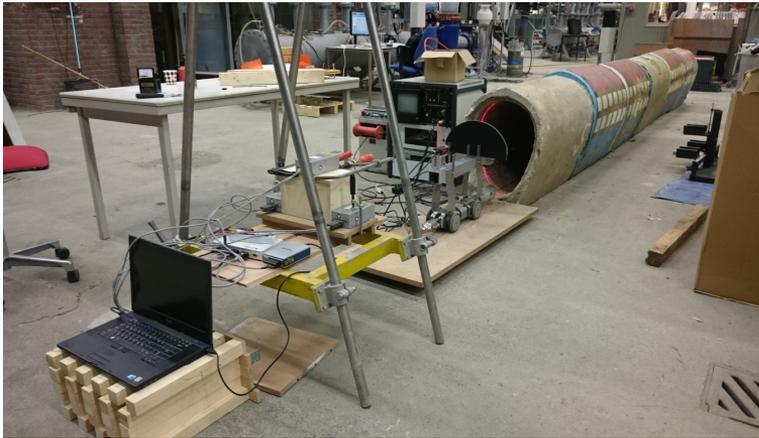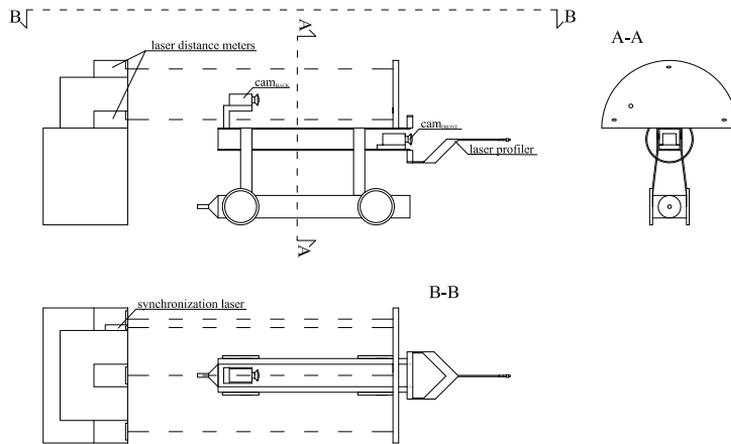
Figure 7.2: The experimental set-up: Sketch (top) and Photograph (down).

The set-up consists, like for the ordinary laser profiling technique, of a laser profiler (Ibak, ILP) combined with a camera (Allied Vision Technology, Prosilica GT3400C), referred to as cam_{FRONT}. The laser profiler uses a reflecting cone to project a laser sheet on the inner pipe wall, creating a line perpendicular to the profiler and thus the moving platform of the apparatus, which is captured by the cam_{FRONT}.

The fixed platform of the set-up consists of the three laser distance meters (Dimetix, FLS-C10) each measuring the distance between the parallel lasers and the reflection board mounted on the moving part. The lasers point at the reflection board mounted on the moving platform of the apparatus thus acquiring the information on the positions (z) and rotation angles (θ_x and θ_y). A second camera (Allied Vision Technology, Manta G-282C), referred to as cam_{BACK} and fixed on the moving part, records the position of the three points projected by the parallel lasers on the reflection board. Applying image processing technique and ellipse fitting the x and y location of the centre of the points (in sensor coordinates) is derived; thus acquiring the remaining information on the positions (x and y) and rotation angle (θ_z) (the associated mathematical concept is described in Chapter 4).

The three laser distance meters (on the fixed platform), two cameras and a projected laser (on the moving platform) are the main parts of the first design: additional details and photos have been given in (Clemens *et al.*, 2015). This previous study highlights the reliability of the laser profiling technique and the need of more accurate sensors *i.e.* laser distance meters, higher camera resolutions. The new version tries to tackle these disadvantages by implementing the following improvements (Table 7.1): (*i*) new cameras, (*ii*) adjustable positions of cameras, (*iii*) new laser distance meters and (*iv*) two data acquisition systems optically synchronized (Figure 7.3).
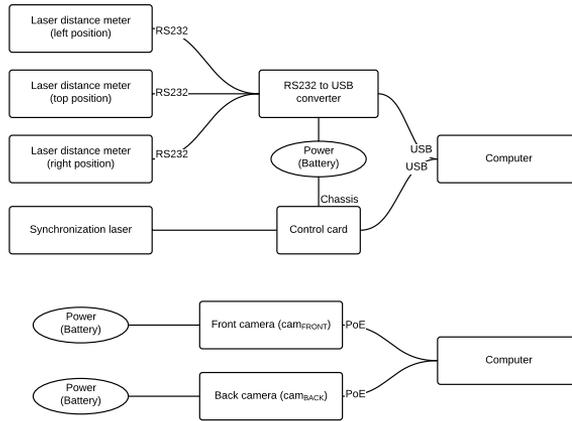
Figure 7.3: Data acquisition systems set up on the device: fixed (top) and moving (down) platform.

Moreover, to properly assess the geometry of the pipe, both data acquisition systems have to be perfectly synchronized. What should be emphasized is that synchronisation between parts for the first version of apparatus was not needed due to the fact that fixed and moving platforms were connected to the same computer thus same internal clock. In the new design it was decided to avoid synchronisation by cables since these are not reliable because of mechanical stresses during the operation, therefore another form of synchronisation between the two data acquisition systems has to be implemented (Figure 7.3). The synchronization was ensured with the 4th laser (Osela, Streamline laser (660 nm)), behaving like a pulse laser (through a bijective time series On-Off), on the fixed platform recorded by the back camera (Figure 7.4); both system clocks could be lagged with an accuracy due to light travel duration (negligible). Overall, the wireless synchronization was achieved. Table 7.1 highlights the main improvements between the two prototypes.
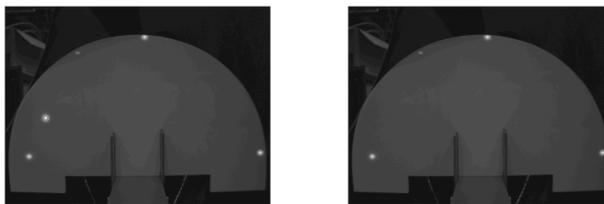
Figure 7.4: View from cam_{BACK} in the right picture the three dots projected by the laser distance meters can be seen, while on the left picture (frame taken 0.083 s later) a fourth laser dot, the pulsed laser, is visible. Synchronization using the fourth laser: frame captured at 3.5 s (left) and at 3.583 s (right).

Table 7.1: 1st vs. 2nd version of the laser profiling technique.

Elements of comparison	Prototype v1.0 (Clemens et al., 2015)*	Prototype v2.0 (this chapter)
Wires between parts	Yes	No
Camera position adjustments	No	Yes
Synchronization between parts	No need	Yes (wireless)
Laser accuracy (σ in mm)	2	0.5
Resolution of cam_{FRONT}	1 MPix	9 MPix
Pixel size of cam_{FRONT} (μm)	2.8×2.8	3.69×3.69
Resolution of cam_{BACK}	1 MPix	2.8 MPix
Pixel size of cam_{BACK} (μm)	2.8×2.8	3.69×3.69
Cost (materials only, in euros)	2,000	30,000

* the cam_{FRONT} same as cam_{BACK}

7.1.1 The fixed platform

This part is basically a platform on which four lasers are fixed: three laser distance meters to assess positions and rotation angles; and a pulsed laser to ensure an optical synchronization through a known sequential time series between data acquisition systems located on both platforms. The distances between the three lasers distance meters on the fixed platform were determined using a program written in Matlab® to calculate the apparatus optimal settings for a given set of sewer dimensions, accuracy in distance metering and geometrical properties of the set-up.

LabVIEW was used for data acquisition and control of the four laser sensors. Communication between three accuracy lasers and computer was achieved using the converter RS232-USB (National Instrument, USB-232/4). Further, the pulse laser was controlled using the USB Chassis (National Instrument, cDAQ-9171) and the card (National Instrument, NI 9472). One battery of 11.1V (Robbe, Roxxy® 3S/5000 mAh) was used as power supply for the lasers of the fixed part. The battery needs to be replaced after eight hours of continued usage to avoid a deep discharge and decrease of the battery life.

7.1.2 The moving platform

This part consists of a rectangular aluminium platform fixed on the CCTV camera. Two cameras with lenses were placed and fixed on it: one in front of the platform (cam_{FRONT}) and another one at the back (cam_{BACK}). Furthermore, the back camera is looking directly at the white-reflective-plastic-board in order to increase measuring rate (suggested by manufacturer (Dimetix FLS-C10 Technical Reference Manual V5.02)). The lenses for the cameras were chosen according to minimum of mean pixel error values, the lowest distortion and the expected size of object of interest.

Synchronization of cameras and data recording are ensured by a computer (Apple, Mac Pro 2013) and Matlab® code that initialises the camera recordings simultaneously. A battery of 22.2V (Pichler, Lemon RC 6S/4400 mAh) provides energy supply for approximately four hours of continuous usage.

7.1.3 Accuracy of laser distance meters

Multiple measuring characteristics are available in the Dimetix, FLS-C10 laser measuring device, found in manual, to meet different requirements for various applications (Dimetix FLS-C10 Technical Reference Manual V5.02). For the apparatus purposes of high accuracy the laser distance meter device is set to precise measuring characteristics, i.e. (max.) measuring rate of 6 Hz, confidence interval of ±0.8 mm (Dimetix FLS-C10 Technical Reference Manual V5.02). The measurement accuracy by the producer (Dimetix) corresponds to the ISO-recommendations ISO/R

1938-1971 (International Organization for Standardization, 1971) with a confidence interval of 95.4% (4σ). In order to assess the uncertainties as a function of distance, for each laser repetitive measurements (circa 1000 times) were carried out at distances of 1, 2. . . 30 m (Figure 7.5). With precise measuring settings the recorded accuracy was higher than that recorded by the manufacturer - until 15 m distance the σ is 0.05-0.19 mm. The results for the right laser deviate from the results of the left and top laser probably due to the airflow velocity *i.e.* the disturbance during measuring.

(a)

(b)

(c)
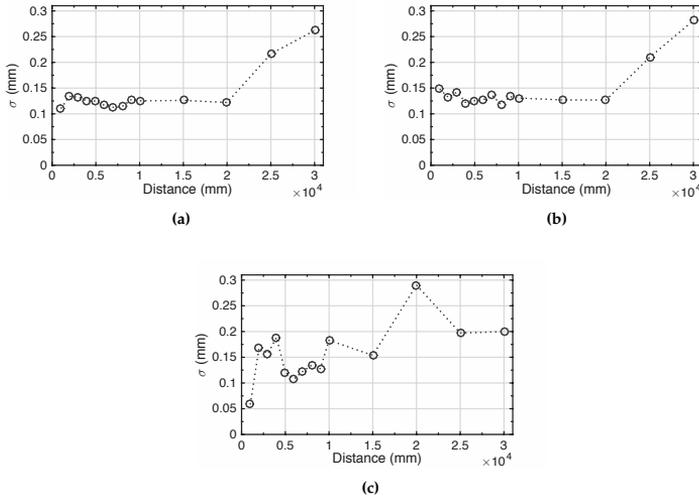
Figure 7.5: Standard deviation of distance measurement for: (a) left laser; (b)] top laser; (c) right laser.

7.1.4 *Accuracy of camera sensors*

The uncertainty of the 2D projection of the wall of the pipe is quantified using the average number of pixels that are illuminated on the sensor of cam_{FRONT}, depending on the scale factor, defined by the ratio between the distance between the laser sheet and the lens and the distance between the lens and sensor plane. The sensor used in cam_{FRONT} is a 1" sensor with 3384 $\times$ 2704 pixels, pixel dimensions are 3.69 μm $\times$ 3.69 μm. Based on an analysis of 20 repetitive samples in 20 different video frames, in which the measuring system was stationary, all rotation angles were equal to zero and the camera positioned in the axis of the conduit revealed that the laser sheet illuminated about 7-8 pixels. Figure 7.6 shows the results of the distribution of the recorded light intensity across the projected line on the camera sensor. Based on these experiments, the standard deviation in the position was estimated to be $\sigma_{x,y,cam_{FRONT}} = 7.3$ μm. Furthermore, the sensor of cam_{BACK} is a 1/1.8" sensor with a resolution of 1936 x 1458 pixels with a pixel width of 3.69 μm $\times$ 3.69 μm, resulting in estimated standard deviation of $\sigma_{x,y,cam_{BACK}} = 7.3$ μm, same as in the case of the cam_{FRONT}.

7.2 APPARATUS CALIBRATION: PROTOCOLS APPLIED AND DATA PROCESSING

All the mathematical backgrounds and tools used in this study are in detail presented in this part and organized as follows (Figure 7.7).

The first step (top line) consists of an independent calibration of all the devices on both platforms: cameras and laser distance meters. Further, both uncertainties in apparatus construction
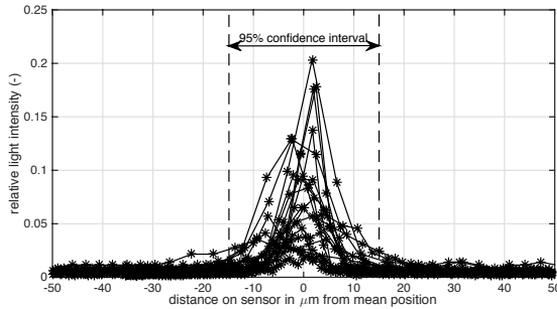
Figure 7.6: Distribution of the light intensity on the sensor of cam_{FRONT}.
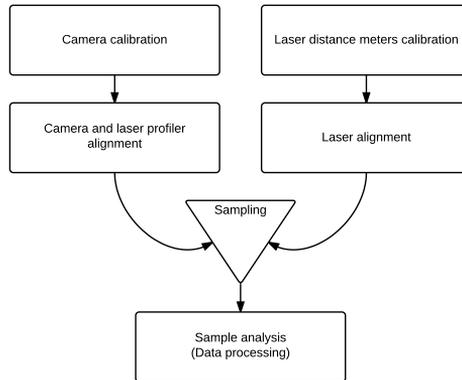
Figure 7.7: The schematic diagram of the experimental protocol.

and in distance meters assembly create misalignments of laser sensors, cameras and laser profiler that can lead to biased and inaccurate results (Clemens *et al.*, 2015). Cameras and laser profiler were easily aligned on the moving platform of the apparatus. The laser alignment protocol is described hereafter in the second step. These important issue were not addressed by Clemens *et al.*, (2015).

7.2.1 *Camera calibration*

Image distortion is caused by either the position of the camera in relation to the subject and/or a lens construction. For each frame recorded by both cameras, the exact position and orientation of this camera should be known; therefore, for each frame, the positions of the three laser points projected on the reflection board have to be known. Further, lens distortion can heavily distort features around the image border making them difficult to detect. To overcome this problem the image can be undistorted as if an idealized camera is being used. Calibrating the cameras and correcting for the distortions can accomplish this. The measurement of distances in a real world from their projections on the image plane becomes possible with proper camera calibration protocols (Faugeras, 1993; Salvi *et al.*, 2002). In this process the internal camera geometric and optical characteristics are determined - intrinsic parameters of camera; as well as the 3D position

and orientation of the camera frame relative to a certain world coordinate system - extrinsic parameters of camera are determined (Tsai, 1987).

Salvi *et al.*, (2002) present a detailed review of some of the most applied calibrating techniques; showing that the accuracy of non-linear methods (*e.g.* Tsai optimised and Weng two-step methods) on the image plane is superior to linear calibration methods. Heikkila and Silvén (1997) present a four-step calibration method that is an extension to the two-step procedure. This technique is most beneficial in camera based 3D measurement and in robot vision, where high geometrical accuracy is needed. This calibration method is incorporated in the standard Matlab$^{\circledR}$ toolbox, which was used for calibrating the cam_{FRONT} and the cam_{BACK} and for selecting the most suitable lenses for the cameras.

Further, due to the construction processes and geometry, the camera-lens combinations create some additional deformations like a reduction of an image's brightness or saturation at the periphery compared to the image centre (vignetting) and chromatic errors. These aberrations are specific to each camera - lens combination and vary with the aperture and focal length. In this study, camera calibration efforts have focused only on the distortion while vignetting and respectively chromatics errors were neglected due to the almost circular section of sewer pipes and respectively the insensitivity of the data processing to vignetting and chromatic errors (since the light from the lasers can be regarded as monochromatic).

The camera calibration protocol is broken down into steps (Figure 7.8).
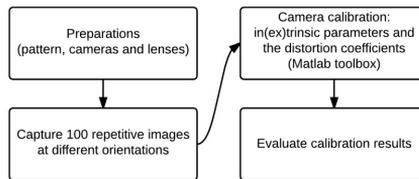
Figure 7.8: Schematics of the camera calibration protocol.

The first step was to prepare a rigid flat and smooth plastic surface with a checkerboard pattern (chessboard square size of 40 mm). Three Kowa lenses, (LM3NCM, LM4NCM and LM6HC) were tested one by one for each camera. When the lens was placed the camera was focused and the light intensity was adjusted for the selected lens aperture. The second step was to take 100 repetitive images for each camera-lens-aperture of the target-board at 9 different orientations (all possible combinations of -15, 0, +15 degrees around horizontal - left and right - and vertical - up and down - axes). Finally, images were loaded and camera was calibrated using the Matlab$^{\circledR}$ Single Camera Calibration App.

The camera calibration procedure estimates the values of the intrinsic and the extrinsic parameters, and the distortion coefficients. In the first step the intrinsic and extrinsic parameters were estimated in closed form, assuming that the lens distortion is 0 (Zhang, 2000). Further, all parameters were simultaneously estimated, including the distortion coefficients by application of a nonlinear least-squares minimization (Levenberg-Marquardt algorithm (Marquardt, 1963)). The closed-form solution was used from the preceding step as the initial estimate of the intrinsic and extrinsic parameters, assuming that the initial estimate of the distortion coefficients is 0 (Heikkila & Silvén, 1997; Zhang, 2000).

The calibration method assumes a pinhole camera model:

$$w \begin{bmatrix} x \\ y \\ 1 \end{bmatrix} = \begin{bmatrix} X & Y & Z & 1 \end{bmatrix} \begin{bmatrix} R \\ T \end{bmatrix} K \tag{7.1}$$

where X, Y, Z are world coordinates of a point; x, y are image coordinates of the corresponding image point in pixels; R matrix (3 × 3 matrix) represents the 3D rotation of the camera; T is translation (1 × 3 vector) of the camera relative to the world coordinate system; w is arbitrary homogeneous coordinates scale factor. Without loss of generality, it is assumed the model plane is on Z = 0 of the world coordinate system (Zhang, 2000); thus reducing the matrices in the equation (7.1).

While K is camera intrinsic matrix, defined as:

$$K = \begin{bmatrix} f_x & 0 & 0 \\ s & f_y & 0 \\ c_x & c_y & 1 \end{bmatrix} \tag{7.2}$$

where coordinates c_x, c_y represent the optical centre (the principal point), in pixels. When the x and y axis are exactly perpendicular, the skew parameter, s, equals 0. The parameters $f_x = F \cdot s_x$ and $f_y = F \cdot s_y$ represent the focal length in terms of pixels, where s_x and s_y are the number of pixels per world unit in the x and y direction respectively and F is the focal length in terms of distance. The information from the intrinsic matrix obtained during the camera calibration was used to determine image scaling factor.

Further, the distorted points $x_{distorted}$, $y_{distorted}$ and their radial (Eq. 7.3) and tangential (Eq. 7.4) distortion coefficients of the lens are denoted as k_1, k_2, k_3, p_1, p_2:

$$\begin{cases} x_{distorted} = x \cdot (1 + k_1 \cdot r^2 + k_2 \cdot r^4 + k_3 \cdot r^6) \\ y_{distorted} = y \cdot (1 + k_1 \cdot r^2 + k_2 \cdot r^4 + k_3 \cdot r^6) \end{cases} \tag{7.3}$$

$$\begin{cases} x_{distorted} = x + [2 \cdot p_1 \cdot y + p_2 \cdot (r^2 + 2 \cdot x^2)] \\ y_{distorted} = y + [p_1 \cdot (r^2 + 2 \cdot y^2) + 2 \cdot p_2 \cdot x] \end{cases} \tag{7.4}$$

where x and y are undistorted pixel locations, $x_{distorted}$ and $y_{distorted}$ are distorted pixel locations, $r^2 = x^2 + y^2$, k_1, k_2 and k_3 are the radial distortion coefficients of the camera-lens for given aperture and p_1 and p_2 are the tangential ones.

The calibration accuracy was evaluated by examining the re-projection errors - the distances in pixels between the detected and the re-projected points. Based on the obtained values of radial, tangential distortion, skew and mean re-projection error, the best camera-lens-aperture combination was selected for the apparatus.

7.2.2 *Laser distance meters calibration*

The three laser distance meters are calibrated using the ordinary least squares method. Monte-Carlo simulations are used to estimate the regression coefficients, their standard uncertainties (same as the one in Fig. 7.5) and covariance between them (in a similar manner as (Bertrand-Krajewski, 2008)). The calibration is carried out for distances of 1 to 30 m and it can be described with the Eq. (5-6).

$$M = b_0 + b_1 \cdot A \tag{7.5}$$

$$\sigma^2(A) = \frac{\sigma^2(M)}{b_1^2} + \frac{\sigma^2(b_0)}{b_1^2} + \frac{\sigma^2(b_1) \cdot (M - b_0)^2}{b_1^4} - 2 \cdot cov(b_0, b_1) \cdot \frac{(M - b_0)}{b_1^3} \tag{7.6}$$

where M is a measured value; A is a true value for the measured distance; b_0 and b_1 are the estimated regression coefficients.

7.2.3 *Laser alignment*

The alignment of the lasers is determined on a 10 m long distance calibration bench. The lasers are installed on a fixed controlled carriage at one end of the bench and a flat PVC board perfectly perpendicular to the bench was installed on the fixed location at the other end. On the board the exact position of the laser distance projection points were carved in. The positions of the lasers were adjusted until the moment when all the laser distances were the same and the projections were positioned in the centre of printed points on the board. These results were validated by repeated measurement on a distance of 1 m. The uncertainty of laser alignment is determined by repeated measurement of the distance between the three projected points at a distance of 10 m.

7.2.4 *Data processing*

Processing of raw data consists of five steps as follows (Figure 7.9).
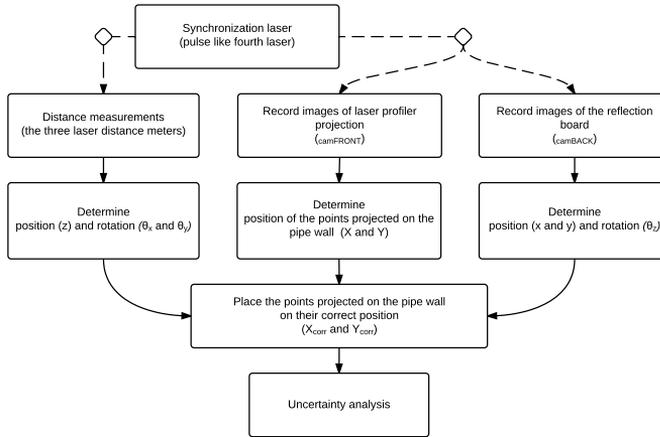
Figure 7.9: Data processing flow chart.

The methods and the mathematics applied in the data processing are addressed and published in Clemens *et al.*, (2015). A few improvements and modifications, however, were addressed in this study. The method is described in detail in Chapter 4. The only thing that was done differently within the method is the calculation of the scaling factor for the cam_{FRONT} and the cam_{BACK}. Scaling factor ($s_{x,y,BACK}$, $s_{x,y,FRONT}$) was determined based on the information from the intrinsic matrix obtained during the camera calibration. The intrinsic matrix parameters represent focal length (f_x and f_y) in terms of pixels (Eq. 7.2); and for the known pixel size ($pixel$) and distance between the pattern board and camera ($d_{z_{BACK}}$) it was possible to determine the value of the s_{BACK} which has components in x and y direction (Eq. 7.7). The s_{FRONT} was calculated in the same manner where distance between cam_{FRONT} and the laser sheet on the z-axis in the reference coordinate system.

$$\begin{cases} s_{x_{FRONT}} = \frac{d_{z_{FRONT}}}{f_x \cdot pixel}, & s_{x_{BACK}} = \frac{d_{z_{BACK}}}{f_x \cdot pixel} \\ s_{y_{FRONT}} = \frac{d_{z_{FRONT}}}{f_y \cdot pixel}, & s_{y_{BACK}} = \frac{d_{z_{BACK}}}{f_y \cdot pixel} \end{cases} \tag{7.7}$$

The method presents the calculation up to the construction of the 3D image of pipes and its uncertainties. Subsequent steps to calculate parameters or characteristics of a pipe are described

in second paper devoted to application examples (*e.g.* of roughness assessment in Stanić *et al.*, 2015; Stanić *et al.*, 2013b).

7.3   ACCURACY OF THE APPARATUS

The experiments were performed in the laboratory to: (*i*) assess the accuracy of the new set of components (cameras, lenses, and laser distance meters) and (*ii*) to obtain examples of the possibilities and limitations of the new version of the apparatus. For the experimental purposes five egg-shaped concrete deteriorated sewer pipes of 600/400 mm were placed one after the other (see Figure 7.2). Furthermore, for the experiments was adopted the experimental distance limit of 10 m.

Specifications and standard uncertainties (obtained by repeated measurement) of the instrumentation applied are summarised in Table 7.2.

Table 7.2: Specifications and standard uncertainties of the instrumentation.

	Brand / Model	Std. uncertainty σ (in mm)
cam_{FRONT}	Allied Vision / Prosilica GT3400C	0.0073
cam_{BACK}	Allied Vision / Manta G-282C	0.0073
Laser distance meters	Dimetix / FLS-C10	0.1888*
Circular projected laser	Ibak / ILP	-
Dimensions of the measuring setup	-	0.25

* At a distance of 10 m (experiment limit)

The program, written in Matlab$^{\circledR}$, calculates the settings of the set-up in order to minimise the expected uncertainty in the end result, using the methods described in Chapter 4 and the dimensions of the sewer to be inspected, while obtaining a practical feasible settings in terms of freedom of movement. It was determined that the optimal distance between the three lasers distance meters is 0.16 cm in both x and y direction.

7.3.1   *Apparatus improvements in the second design*

Table 7.3 shows the median values of radial, tangential distortion, skew and mean re-projection error for all the camera-lens-aperture combinations. The results clearly suggest that the lens LM6HC is the best fit for the cam_{BACK}. Consequently, leaving the lenses LM3NCM and LM4NCM for the cam_{FRONT}. In order obtain the best estimate of the actual position of the three laser points (consequently x, y, θ_x, θ_y and θ_z) it is essential to have the most accurate correction for the distortions and hence the best-fit lens for the cam_{BACK}. On the one hand the LM3NCM lens has slightly lower distortion coefficients values in comparison with the LM4NCM lens; on the other hand the mean error is slightly higher. Finally, the LM4NCM lens was chosen because there are fewer outliers in the results in comparison with the LM3NCM lens results. Largest apertures were adopted due to the low light intensities inside the sewer pipes. The Figure 7.10 shows the boxplot of the selected camera-lens-aperture combinations.

Figure 7.11 shows the three calibrations lines associated with the laser distance measurements. Due to the good linearity of laser distance meters, only straight lines have been calculated. The values of the estimated regression coefficients, their standard uncertainties and covariance between them are given in the Table 7.4.

Further, during the laser alignment procedure it was determined that the standard deviation of the alignment was estimated to be 1.3×10^{-6} radials for the all three lasers at the experimental distance. Overall, the new design increases the accuracy of laser alignment with a factor of 19.

Table 7.3: The camera-lens-aperture the camera calibrations median values.

Camera	Lens	Aperture	Radial distortion			Tangential distortion		Skew	Mean error in pixels
			k_1	k_2	k_3	p_1	p_2		
cam_{FRONT}	Kowa (LM4NCM)	1.6	-0.0755	0.0848	-0.0436	-0.0003	0.0011	-0.8386	0.4407
		16	-0.0866	0.1260	-0.0789	0.0003	0.0005	-0.9424	0.4567
	Kowa (LM3NCM)	2.4	-0.0572	0.090	-0.040	0.0011	0.0007	-0.8115	0.5397
		4	-0.060	0.0957	-0.0427	0.0007	0.0006	-0.6395	0.5075
		8	-0.0592	0.0948	-0.0421	0.0007	0.0005	-0.6727	0.4989
	Kowa (LM6HC)	1.8	-0.1707	0.1202	-0.0331	0.0004	0.0017	-11.219	0.5528
		2.8	-0.1661	0.1101	-0.0249	0.0004	0.0014	-14.247	0.5514
		4	-0.1676	0.1151	-0.0295	0.0002	0.0012	-14.663	0.5552
		5.6	-0.1673	0.1137	-0.0283	0.0004	0.0012	-14.232	0.5591
		8	-0.1684	0.1164	-0.0312	0.0006	0.0012	-14.005	0.5758
		11	-0.1679	0.1115	-0.0256	0.0006	0.0012	-13.463	0.5896
cam_{BACK}	Kowa (LM4NCM)	1.6	-0.0755	0.0991	-0.0630	0.0002	0.0012	-14.013	0.4438
		16	-0.0832	0.1153	-0.0672	0.0008	0.0014	-10.841	0.5134
	Kowa (LM3NCM)	2.4	-0.0489	0.0708	-0.0287	0.0009	0.0031	-11.111	0.7669
		4	-0.0564	0.0878	-0.0382	0.0008	0.0021	-12.166	0.5821
		8	-0.0572	0.0898	-0.0389	0.0008	0.0025	-12.020	0.5194
	Kowa (LM6HC)	1.8	-0.1799	0.1718	-0.0926	-0.0005	0.0018	-0.7251	0.3924
		2.8	-0.1781	0.1646	-0.0739	-0.0003	0.0018	-0.845	0.3954
		4	-0.1779	0.1651	-0.0754	-0.0003	0.0017	-0.8167	0.3934
		5.6	-0.1794	0.170	-0.0815	-0.0003	0.0016	-0.8178	0.3972
		8	-0.1796	0.1613	-0.0637	-0.0004	0.0014	-0.9543	0.4280
		11	-0.1814	0.1770	-0.0961	-0.0003	0.0016	-0.8994	0.4390
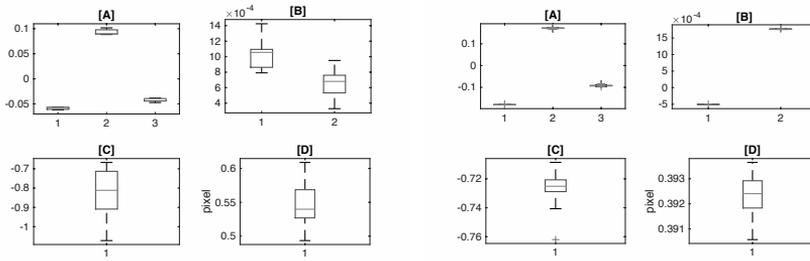
Figure 7.10: Boxplot of cam_{FRONT}-LM3NCM-2.4 (left) and cam_{BACK}-LM6HC-1.8 (right): [A] Radial distortion; [B] Tangential distortion; [C] Skew; [D] Mean error in pixels; On each box, the central mark is the median, the edge of the box are 25th and 75th percentiles, the whiskers extend to the most extreme data points not considering outliers (approximately $\pm 2.7\sigma$), and outliers are plotted individually.

Table 7.4: Estimated calibration coefficients, their uncertainty and covariance calculated using Monte-Carlo simulations.

	b_0	b_1	$\sigma(b_0)$	$\sigma(b_1)$	$cov(b_0, b_1)$
Left laser	-2.136	1.0	0.0587	6×10^{-6}	-3×10^{-7}
Top laser	-2.592	1.0	0.0626	6×10^{-6}	-3×10^{-7}
Right laser	-3.654	1.0	0.0623	6×10^{-6}	-3×10^{-7}

7.3.2 *Experimental results and potentials*

In the laboratory (Figure 7.2), first experiments were conducted on one sewer pipe using the Prototype v1.0 followed by the application of the Prototype v2.0 on the same pipe in order to compare two versions. Second, the experiment was conducted over the whole sewer reach, representing field conditions in a controlled laboratory environment.

Figure 7.12 presents a comparative measurement between the two prototypes. The results show that there is a difference in estimation of the loss of wall thickness (compared to a theoretical,
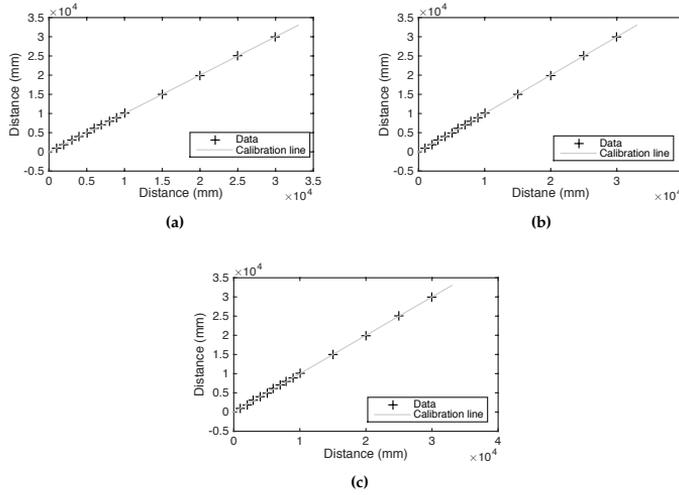
Figure 7.11: Distance meters calibration line for: (a) left laser; (b) top laser; (c) right laser.

un-corroded, initial geometry). Due to the fact that the distortion of the image and consequently its corrections were not taken into account within the Prototype v1.0 there is an over-estimation of the loss of wall thickness in the area closely located to the invert level and under-estimation in the area in close proximity of the crown region. These results (Figure 7.12) are expected due to the effect of moustache distortion for the Prototype v1.0 cam_{FRONT}. On the other hand, for the Prototype v2.0 cam_{FRONT} negative values of k_1 radial distortion coefficients barrel distortion was present; and corrected by warping the image with a reverse distortion. Based on the tangential coefficient values pixel locations were returned in normalized image coordinates, with the origin at the optical centre. If the other cameras would had been used for the Prototype v1.0 different results would have been yielded.

Uncertainty analysis was performed to determine the standard uncertainties in the x, y and z directions. Assuming that the uncertainties in the x and y directions are mutually independent, the $\sigma_{wall\ loss} = \sqrt{\sigma_x^2 + \sigma_y^2}$ was determined. Figure 7.13 shows the standard uncertainties of loss of wall thickness between the two versions of the apparatus. The results show the improvements added by the new hardware and improved protocols applied. From the figure it can be seen that the standard uncertainties vary from 1 to 1.8 mm for the Prototype v2.0; while for the Prototype v1.0, the standard uncertainty varies from 4.5 to 11.5 mm. In both cases, the uncertainties are the lowest in the invert level and they grow towards the crown region. This result was expected due to the fact that the laser profiler and its projection is closer to the invert level. Overall, the new design increases the accuracy with a factor of 5 to 10.

There are, however, some issues associated with the new version of the apparatus (Prototype v2.0). While the moving platform of the device moves through the pipe, due to the uneven nature of the surface, it can suddenly in a second or a part of a second, show a significant change in position and orientation. The frame rate of cam_{FRONT} and cam_{BACK} were set to 12 frames/s, while the laser distance meters measuring rate were set to 6 Hz (maximum rate for the accurate measuring settings (Dimetix FLS-C10 Technical Reference Manual V5.02). Laser distance meters were not able to always keep track of these sudden changes in the position, thus yielding results that are of questionable accuracy at a few locations - frame positions (Figure 7.14). Furthermore, the earlier experiments using the Prototype v1.0 were conducted using a ramp and without actual entering of the moving platform inside the pipe. Consequently there were no sudden and/or major changes in the position thus yielding results that follow accurate one. As can be seen in
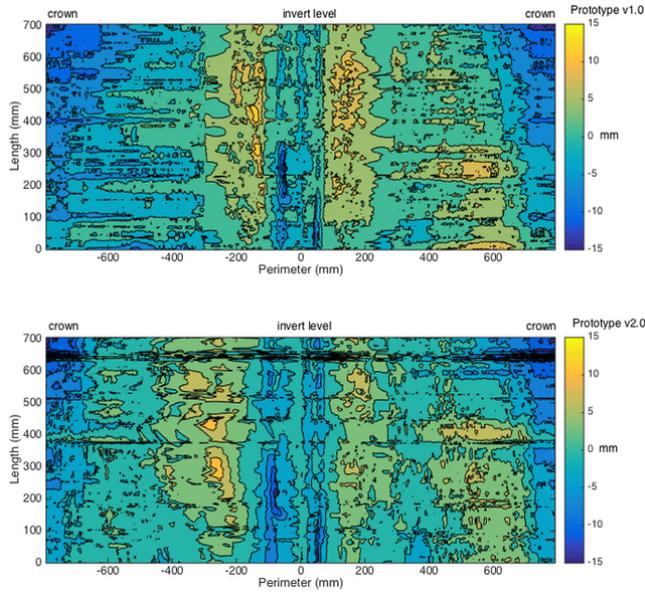
Figure 7.12: Difference between theoretical and measured geometry for the old pipe. The upper chart shows the result obtained from using the 1st (old) version of the apparatus, and the lower chart shows the result of the 2nd (new) version of the apparatus.

Figure 7.14, looking from the side there is a small deviation between two versions in the pipe interior estimation. This deviation is not noticeable while looking from front to top.

In order to estimate the deviation in image processing results for the cam_{FRONT} and cam_{BACK} sensitivity analysis is performed. Using 100 repetitive processed frames/images, where the measuring system was stationary, a 'true' image of a given location was obtained. Figure 7.15 shows the difference between the true image and 100 repetitive video frames. Results suggest that for the cam_{FRONT} image processing results deviate in the lateral and crown region in order of 1 pixel. In the invert region this deviation is 1-3 pixels. This is due to the presence of reduced light intensity and sharpness in the lower part of video frame. On the other hand, for the cam_{BACK} there is barely any deviation in image processing results present, which is more important for an accurate estimation of position of the apparatus.

Further, the experiment was carried out over the whole stretch of the connected pipes in the laboratory (Figure 7.2). As mentioned earlier while moving through the pipes and especially when leaving one pipe and entering the next one, there were sudden shifts in position and orientation of the moving platform; consequently leading sometimes to the loss of the projection of the laser beam on the reflection board. This lack of data during data processing generates a significant systematic error in estimating of the pipe interior geometry. These measurements were discarded from the final results. In addition, in some cases the projected laser point on the reflection board, when is close to the edge of the captured image, may disappear from the image during the process of correcting for the distortion. These measurements were also discarded from the final results.

Moreover, what was noticed is that during some time intervals the synchronization between the three distance meters is not guaranteed (Figure 7.16). This was caused by incorrect laser software control. This lack of synchronization results in wrong estimation of the pitch θ_x and yaw θ_y and continuing with the estimation of translation in x and y and roll θ_z. Additionally,
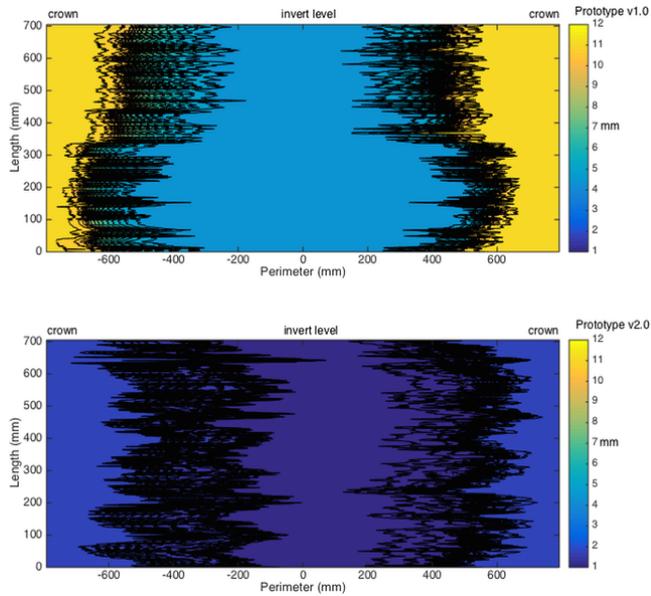
Figure 7.13: Difference between uncertainties associated to the estimation of the loss of wall thickness. The upper chart shows the result obtained from using the 1st (old) version of the apparatus, and the lower chart shows the result of the 2nd (new) version of the apparatus.

synchronization using the fourth laser is delayed for about half of second; this was caused by the issues in laser software initiation that was easily corrected (Figure 7.17). Firstly the camera recording was initialised followed by the laser system activation. When the lasers are initiated the fourth laser pulsing is initiated and recorded by cam_{BACK}. The moment of the first pulse is the synchronisation time (Figure 7.17). Overall, it is hereby again necessary to emphasize the importance of perfect synchronization between all elements of the two platforms in order to yield results free of (systematic) error. Figure 7.18 shows the results of 3D reconstruction of the pipe interior with the visible systematic error that were discussed above.

Currently the amount of raw data that is generated during the experiment data acquisition over the 1 m of pipe length is around 4.86 GB. This can be significantly reduced. Accelerating time is very challenging and will facilitate the synchronization of the entire process. In addition, the laser distance measurement with double measuring frequency in comparison with the image capturing frequency could strongly reduce the effects of sudden changes in the position of the moving platform of the apparatus.

7.4 EXTENSIVE APPARATUS TESTING

7.4.1 *Empty pipe under various conditions*

Water and vaseline were applied inside the pipe, on the wall, in order to create conditions that may occur in sewers: water saturated atmosphere (temperature, humidity, diffuse infiltration through the wall) and fat deposits. The goal of these experiments was to study of potential effects (bias, additional uncertainties) created by such conditions. No disturbances in the processes and the calculations have been seen with these experiments: humid and/or fat covered pipe can be scanned without difficulties. A small adjustment in the image processing is required for wet
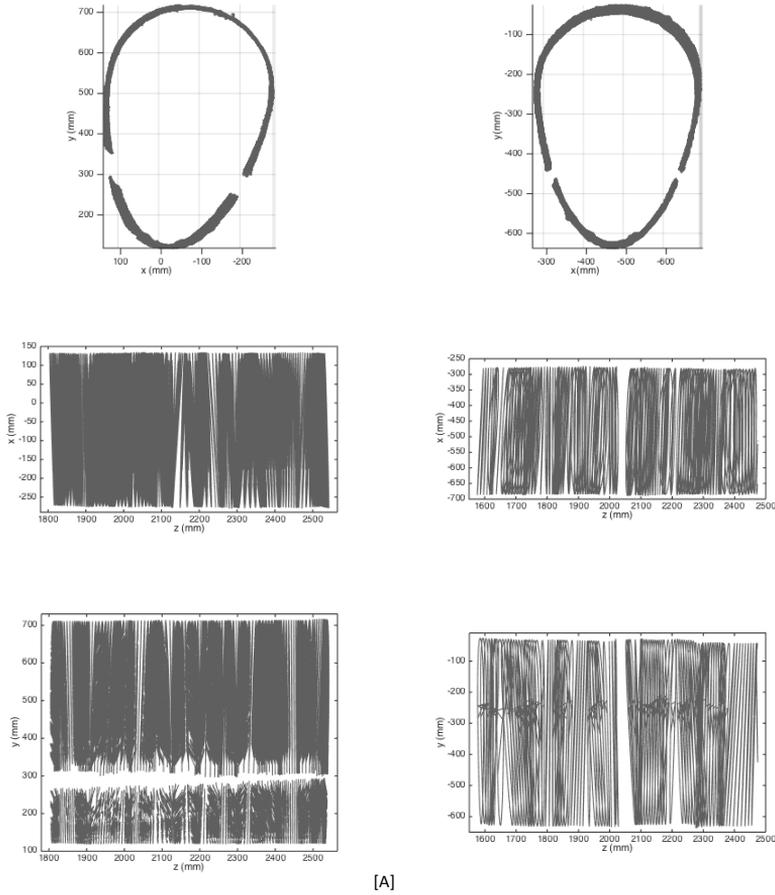
Figure 7.14: Front (first row), top (second row) and (third row) side view of the results of 3D reconstruction of the scanned pipe interior geometry using: [A] Prototype v1.0; [B] Prototype v2.0.

and/or fat covered pipes; light intensities are weaker and the threshold on pixel value needs to be changed. However, this adaptation does not change the accuracy on the result.

7.4.2 *Various object and material types*

Various objects and materials were placed in an egg-shaped pipe (dimensions 400/600 mm) to cover the wide range of solid materials and study effect of size, shapes, colours, roughness or the kind of deposits, which can be found in sewer systems. The scanned (S_{SCANNED}) and the measured (S_{MEASURED}) sizes independently obtained were compared with a simple variance test. When Eq. 7.8 was satisfied, the prototype provides a measurement consistent with the one given by the calliper. Otherwise, the prototype provides biased estimations of the object dimensions.

$$| S_{\text{SCANNED}} - S_{\text{MEASURED}} | \leqslant 2 \cdot \sqrt{\sigma^2 (S_{\text{SCANNED}}) + \sigma^2 (S_{\text{MEASURED}})} \qquad (7.8)$$
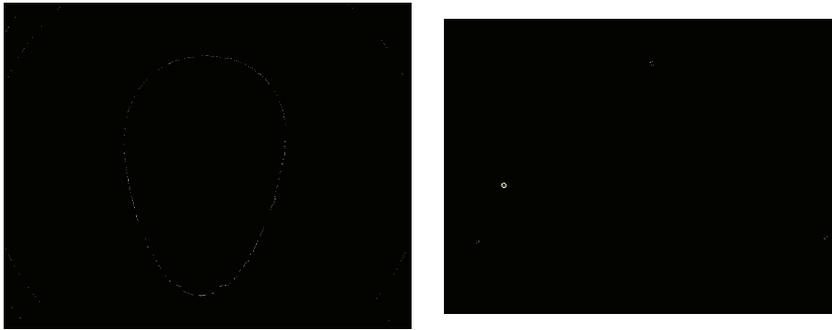
Figure 7.15: Deviation in repetitive image processing results for cam_{FRONT} (left) and cam_{BACK} (right).
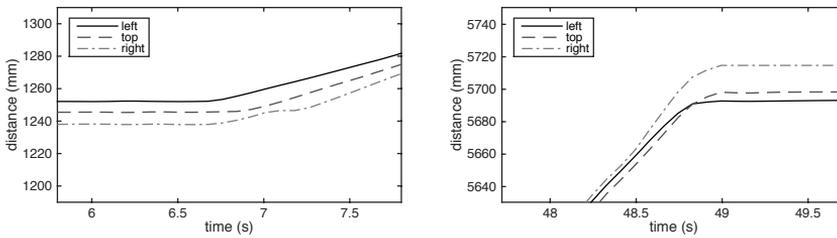
Figure 7.16: Examples of the synchronization problems between the three laser distance meters for the experiments over the whole sewer pipe stretch.
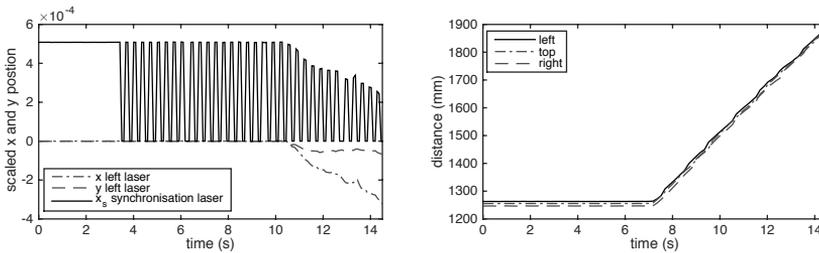
Figure 7.17: Synchronisation between moving platform (left) and fixed platform (right).

where $\sigma^2(S_{SCANNED})$ and respectively $\sigma^2(S_{MEASURED})$ are the standard uncertainties associated to the laser and respectively the calliper measurements.

Further, some scanned objects were grouped (Table 7.5) and consistency rates (R_C) were calculated for each group by:

$$R_C = \frac{N_C}{N_T} \qquad (7.9)$$

where N_C, is the number of scanned objects of the group for which the Eq. 7.8 was satisfied and N_T is total number of objects in the group.
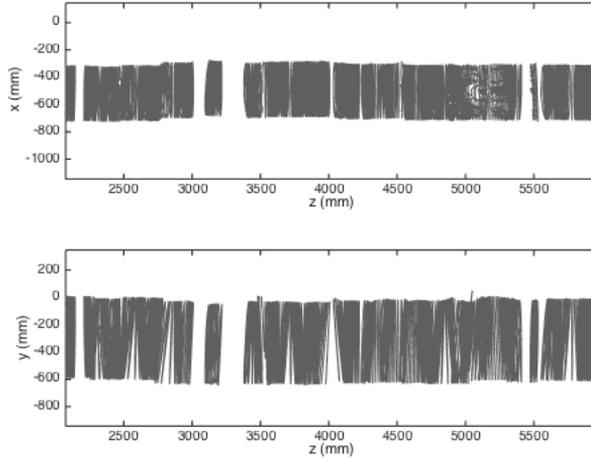
Figure 7.18: Top and side view of the results of 3D reconstruction of the scanned sewer pipe stretch.

Table 7.5: List of material groups.

Group name	Objects included in the experiment group
Bricks and concrete	brown brick, Deltares tetrahedrons, scarred cube, headless pyramid, double rotated T, bollard
Tiles	brown, white, zebra and blue tile
Metal	various metal and cylindrical shapes, battery, U steel bar

Due to the construction and the manner in which the devices is used, the data density (*i.e.* frame resolution) along the z-axis is directly dependent on two parameters: the value of the cam_{FRONT} frame frequency (12 fps for the presented prototype) and the speed of the moving platform (2-3 cm/s). The desired speed was 4 cm/s thus theoretically recording a frame every 3.3 mm (1.7 - 2.5 mm in reality). This value was not constant and varies from frame to frame due to non-constant speed, pitch, yaw and roll angles. The low-resolution along the z-axis may be responsible for some inconsistencies (*e.g.* various metal and cylindrical shapes, battery, scarred cube, headless pyramid) between scanned and measured sizes. From one frame where an object can be seen to the following one where the same object is not visible anymore, the real object edge is somewhere between these frames and the accuracy of the measurement is dependent on the data or frame density. In order to reduce this weakness of the Prototype v2.0, two solutions may be applied: (*i*) increase the image acquisition frequency (24 or 36 fps) and/or (*ii*) reduce the speed of the moving platform. The first solution will create more problems due to the aforementioned issues with the generated amount of raw data. On the other hand, the second solution is more feasible for research purposes, but not for routine applications. Consequently concluding that it is essential to switch to the image pre-processing, in order to reduce the required data transmission capacity while improving accuracy of the results along the main axis of pipe.

Table 7.6 presents consistency rates of groups given in Table 7.5. For the concrete objects, the consistency rate was 0.47 and when the distances along the direction of movement were the consistent this rate increased up to 0.67. The same can be concluded for the metal objects, however, they possess a higher consistency rate. Moreover, simple shapes like tiles were accurately measured (except along the main axis of the pipe) and offer a consistency rate of 1. Overall, these rates emphasize the effect of the low-resolution along the z-axis.

Table 7.6: Consistency rates of the groups.

Group name	R_C
Bricks and concrete	0.47 (0.67)
Tiles	1
Metal	0.67 (0.875)

Further, surfaces of the blue tile could not be scanned due to its bright (reflective) nature which lead to pixel saturation. Fortunately, most frequently used materials for sewer constructions (*e.g.* concrete, steel) are not reflective, especially when affected by corrosion processes. Transparent objects *i.e.* glass bottle disturb the measurements as show in Figure 7.19. The device was only able to scan the top crest of the bottle; transparent objects create diffraction and distorted shadow while the projected laser was passing through the object. Only the perpendicular parts (to the projected laser) of transparent objects may be measured. The distorted shadow created the gap in the 3D data (Figure 7.19). In general bright and transparent objects are relatively uncommon in sewers.
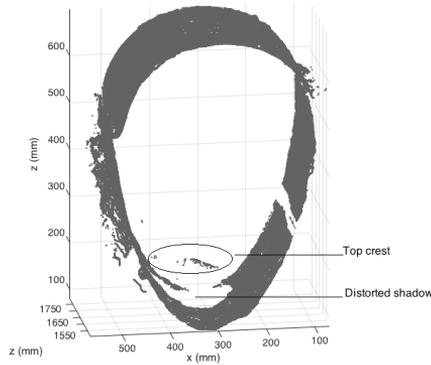
Figure 7.19: Glass bottle scanned by prototype.

7.4.3   *Deposits, displaced joints and other defects found in sewer*

Laser profiling technique allows quantification of deposit volumes. This can be achieved by scanning the pipe two times: once with sediments and a second time while the pipe is empty. Firstly, an experiment was carried out with the wooden board present in the pipe. Then about 67 g (approximately 46.5 cm^3 - based on typical loose sand density of 1442 kg/m^3) of sand was placed on the board and the pipe was scanned again (Figure 7.20). The difference between consecutive measurements without and with sand present gave the estimation of the volume $V = 45.2\ cm^3$. The deviation of the measured value from the actual is in the order of 3%.

Sludge deposits were detected wih no difficulties by the apparatus. The outcome was consistent with the ones previously mentioned (*i.e.* fat and wet wall). Furthermore, displaced joints and section reductions were experimentally simulated (Figure 7.21). The profiler was able, with ease, to scan both objects. Shapes were faithfully reproduced including the valve of the inner tube. However, shadow effect was visible. the part of the joint that hangs (see Figure 7.21 left) hindered the measurement of the crown region of the pipe. The camera is not able to see behind the obstacle. The same issue persisted with the back part of the inner tube (see Figure 7.21 right). Furthermore, to the shadow effect can be attributed also gaps in the laser projection. This can be clearly seen in the inner tube (see Figure 7.21 right). The wooden piece placed to maintain the
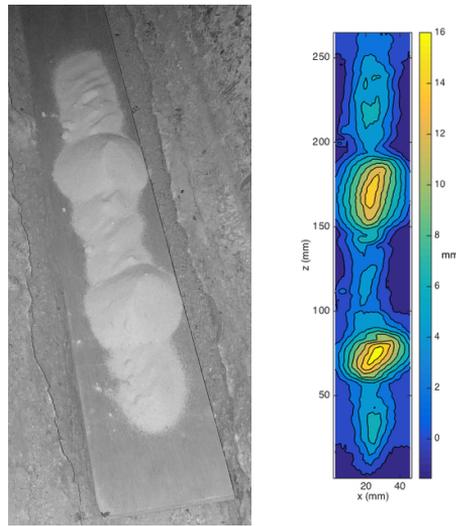
Figure 7.20: Quantification of the sand deposit volume: photo of the experiment (left) and scanned sand relief (right).

inner tube in its position was not visible due to blocked laser projection by the inner tube. These experiments highlighted issues that need to be addressed: (*i*) to limit or avoid shadow effect, both camera and laser sources should be multiple (facing each other) and (*ii*) potential information can be extracted from gaps in the data. This promising outcome may lead to new methods for pattern recognition.

The Prototype v2.0 provided consistent measurements for the diameter and the lengths of various cylindrical shapes (Figure 7.22). Therefore, such a device used *in situ* will be able to locate and quantify accurately intrusive connections.
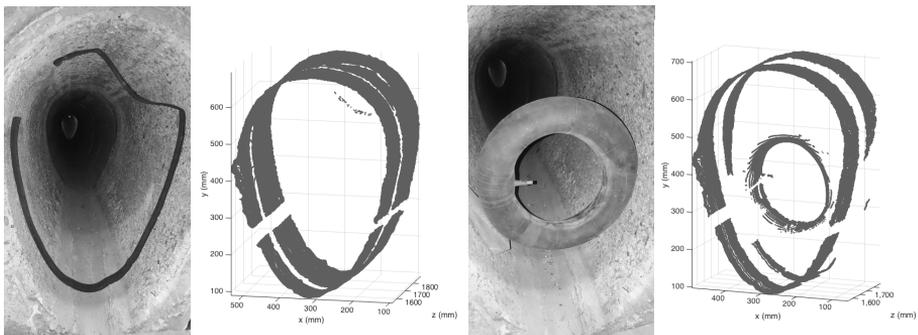
Figure 7.21: Displaced joint (left) and section reduction with one inner tube (right); picture and scanned data.

Root intrusion was simulated by gluing fine roots to the pipe crown (Figure 7.23). Roots and their main direction are visible in the scanned data. Overall, space filled with roots can be easily assessed. Figure 7.24 confirms this statement.
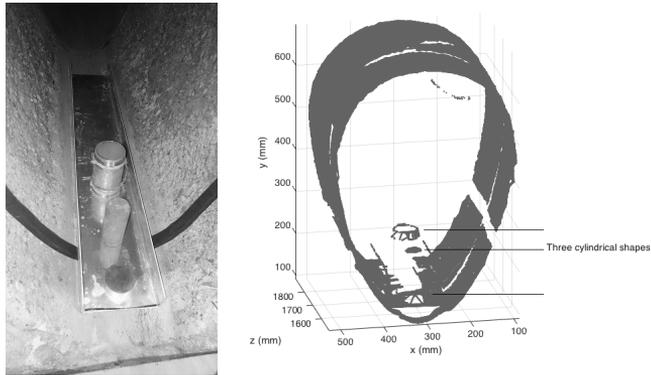
Figure 7.22: Various cylindrical shapes scanned with the device: photo (left) and scanned data (right).
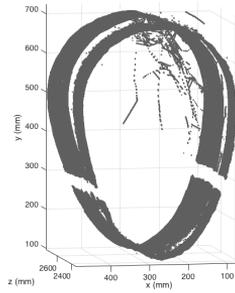
Figure 7.23: Roots scanned by the prototype.
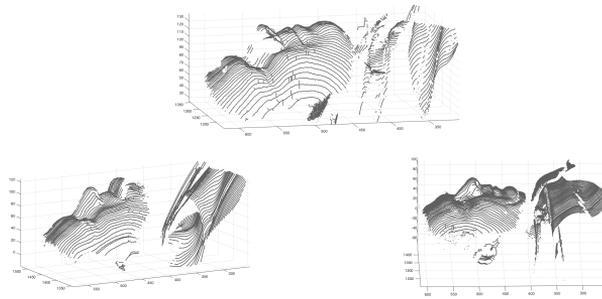
Figure 7.24: Faces of people who worked on the development of the Prototype v2.0.

Further, an attempt was made to simulate reality, thus numerous objects that can be found in a sewer were placed inside the pipe. Results show that it is possible to detect all objects. In order to detect the objects, however, the light intensity had to be adjusted in the image processing.

At the very end of the experiments the pipe was cracked using a professionally operated sledgehammer. Besides cracks a partial break (hole) on one side was created. The profiler was

able to recognise cracks and their size and orientation as well as the partial break (Figure 7.25); hence demonstrating once again the potential of laser profiling technique.
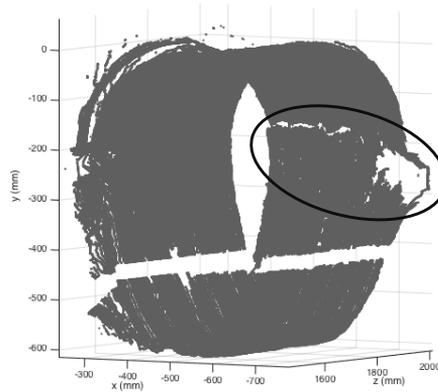
Figure 7.25: Fissures and break scanned by the prototype.

7.4.4 *Estimation of wall roughness*

As mentioned earlier there is perspective of the application of the laser profiler technique for measuring apart from the pipe interior geometry, the wall (physical) roughness. With pipe deterioration the pipe geometry changes and thus the hydraulic diameter changes; thereby pipe geometry becomes important for quantifying the actual hydraulic resistance (Figure 7.25). As stated earlier the wall roughness can be quantified by using the analysis, as proposed by Pegram and Pennington (1996), of the scanned surface data. The total uncertainty σ_{tot}, is defined by Eq. 6.7 - $\sigma_{tot} = \sqrt{\sigma_m^2 + \sigma_{in}^2}$ and is composed of a measurement and an interpolation component. The only way to reduce the σ_{tot} is by reducing the part of uncertainty associated with measuring. The improvement of the new version of the laser profiling technique shows that this accuracy can be increased to $\sigma = 1\text{-}1.8$ mm. For the studied pipe diameter and based on the position of the laser projection source in the pipe (Figure 7.26) the standard deviation or the 95% uncertainty interval of the laser profile is somewhere between 2-4 mm. It should be noted that wall roughness varies with a region, being the lowest at the invert region and being the highest at the crown region. Consequently, with the current accuracy the prototype will yield results with a relatively high uncertainty, especially in the invert and lateral region. The earlier study (see Chapter 6) showed that the largest part of the total uncertainty is associated with the measuring uncertainty. When the surfaces $k_s > 10$ mm, the interpolation uncertainties may increase significantly if the elevation between the neighbouring measured points is high. In conclusion, the measuring accuracy should be, in this case, around 0.5 mm (at least 50% less than k_s) for the invert and lateral region ($k_s \leqslant 2$ mm), otherwise it could be regarded that the results of the roughness are unreliable. This can be achieved by further improving the apparatus accuracy and in addition with possible shifting the laser profiler closer to the scanned surface. In the case of the crown region ($k_s > 10$ mm) of the measuring uncertainty of 3 mm will not yield results, which are unreliable. Overall, the regions with higher roughness will most affect the hydraulic resistance; hence the higher measuring accuracy will yield more reliable estimations of hydraulic roughness. For instance, with the improved prototype the initial estimation of the physical roughness can be obtained using laser profiling. From a generated 3D model of the pipe interior, using the laser profiler technique, it can be decided whether the scanning should be repeated with the re-positioned laser profiler to yield a more accurate estimation of the roughness.
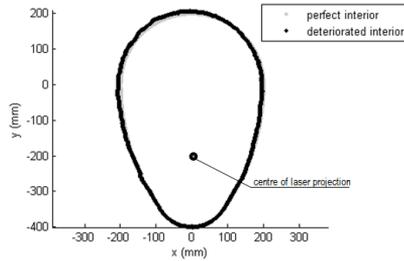
Figure 7.26: Example of the laser profiler results; deteriorated pipe cross-section vs. perfect pipe cross-section.

Further, for the known aggregate sizes the physical roughness was estimated using the new version of the apparatus and the results are summarised in the Table 7.7. Due to the lack of accuracy and the low-resolution, standard uncertainties are of the same order of magnitude (mm) as the roughness itself: the prototype is not sufficiently accurate to estimate roughness. As already stated the third version of the apparatus (Prototype v3.0) is required for *in situ* roughness measurements. By applying the same calculations, for determining the relative contribution of the individual source of error to the overall measuring error, presented in Chapter 4 to reach a target accuracy of 0.5 mm, the following improvements should be implemented: laser distance meters should be 100 times more accurately aligned, distances provided by these device should be 10 times more accurate, camera accuracy needs to be improved by a factor of 3.3, camera offset and respectively scaling factor should be 10 times more accurate. Relative contributions to the total uncertainty have been plotted in Figure 7.27. Furthermore, the laser profiler with the narrower and a more light intensive beam would further contribute to the increase of the accuracy. Overall, the *in situ* roughness measurements are likely unrealistic with the current prototype of the laser profiling devices.

Table 7.7: Results of the roughness calculations.

Material	Granulometry	k_s (mm)	σ_{k_s} (mm)
Sand	0.1 mm	1.74	2.01
Gravel	5-8 mm	6.13	2.26
Small stones	22-30 mm	11.25	2.68
Medium stones	30-40 mm	15.62	3.07
Large stones	40-63 mm	17.34	3.66

Moreover, this combination of the information on the interior geometry and on the physical roughness will yield an accurate estimate of the hydraulic roughness; furthermore provide the information on the actual relation between water depth in the pipe and the flow velocity and discharge respectively. For instance, this can be simulated using the results and methods from the Chapter 4 and 6. Figure 7.28 shows the relation between water depth in the pipe (h/H) and the flow velocity and discharge respectively (v/v_{full}, Q/Q_{full}). It can be seen the importance of both knowing the physical roughness and internal geometry. The pipe's capacity, water-flow velocity in the pipe, will somewhat change with an increase of the physical roughness k_s only from 0.54 mm (new pipe) to 3.88 mm (equivalent k_s for The Hague (Po8) pipe). When the water depth in the pipe is below 60% the velocity will be slightly lower compared to the velocity in the new pipe. In contrast it will slightly increase when the water depth in the pipe is above 60%. When added on top of that the information on the interior geometry (example from the scanning of The Hague (Po8) pipe) the velocity and discharge in the partially filled pipe will somewhat change again. However, the major change in the pipe's capacity will occur when in the calculation are considered the roughness for each region; hence demonstrating once again the importance of knowledge of both parameters.

Relative mean contribution error terms for θ_x=0.89629°, θ_y=0.2307°, θ_z=-1.9616°
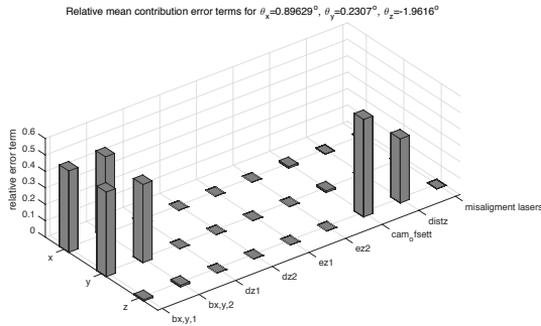
Figure 7.27: Expected accuracy of a theoretical third version of a laser-scanning device to reach a standard uncertainty of the position of the cross-section of 0.5 mm.
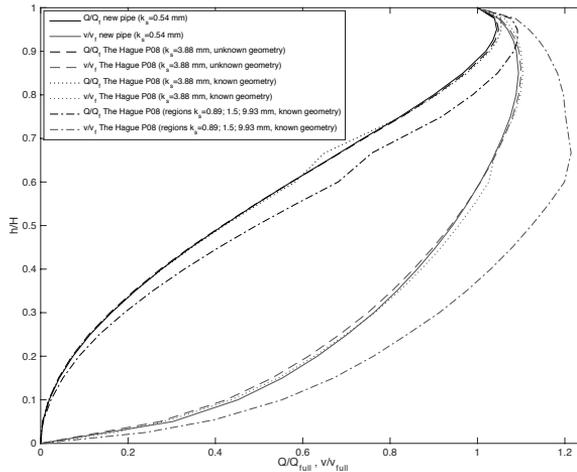
Figure 7.28: Velocity and discharge in partially filled egg-shaped pipe and the effects of the change of the physical roughness and the interior geometry.

7.5 CONCLUSIONS

The potential application of the improved laser profiling technique are comprehensive *e.g.* deposit measurements, roughness measurements, crack recognition. Collected information on 3D geometry may be used: to calculate realistic discharge capacities (making a distinction between DWF and storm conditions), as input in CFD modelling instead of common assumptions on roughness, to study pipe collapsing behaviour, to predict network aging and efficiently plan maintenance works.

The new design of the apparatus (Prototype v2.0) and the improvements in the protocol applied (*e.g.* camera calibrations) showed that measuring accuracy can increase up to 5-10 times. It must be emphasized, however, that if the system is not fully synchronized the obtained results

will be accompanied by a constant systematic error in the estimation of the interior geometry. There are several improvements that can be applied to the Prototype v2.0 *i.e.* amount of raw should be significantly reduced (recently learned that it is possible to reduce the amount of raw data about 100 times), increase the apparatus accuracy. In addition, the laser distance measurement with double measuring frequency in comparison with the image capturing frequency could strongly reduce the effects of sudden changes in the position of the moving platform of the apparatus.

Various objects and materials were detected inside the sewer pipes *e.g.* sludge deposits, displaced joints, intrusive connections. The Prototype v2.0 was also able to detect fissures, breaks and roots; hence demonstrating the potentials of this technique. Further, laser profiling technique allows quantification of deposit volumes. Moreover, this technique has a potential in estimating the pipe wall roughness. However, the Prototype v2.0 is not accurate enough for the task at hand. It should also be noted that this technique is able to detect attached deposits *i.e.* build-up grease and settled deposits *e.g.* muck, which can significantly influence the system functionality, and quantify corresponding roughness. A more accurate device (Prototype v3.0) will enable *in situ* roughness measurements estimation. For instance, increasing the accuracy by using the large camera sensors and/or narrower more light intensive laser beans.

Overall, this study strengthens the reliability of such a technique thus suggesting its wider application in inspection practice. Information provided to sewer managers will be more accurate and objective in order to take appropriate decisions. The present version, however, can still be improved to provide spatially distributed accurate roughness measurements: better input data for sewer modellers.

8

CONCLUSIONS AND RECOMMENDATIONS

This thesis discusses the limitations of the currently used information sources on the structural and hydraulic conditions of concrete pipes in sewer asset management. Suggestions for some solutions to the challenges posed by these limitations are also presented. In this chapter the main research contributions together with summarized chapter conclusions and recommendations for future work are presented.

8.1 RESEARCH CONTRIBUTION

This research aims at (*i*) identifying the required information on the structural and hydraulic performance of the sewer pipes, (*ii*) quantifying the uncertainties of information and (*iii*) improving the quality of this information. The thesis provides the enhancements of existing sewer inspection techniques and new inspection methods thus contributing to a better understanding of the structural and hydraulic behaviour of sewer pipes that serve as a basis from which asset management can benefit. This increased knowledge about system performance and information, of sufficient quality, on the actual status of the assets will contribute to the increased confidence in the decision making process on sewer rehabilitation needs; thus attaining a preferred service level at an acceptable level of public costs. Furthermore, a proper serviceability of the asset in the long term will allow the prevention of adverse effects on human health and environment.

8.2 CONCLUSIONS

First of all, it is concluded that there are numerous factors that can influence the structural and hydraulic performance of the sewer pipes, eventually leading to failure. The HAZOP technique was demonstrated that it can be used as a first indication for determining these causes and basic information on them needed for sewer asset management. Furthermore, the presented HAZOP analysis ultimately helps to define what information is required to be able to detect and quantify any given failure mechanism. It is possible that, due to expert subjective judgment based on hindsight, some failure causes were not identified. In order to avoid this the experts from various fields of work and expertise were interviewed. Moreover, the same failure mechanism were discussed with different experts eventually leading to the same conclusions. Overall, the greater number of possible failure causes is linked to human activity - around 65% (*e.g.* workmanship errors, design errors). The assumption that a newly built sewer is perfect is hampering effective and efficient sewer maintenance strategies. In order to better understand the changes in the condition of the assets, it is essential to gather information on relevant deterioration. It is concluded that important parameters related to the structural condition of concrete sewer pipes are wall thickness, geometry and material properties. On the other hand, looking from the perspective of hydraulic performance information such as hydraulic roughness and the interior geometry will allow an estimation of whether or not a given pipe has adequate hydraulic capacity. This can be achieved generally by using sewer inspection techniques.

Conventional inspection techniques for concrete sewer pipes *i.e.* CCTV and core sampling are commonly applied for assessing structural conditions. It is concluded that the quality of visual inspection and drill core results are insufficient to guide proper decision making. The results showed that the quality of final core classification depends on the selected parameters and their classification range. Different factors such as non-uniform deterioration, height/diameter ratio, experimental uncertainty and damage during drilling all influence the proper estimation of

splitting tensile strength, which makes the results unreliable. Consequently, the understanding of uncertainty of inspection data is relevant for future decision making and model development. Uncertainties related to the application of both CCTV inspection and core analysis in today's practice could be and should be determined and quantified, being an essential parameter in risk qualification. Moreover, there is a need for further study of material property parameters of core sampling in order to be able to assess the associated uncertainties and then to determine the optimal parameters that will enable the assessment of the concrete quality of the pipe.

It is concluded that laser profiling is potentially a technique that allows the interior geometry to be measuring accurately enough to be able to quantify the interior geometry for heavily deteriorated pipes, provided that the position and alignment of the camera and laser are adequately accounted for. Laser profiler results that are not corrected are subject to unknown, and potentially very large, errors, which systematically overestimate the loss of wall-thickness resulting in an overestimation of the risk of collapse. As a result, an assessment with a laser profiler might increase costs, but not risks of failure. The accuracy of the experimental set-up (Prototype v1.0) is mainly determined by the uncertainty of the distance measurement and the alignment of the three lasers used to quantify the position and orientation of the camera and the laser sheet. Apart from the inner geometry it is essential to possess information on the amount of healthy material. The thickness of healthy material is defined as the remaining thickness of uncompromised concrete.

As already noted this research has demonstrated that core sampling is associated with a significant uncertainty. Therefore, to evaluate the performance of degraded sewer pipes a laboratory pipe crushing experiments and an extensive drill core analysis were carried out. Further, the presence of cracks does not imply that the pipe will collapse. Cracked pipes could still withstand a reasonable additional load. Different factors, such as road conditions, traffic load and especially local soil conditions influence the sewer's lifespan. It is disputable to regard pipe age and CCTV as main and sufficient information sources in deciding upon sewer system renewal.

Referring to drill core analysis, it is concluded that the tensile splitting strength gives the best information with respect to the material's properties. Further, it is concluded that the remaining healthy concrete thickness *i.e.* carbonation depth test gives the best information with respect to the geometry. This inspection method is more suitable for non-severely deteriorated pipes. It is concluded that the concrete deteriorates non-uniformly in space and time. This variation in material properties will most likely increase with the worsening of the conditions of a pipe. Overall, it is next to impossible to determine all possible concrete degradation mechanisms, due to the influence of numerous factors starting from the production stage to the end of a pipe service life. For very deteriorated pipes other, non-destructive techniques should be developed as an alternative since obtaining a quantification of the variance in the pipe condition would result in a prohibitive large number of samples that have to be taken.

Further, it is concluded that laser scanning offers challenging perspectives for measuring structural characteristics of sewer pipes, such as physical roughness. For the deteriorated concrete pipe surfaces a low-resolution laser scan is able to measure physical roughness and consequently the hydraulic one. The more the sewer pipe surfaces are deteriorated, the more feasible the application of a lower resolution laser becomes. On the other hand, for the regions with lower roughness it is necessary to possess more accurate laser distance-measuring techniques. Potentially a laser profiler (Prototype v1.0) combined with pattern recognition may provide information on these factors as well. However, there is a need for a more accurate laser profiling apparatus (Prototype v2.0), in order to be able to estimate the wall roughness along the whole perimeter.

The combination of the two methods, *i.e.* to use the laser profiler to determine the pipe interior geometry as well as to identify representative patches where roughness should be measured, is an opportunity to strengthen the laser profiling technique as a method. Moreover, this combination of the information on the interior geometry and on the physical roughness will yield an accurate estimate of the hydraulic roughness; furthermore it will provide information on the actual relation between water depth in the pipe and the flow velocity and discharge respectively. Therefore, it will provide an input for the hydrodynamic sewer models thus enabling an accurate estimation

of actual hydraulic characteristics and thus may serve as a basis for a sewer asset management based on actual functionality.

The new design of the laser profiling technique (Prototype v2.0) and the improvements in the protocol applied (*e.g.* camera calibrations) showed that the measuring accuracy can be increased up to 5-10 times. Most of the common defects were quantified: deposits, wall erosion, displaced joints, section reductions, intrusive connections, fissures, breaks and roots; hence the reliability of this technique was demonstrated. Further, this technique allows quantification of deposit volumes, with uncertainty $\sigma \approx 3\%$. It must be emphasized, however, that if the system components of the measuring are not fully synchronized the obtained results will be accompanied by a constant systematic error in the estimation of the interior geometry. There are several improvements that can be applied to the Prototype v2.0 *i.e.* the amount of raw data should be significantly reduced (recently learned that it is possible to reduce the amount of raw data about 100 times) along with an increase in the apparatus accuracy. In addition, the laser distance measurement with double measuring frequency in comparison with the image capturing frequency could strongly reduce the effects of sudden changes in the position of the moving platform of the apparatus. Moreover, this technique has a potential in estimating the pipe wall roughness. It should also be noted that this technique is able to detect attached deposits *i.e.* build-up grease and settled deposits *e.g.* muck, which can significantly influence the system functionality, and quantify corresponding roughness. A more accurate device (Prototype v3.0) will enable *in situ* roughness measurements estimation. Other solutions can be studied in order to increase the accuracy: well-couples cameras and lenses, and/or large camera sensors or narrower more light intensive laser beams.

Overall, this study strengthens the reliability of such a technique thus suggesting its wider application in inspection practice. Information provided to sewer managers will be more accurate and objective in order to take appropriate decisions. The present version (Prototype v2.0), however, can still be improved to provide spatially distributed accurate roughness measurements: better input data for sewer modellers.

8.3 RECOMMENDATIONS FOR FUTURE WORK

Further research on quantifying failure processes, as well as determining the availability of the information will contribute, along with the results of HAZOP analysis, to the continuation of the risk analysis. The information on the actual status of a pipe with repeated measurements over time may reveal information on failure processes evolvement over the period of time. Also, there is a possibility of recording some processes of which we are not yet aware. To quantify the probability of failure occurrence for each component and to identify critical components, the Failure-Tree Analysis (FTA) will be used. It is anticipated that this approach will lead to a better quantitative understanding of the processes that lead to failure. For practical application, it is unlikely that all possible failure mechanisms will be taken into account, because of the vast amount of information that is involved, and due to the fact that it is likely that not all processes that occur are acknowledged yet.

The Prototype v2.0 is still not accurate enough to be suitable for *in situ* roughness measurements, the results of which may be used as input data for CFD modelling instead of common, and maybe inaccurate (especially for an existing sewer), assumptions. Additionally this was a laboratory based study, and for practical use further apparatus improvements and testing are needed. Therefore, future developments of the laser profiling technique (Prototype v3.0) will aim at: (*i*) increasing the accuracy (standard uncertainty up to 0.2 of 0.5 mm) in order to accurately estimate the roughness; (*ii*) improving the design and mathematical methods to process data of such a laser profiler; (*iii*) possibilities of using pattern recognitions of pipe defects (to prevent subjectivity in data interpretation as for CCTV); (*iv*) to propose new devices *e.g.* combining techniques and measurement methods to assess the submersed parts of the pipe, to identify misconnections and to make inspections easier (without disruption of the sewer service) and (*v*) using multiple both

camera and laser profiler sources (facing each other) will overcome a shadowing effect during the measurement. This promising outcome may lead to new methods for pattern recognition.

The results of this research will be used for future development of inspection strategies using core sampling. It is concluded that the carbonation depth test gives the best information with respect to the remaining healthy concrete thickness. There is a need for a new method adjunct to the laser profiling technique, since the drill core analysis is not able to achieve this due to the fact that it is destructive and provides information on the material properties of a few locations only. For instance, an ultrasonic nondestructive technique can be used for an evaluation of concrete structures (Akhtar, 2013; Popovics & Rose, 1994). An ultrasonic device may be coupled to the laser profiling apparatus to differentiate between deteriorated and healthy concrete material.

Further, for sewer rehabilitation decisions, it is necessary to be able to calculate the remaining strength of the soil-pipe construction environment for deteriorated pipes. Therefore, further research should concentrate on simulations with a Finite Element Method (FEM), with the pipe geometry information provided by a laser profiling and material properties by core sampling. The lab test setup presented in this thesis is a simplification of actual field conditions and can be used to verify a finite element model (*e.g.* DIANA (de Borst *et al.*, 1985)). Such a model will be able to accurately predict the structural behaviour of a sewer pipe; thus the structural behaviour of these pipes will be studied in more depth. Furthermore, the effects of the different soil properties and/or conditions can be studied as well as the effects of different kinds of loads (*e.g.* traffic load) on the structural response. The final model can be used to determine the remaining load bearing capacity of a sewer pipe and to determine the type of information needed to further enhance the decision making process.

It is important that sewer managers realise that not every source is relevant at all times, and nor do they give perfect information. This means that data should not be regarded as the 'truth', but as an indication of what might be the current status given specific circumstances. People operate within bounded rationality, forcing them to use intuition to transfer information from multiple sources to judgements and decisions. In addition to that, decision making in multi-actor settings forces people to step away from their own preferences in order to make compromises. Sewer operators should be able to judge the impact of the uncertainties on the decisions they need to make on a day-to-day basis in order to justify their choices properly, even in complicated decision processes.

A APPENDIX

A. Flooding - capacity decrease

A-1. Human error

1.1. Production error	Cause	Information needed on cause	Where to get information
1.1.1. Material error	- poor equipment - software error - insufficient quality control (raw material / final product) - inadequate climate control - transport and handling	1. checking with manufacturer	a. from the manufacturer
1.1.2. Shape and/or dimensions error	- poor equipment - software error - insufficient quality control of final product - inadequate climate control - tear and wear molds - transport and handling	1. checking with manufacturer	a. from the manufacturer

1.2. Design error	Cause	Information needed on cause	Where to get information
1.2.1 Hydraulic design	- un/experienced engineers	1. checking of design protocol	a. inside the company
	- non-validated software	1. providing information on used version of software 2. software acceptance test	a. inside the company b. software developer
	- lack of quality check	1. checking of model input 2. checking of model output	a. inside the company b. standards for hydraulic design
	- lack of appropriate data	1. checking the quality of available initial data necessary for design	a. sources of initial data - population → municipality - precipitation → hydro-meteorological centre - water consumption→ water utility - pollution → wastewater utility - hydraulic load from surrounding area → hydro-geological centre
1.2.2. Structural design	- un/experienced engineers - lack of quality check - lack of appropriate data	1. checking of design protocol 1. checking of final report 1. checking the quality of available initial data necessary for design	a. inside the company a. inside the company a. sources of initial data - material → production phase - structural loads → traffic section of municipality - geotechnical design → geo-logical centre
1.2.3. Inherent design uncertainties	- improper data assessment - climate change - social/political changes - unknown relevant processes	1. checking of final data assessment 1. simulate possible scenarios 1. simulate possible scenarios 1. research	a. inside the company a. expert checking a. expert checking a. scientific research institutions

1.3. Construction error	Cause	Information needed on cause	Where to get information
1.3.1. Improper pipe positioning	- improper quality of backfill	1. soil characteristics of backfill	a. from the constructor b. from the measuring
	- lack of supervision	1. who and if there was supervision	a. from the municipality
	- pipes barely connected	1. position of pipes	a. from the constructor b. from the inspection
1.3.2. Damaging during refilling and/or compaction	- cores material in backfill	1. soil characteristics of backfill 2. how it was compacted	a. from the constructor
	- lack of supervision	1. who and if there was supervised	a. from the municipality
1.3.3. Improper bedding and/or foundation	- improper consolidation of bedding - improper foundation - lack of supervision	1. characteristics of bedding 1. soil characteristics of foundation 1. who and if there was supervised	a. from the constructor a. from the constructor a. from the municipality
1.3.4. Wrongly constructed connections and/or joints	- lack of professionalism during construction	1. as-built report 2. inspection results	a. from the constructor
	- lack of supervision	1. who and if there was supervised	a. from the municipality
	- improvisation due to local conditions	1. as-built report 2. inspection results	a. from the constructor
1.3.5. Improper choice of pipe and joint type and/or material	- un/experienced engineers - lack of quality check - lack of appropriate data	1. checking of design protocol 1. checking of final report 1. checking the quality of initial data necessary for the design	a. inside the design company a. from the contractor a. sources of initial data: (*e.g.* material → manufacture)
1.3.6. Wrong constructed manholes	- lack of professionalism during construction	1. as-built report 2. inspection results	a. from the constructor
	- lack of supervision	1. who and if there was supervised	a. from the municipality
	- improvisation due to local conditions	1. as-built report 2. inspection results	a. from the constructor
	- lack of cooperation with road constructors	1. as-built report of sewer and road construction 2. inspection results	a. from constructors
1.3.7. Absence of inspection after construction	- lack of professionalism and supervision	1. as-built report	a. from the constructor

1.4. Operation and Maintenance	Cause	Information needed on cause	Where to get information
1.4.1. Improper sewer condition assessment	- un/experienced inspector - lack of professionalism - improper data assessment	1. checking of inspection results 1. checking of inspection protocol 1. checking of final data assessment	a. from the municipality a. from the municipality a. inside the municipality
1.4.2. Improper sewer maintenance	- un/experience of maintenance team - improper/absence sewer cleaning - improvisation due to local conditions - use of inappropriate equipment	1. checking of maintenance results 1. checking of maintenance reports 1. checking of maintenance reports 1. checking of maintenance reports	a. from the municipality a. from the municipality a. from the municipality a. from the municipality
1.4.3. Inherent uncertainties	- uncertainty of inspection data	1. research on inspection data quality	a. scientific research institutions
	- lack of appropriate data	1. research	a. scientific research institutions
	- improper standardisation	1. research	a. scientific research institutions
1.4.4. Improper rehabilitation	- un/experience of rehabilitation team - lack of professionalism during rehabilitation	1. checking of rehabilitation results 1. checking of rehabilitation reports	a. from the municipality a. from the municipality
	- improvisation due to local conditions - use of inappropriate equipment	1. checking of rehabilitation reports 1. checking of maintenance reports	a. from the municipality a. from the municipality

1.5. Abuse	Cause	Information needed on cause	Where to get information
1.5.1. Disposal of unsuitable waste	- accidental/deliberate sewer blockage	1. checking the existence of uncommon damages	a. from the inspection
		2. potential sources (*e.g.* industry, hospitals)	a. from survey b. from *in situ* measurements
1.5.2. Illicit connections	- placement of lateral connections	1. checking the existence of illicit connections	a. from the inspection

A-2. External effects

2.1 Root intrusion	Cause	Information needed on cause	Where to get information
2.1.1. Tree species and their position	- trees with deep roots - trees located close-by the sewer	1. type of trees 1. location of trees	a. from the local community a. from the local community
2.1.2 Characteristics of the local environment	- low groundwater table - poor soil conditions - climate conditions - pollution and infection	1. measurement of groundwater table 1. soil texture/structure, moisture, aeration, temperature and root competition 1. light intensity, CO_2 1. toxic material, bacteria, fungi and soil-inhabiting animals	a. from measuring programs (ground water table) a. from measuring programs a. from the meteorological department a. from measuring programs
2.1.3. Wrongly constructed connections and/or joints	- lack of professionalism during construction - lack of supervision - improvisation due to local conditions	1. as-built report 2. inspection results 1. who and if there was supervised 1. as-built report 2. inspection results	a. from the constructor a. from the municipality a. from the constructor
2.1.4. Improper choice of joint type and/or material	- un/experienced engineers -lack of quality check -lack of appropriate data	1. checking of design protocol 1. checking of final report 1. checking the quality of initial data necessary for the design	a. inside the design company a. from the contractor a. sources of initial data: (e.g. material $\rightarrow$ manufacture)
2.1.5. Weakened structural elements	- low strength properties of plastic pipes - sever pipe deterioration	1. deformation of pipes 1. sever cracks, pipe brakes, infiltration	a. from the inspection (e.g. CCTV) a. from the inspection (e.g. CCTV)
2.1.6. Sewer maintenance practices	- improper root removal	1. maintenance procedure	a. from the maintenance team

2.2 Partial collapse	Cause	Information needed on cause	Where to get information
2.2.1. Improper pipe positioning	- improper quality of backfill - lack of supervision - pipes barely connected	1. soil characteristics of backfill 1. who and if there was supervision 1. position of pipes	a. from the constructor b. from the measuring a. from the municipality a. from the constructor b. from the inspection
2.2.2. Damaging during refilling and/or compaction	- cores material in backfill - lack of supervision	1. soil characteristics of backfill 2. how it was compacted 1. who and if there was supervised	a. from the constructor a. from the municipality
2.2.3. Improper bedding and/or foundation	- improper consolidation of bedding - improper foundation - lack of supervision	1. characteristics of bedding 1. soil characteristics of foundation 1. who and if there was supervised	a. from, the constructor a. from the constructor a. from the municipality
2.2.4. Wrongly constructed connections and/or joints	- lack of professionalism during construction - lack of supervision - improvisation due to local conditions	1. as-built report 2. inspection results 1. who and if there was supervised 1. as-built report 2. inspection results	a. from the constructor a. from the municipality a. from the constructor
2.2.5. Weakened structural elements	- low strength properties of plastic pipes - sever pipe deterioration	1. deformation of pipes 1. sever cracks, pipe brakes, infiltration	a. from the inspection (e.g. CCTV) a. from the inspection (e.g. CCTV)
2.2.6. Root intrusion	$\Rightarrow$ Table 2.1	$\Rightarrow$ Table 2.1	$\Rightarrow$ Table 2.1
2.2.7. Inappropriate load transfer	- improper traffic load - load due to construction around the sewer	1. nature and density of the traffic 1. if proper measures were taken during construction 2. structure conditions	a. from the municipality a. from the constructor b. from the inspection
2.2.8. Improper sewer maintenance	- un/experience of maintenance team - improper/absence sewer cleaning - improvisation due to local conditions - use of inappropriate equipment	1. checking of maintenance result 1. checking of maintenance reports 1. checking of maintenance reports 1. checking of maintenance reports	a. from, municipality a. from municipality a. from municipality a. from municipality
2.2.9. Improper rehabilitation	- un/experience of rehabilitation team	1. checking of rehabilitation results	a. from municipality
2.2.10. Extreme events	- earthquakes, landslides etc.	1. occurrence of the events	a. from historical records
2.2.11. Abuse	- (un)purposely placing objects in sewer	1. checking the existence of unsuitable objects	a. from the inspection

2.3 Sedimentation	Cause	Information needed on cause	Where to get information
2.3.1. Design errors	⇒ Table Flooding A-1.2	⇒ Table Flooding A-1.2	⇒ Table Flooding A-1.2
2.3.2. Construction errors	⇒ Table Flooding A-1.3	⇒ Table Flooding A-1.3	⇒ Table Flooding A-1.3
2.3.3. Ingress of soil	⇒ Table Flooding A-2.4	⇒ Table Flooding A-2.4	⇒ Table Flooding A-2.4
2.3.4. Improper sewer maintenance	- un/experience of maintenance team - improper/absence sewer cleaning - improvisation due to local conditions - use of inappropriate equipment	1. checking of maintenance results 1. checking of maintenance reports 1. checking of maintenance reports 1. checking of maintenance reports	a. from the municipality a. from the municipality a. from the municipality a. from the municipality
2.3.5. Abuse	⇒ Table Flooding A-1.5	⇒ Table Flooding A-1.5	⇒ Table Flooding A-1.5
2.3.6. Usage of urban area	-no cleaning of urban areas -abuse of surface areas	1. checking frequency of cleaning of urban areas 1. checking complaints reports	a. from the municipality a. from the municipality
2.3.7. Uneven soil settlement	⇒ Table Structural B-2.2	⇒ Table Structural B-2.2	⇒ Table Structural B-2.2
2.3.8. Pump operation and maintenance	⇒ Table Mechanical A-1.4	⇒ Table Mechanical A-1.4	⇒ Table Mechanical A-1.4

2.4 Ingress of soil	Cause	Information needed on cause	Where to get information
2.4.1. Improper pipe positioning	- improper quality of backfill - lack of supervision - pipes barely connected	1. soil characteristics of backfill 1. who and if there was supervision 1. position of pipes	a. from the constructor b. from the measuring a. from the municipality a. from the constructor b. from the inspection
2.4.2. Damaging during refilling and/or compaction	- cores material in backfill - lack of supervision	1. soil characteristics of backfill 2. how it was compacted 1. who and if there was supervised	a. from the constructor a. from the municipality
2.4.3. Improper bedding and/or foundation	- improper consolidation of bedding - improper foundation - lack of supervision	1. characteristics of bedding 1. soil characteristics of foundation 1. who and if there was supervised	a. from the constructor a. from the constructor a. from the municipality
2.4.4. Wrongly constructed connections and/or joints	- lack of professionalism during construction - lack of supervision - improvisation due to local conditions	1. as-built report 2. inspection results 1. who and if there was supervised 1. as-built report 2. inspection results	a. from the constructor a. from the municipality a. from the constructor
2.4.5. Improper choice of pipe and joint type/material	- un/experienced engineer - lack of quality check - lack of appropriate data	1. checking of design protocol 1. checking of final report 1. checking the quality of initial data necessary for the design	a. inside the design company a. from the contractor a. sources of initial data: (e.g. material → manufacture)
2.4.6. Weakened structural elements	- low strength properties of plastic pipes - sever pipe deterioration	1. deformation of pipes 1. sever cracks, pipe brakes, infiltration	a. from the inspection (e.g. CCTV) a. from the inspection (e.g. CCTV)
2.4.7. Groundwater table	- high groundwater table - aggressive ground water	1. measurement of groundwater table 1. ground water quality	a. from measuring programs (ground,water table) a. from measuring programs
2.4.8. Root intrusion	⇒ Table Flooding A-2.1	⇒ Table Flooding A-2.1	⇒ Table Flooding A-2.1
2.4.9. Inappropriate load transfer	- improper traffic load - load due to construction around the sewer	1. nature and density of the traffic 1. if proper measures were taken during construction 2. structure conditions	a. from the municipality a. from the constructor b. from the inspection

A-3. Human error & External effects

3.1. Other construction	Cause	Information needed on cause	Where to get information
3.1.1. Design management	- lack of coordination of disciplines of urban planning - changes in design of master plan	1. all the disciplines of master plan design (too complex)	a.project developer (-)
3.1.2. Documentation of design	- improper management of documentation - final built situation design report	1. checking report 1. checking report / if it exists	a. inside company a. inside company
3.1.3. Abuse	- (un)purposely placing objects in sewer	1. checking the existence of unsuitable objects	a. from the inspection

B. FLOODING - CAPACITY INCREASE

B-1. Natural impact

1.1. Climate change	Cause	Information needed on cause	Where to get information
1.1.1. Natural causes	- variations in solar radiation; variations in the Earth's orbit; continental drift *etc.*	- monitor the climate conditions	a. from meteorological institute
1.1.2. Human causes	- greenhouse gas emission	- monitor the greenhouse effect	a. from meteorological institute

1.2. Local area characteristics	Cause	Information needed on cause	Where to get information
1.2.1. Topography	- surface shape and features themselves	1. topographic maps	a.from the municipality
1.2.2. Soil permeability	- more impervious soil - amount and type of vegetation	1. area soil maps 2. area vegetation maps	a.from geological institute b. from the municipality; survey

B-2 Anthropogenic impact

2.1. Urbanisation	Cause	Information needed on cause	Where to get information
2.1.1. Water consumption	- increase in population	1. population projections	a. survey
2.1.2. Amount of impervious surface	- increase in impervious surface	1. urbanisation planning	a. from the municipality
2.1.3. Usage of urban area	- change in usage of certain urban area	1. urbanisation planning	a. from the municipality

2.2. Urban water management	Cause	Information needed on cause	Where to get information
2.2.1. Water consumption	- increase in population	1. population projections	a. survey
2.2.2. Rationality of water consumption	- awareness of rational water consumption	1. informed citizens	a. from the municipality; survey
2.2.3. Infrastructure development	- underdeveloped infrastructure	1. current asset	a. from the municipality

B-3. ANTHROPOGENIC IMPACT & NATURAL IMPACT

3.1. Surface water bodies	Cause	Information needed on cause	Where to get information
3.1.1. Water level of water bodies	- increase of water level	1. water level	a. from the water board
3.1.2. Management of surface water	- improper surface water management	1. surface water storage	a. from the municipality and the water board

A. FREQUENT CSOs - CAPACITY DECREASE

A-1.Human error

A-1.1. Design error ⇒ Flooding A-1.2

1.2. Construction error	Cause	Information needed on cause	Where to get information
1.2.1. Improper pipe positioning	⇒ Table Flooding A-1.3.1	⇒ Table Flooding A-1.3.1	⇒ Table Flooding A-1.3.1
1.2.2. Improper bedding/foundation	⇒ Table Flooding A-1.3.3	⇒ Table Flooding A-1.3.3	⇒ Table Flooding A-1.3.3
1.2.3. Wrongly constructed weirs	- lack of professionalism during construction	1. as-built report 2. inspection results	a. from the constructor
	- lack of supervision	1. who and if there was supervised	a. from the municipality
	- improvisation due to local conditions	1. as-built report 2. inspection results	a. from the constructor a. from inspection
1.2.4. Absence of inspection after construction	⇒ Table Flooding A-1.3.7	⇒ Table Flooding A-1.3.7	⇒ Table Flooding A-1.3.7

A-1.3. Operation and Maintenance ⇒ Flooding A-1.4

B. FREQUENT CSOs - CAPACITY INCREASE

B-1. Natural impact ⇒ Flooding B-1

SOIL CONTAMINATION AND EXPOSE TO HEALTH HAZARDS

A. Soil contamination

1. Exfiltration	Cause	Information needed on cause	Where to get information
1.1. Groundwater table	⇒ Table Flooding A-2.3.7	⇒ Table Flooding A-2.3.7	⇒ Table flooding A-2.3.7
1.2. Pressurised sewer	- increase and/or decrease of flow capacity	1. monitor water level in the system	a. from the municipality
1.3. Wrongly constructed connections and/or joints	⇒ Table Flooding A-1.3.4	⇒ Table Flooding A-1.3.4	⇒ Table Flooding A-1.3.4
1.4. Weakened structural elements	⇒ Table Flooding A-2.3.6	⇒ Table Flooding A-2.3.6	⇒ Table Flooding A-2.3.6

B. Exposure to health hazards

B-1. ⇒ Flooding (*prolonged period of exposure*)

2. Wastewater characteristics	Cause	Information needed on cause	Where to get information
2.1. Concentration of pollutants	- *e.g.* wastes with substantial sulphide or organic sulphur/sulphate contents	1. amount of organic material 2. concentration of sulphide/sulphate	a. from *in situ* sampling and measurements
	- presence of forbidden pollutants in sewer	1. potential sources (*e.g.* industry, hospitals)	a. from survey b. from *in situ* sampling and measurements

3. Public awareness	Cause	Information needed on cause	Where to get information
3.1. Contact with wastewater	- lack of awareness regarding the danger of having contact with wastewater	1. informed citizens	a. from the municipality; survey
3.2. Inadequate protection	- lack of awareness regarding the proper protection from contamination	1. informed citizens	a. from the municipality; survey

B-4. Operation and Maintenance ⇒ Flooding A-1.4

5. Abuse	Cause	Information needed on cause	Where to get information
5.1. Disposal of unsuitable waste	- accidental/deliberate of polluted water	1. checking the existence of uncommon damages 2. potential sources (*e.g.* industry, hospitals)	a. from the inspection a. from survey b. from *in situ* measurements

6. Danger for sewer workers	Cause	Information needed on cause	Where to get information
6.1. Danger from traffic	- lack of awareness	1. informed workers	a. from the municipality and/or inspection company; survey
6.2. Danger from toxic gasses	- lack of awareness	1. informed workers	a. from the municipality and/or inspection company; survey
6.3. Improper handling of manhole covers	- lack of awareness	1. informed workers	a. from the municipality and/or inspection company; survey
6.4. Improper handling of inspection equipment	- lack of awareness	1. informed workers	a. from the municipality and/or inspection company; survey
6.5. Inadequate protection	- lack of awareness	1. informed workers	a. from the municipality and/or inspection company; survey

A Structural collapse - strength decrease

A-1. Human error ⇒ Flooding A-1

A-2. External effects

2.1. Wastewater characteristics	Cause	Information needed on cause	Where to get information
2.1.1. Concentration of pollutants	- wastes with substantial sulphide or organic sulphur/sulphate contents - chlorine from brackish/see water - presence of forbidden pollutants in sewer	1. amount of organic material 2. concentration of sulphide/sulphate 1. concentration of chlorine 1. potential sources (*e.g.* industry, hospitals)	a. from *in situ* sampling and measurements a. from in-situ sampling and measurements a. from survey b. from *in situ* sampling and measurements
2.1.2. Nature of pollutants	- low wastewater velocities - wastewater temperature and its fluctuation - high wastewater velocities with solid material - low pH and low dissolved oxygen content	1. wastewater velocities 1. temperature 1. wastewater velocity 2. nature of sewer deposit 1. pH value 2. amount of dissolved oxygen	a. from *in situ* sampling and measurements a. from *in situ* sampling and measurements a. from *in situ* sampling and measurements a. from *in situ* sampling and measurements

2.2. Groundwater characteristics	Cause	Information needed on cause	Where to get information
2.2.1. Groundwater table	- high groundwater table - aggressive ground water	1. measurement of groundwater table 1. ground water quality	a. from measuring programs a. from *in situ* sampling and measurements

A-3. Human error & External effects

3.1. Other construction	Cause	Information needed on cause	Where to get information
3.1.1. Design management	- lack of coordination of disciplines of urban planning - changes in design of master plan	1. all the disciplines of master plan design (too complex)	a.project developer (-)
3.1.2. Documentation of design	- improper management of documentation - final built situation design report	1. checking report 1. checking report / if it exists	a. inside company a. inside company
3.1.3. Abuse	- (un)purposely placing objects in sewer	1. checking the existence of unsuitable objects	a. from the inspection

B. Structural collapse - load increase

B-1. Anthropogenic impact

1.1. Traffic load	Cause	Information needed on cause	Where to get information
1.1.1. Heavy traffic	- improper traffic control	1. checking the real time traffic control systems	a. traffic control centre
	- decreased motorway capacity	1. number of vehicle per inhabitant 2. number of inhabitants	a. surveys b. census reports
	- inefficient motorway design	1. (too complex)	a. (-)
1.1.2. Poor quality of road	- lack of professionalism during construction	1. as-built report 2. inspection results	a. from the constructor
	- lack of supervision	1. who and if there was supervised	a. from the municipality
	- poor quality of road material	1. checking with manufacturer	a.from manufacturer
	- poor structural design	1. checking of final report	a. inside company

1.2. Structures in proximity of sewer	Cause	Information needed on cause	Where to get information
1.2.1. Design management	- lack of coordination of disciplines of urban planning	1. all the disciplines of master plan design	a.project developer
	- changes in design of master plan	(too complex)	(-)
1.2.2. Documentation of design	- improper management of documentation	1. checking report	a.inside the company
	- final built situation design report	1. checking report / if it exists	a. inside the company
1.2.3. Construction in proximity of sewer	- load and vibrations due to construction	1. construction practices in the area	a. from the municipality

1.3. Abuse	Cause	Information needed on cause	Where to get information
1.3.1. High load disposal of waste	- unauthorized waste disposal (*e.g.* industry)	1. industrial waste disposal practise	a. from particular company

B-2. Natural impact

B-2.1 Root intrusion ⇒ Flooding A-2.1

2.2. Uneven soil settlement	Cause	Information needed on cause	Where to get information
2.2.1. Improper pipe positioning	- improper quality of backfill	1. soil characteristics of backfill	a. from the constructor b. from the measuring
	- lack of supervision	1. who and if there was supervision	a. from the,municipality
	- pipes barely connected	1. position of pipes	a. from the constructor b. from the inspection
2.2.2. Improper bedding and/or foundation	- improper consolidation of bedding	1. characteristics of bedding	a. from the constructor
	- improper foundation	1. soil characteristics of foundation	a. from the constructor
	- lack of supervision	1. who and if there was supervised	a. from the municipality
2.2.3. Improper refilling and/or compaction	- improper consolidation of backfill	1. soil characteristics of backfill 2. how it was compacted	a. from the constructor
	- lack of supervision	1. who and if there was supervised	a. from the municipality
2.2.4. Traffic load	⇒ Table Structural B-1.1	⇒ Table Structural B-1.1	⇒ Table Structural B-1.1
2.2.5. Soil conditions	- groundwater drawdown	1. measurement of groundwater table	a. from measuring programs
	- poor soil conditions	1. soil texture/structure moisture and temperature	a. from measuring programs

2.3. Extreme events	Cause	Information needed on cause	Where to get information
2.3.1. High discharge	- floods, natural water catastrophes (*e.g.* tsunami)	1. occurrence of the events	a. from historical records
2.3.2. Ground movement	- earthquakes, landslides *etc.*	1. occurrence of the events	a. from historical records

B-3. Anthropogenic impact & Natural impact

3.1. Sinkholes	Cause	Information needed on cause	Where to get information
3.1.1. Ingress of soil	⇒ Table Flooding A-2.4	⇒ Table Flooding A-2.4	⇒ Table Flooding A-2.4
3.1.2. Traffic load	⇒ Table Structural B-1.1	⇒ Table Structural B-1.1	⇒ Table Structural B-1.1
3.1.3. Construction in proximity of sewer	- load and vibrations due to construction	1. construction practices in the area	a. from municipality

A. Mechanical collapse - strength decrease

A-1. Human error

A-1.1 Production error ⇒ Flooding A-1.1

A-1.2 Design error ⇒ Flooding A-1.2

1.3. Construction error	Cause	Information needed on cause	Where to get information
1.3.1. Improper choice of pipe and joint type/material	- un/experienced engineers - lack of quality check - lack of appropriate data	1. checking of design protocol 1. checking of final report 1. checking the quality of initial data necessary for the design	a. inside the design company a. from the contractor a. sources of initial data: (*e.g.* material → manufacture)
1.3.2. Wrong constructed weirs	- lack of professionalism during construction - lack of supervision - improvisation due to local conditions	1. as-built report 2. inspection results 1. who and if there was supervised 1. as-built report 2. inspection results	a. from the constructor a. from the pump operators a. from the constructor a. from inspection
1.3.3. Wrong constructed pumping station	- lack of professionalism during construction - lack of supervision - improvisation due to local conditions	1. as-built report 2. inspection results 1. who and if there was supervised 1. as-built report 2. inspection results	a. from the constructor a. from the municipality a. from the constructor a. from inspection
1.3.4. Wrong constructed connections/joints and/or (revers) valves	- lack of professionalism during construction - lack of supervision - improvisation due to local conditions	1. as-built report 2. inspection results 1. who and if there was supervised 1. as-built report 2. inspection results	a. from the constructor a. from the pump operators a. from the constructor a. from inspection
1.3.5. Wrong constructed inlet and/or outlet	- lack of professionalism during construction - lack of supervision - improvisation due to local conditions	1. as-built report 2. inspection results 1. who and if there was supervised 1. as-built report 2. inspection results	a. from the constructor a. from the pump operators a. from the constructor a. from inspection
1.3.6. Improper PLC installation	- lack of professionalism and supervision	1. as-built report	a. from the constructor
1.3.7. Absence of inspection after construction	- lack of professionalism and supervision	1. as-built report	a. from the constructor

1.4. Operation and Maintenance	Cause	Information needed on cause	Where to get information
1.4.1. Improper sewer condition assessment	- un/experienced inspector - lack of professionalism - improper data assessment	1. checking of inspection results 1. checking of inspection protocol 1. checking of final data assessment	a. from the pump operators a. from the pump operators a. inside the municipality
1.4.2. Improper sewer maintenance	- un/experience of maintenance team - improper/absence pump cleaning - improvisation due to local conditions - use of inappropriate equipment	1. checking of maintenance results 1. checking of maintenance reports 1. checking of maintenance reports 1. checking of maintenance reports	a. from the pump operators a. from the pump operators a. from the pump operators a. from the pump operators
1.4.3. Inherent uncertainties	- lack of appropriate data - improper standardisation	1. research 1. research	a. scientific research institutions a. scientific research institutions
1.4.4. Improper rehabilitation	- un/experience of rehabilitation team - lack of professionalism during rehabilitation - improvisation due to local conditions - use of inappropriate equipment	1. checking of rehabilitation results 1. checking of rehabilitation reports 1. checking of rehabilitation reports 1. checking of maintenance reports	a. from the pump operators a. from the pump operators a. from the pump operators a. from the pump operators

1.5. Abuse	Cause	Information needed on cause	Where to get information
1.5.1. Unsuitable waste	- accidental/deliberate disposal of inappropriate waste	1. checking the existence of uncommon damages 2. potential sources	a. from the inspection a. from survey b. from *in situ* inspection
1.5.2. Illegal access to pumping station	- damaging and/or stealing - PLC manipulation	1. surveillance information 1. surveillance information	a. from the surveillance a. from the surveillance

A-2. External effects

A-2.1 Wastewater characteristics ⇒ Structural A-2.1

A-3. Human error & External effects

3.1. Control system failure	Cause	Information needed on cause	Where to get information
3.1.1. Power system failure	- *e.g.* thunder strike	1. reported failures	a. from the pump operators
3.1.2. PLC malfunction	- *e.g.* short circuiting; manipulation	1. reported failures	a. from the pump operators

B. MECHANICAL COLLAPSE - LOAD INCREASE

B-1. Human error

1.1. Operation and Maintenance	Cause	Information needed on cause	Where to get information
1.1.1. Improper sewer condition assessment	⇒ Table Mechanical A-1.4.1	⇒ Table Mechanical A-1.4.1	⇒ Table Mechanical A-1.4.1
1.1.2. Improper sewer maintenance	⇒ Table Mechanical A-1.4.2	⇒ Table Mechanical A-1.4.2	⇒ Table Mechanical A-1.4.2
1.1.3. Inherent uncertainties	⇒ Table Mechanical A-1.4.3	⇒ Table Mechanical A-1.4.3	⇒ Table Mechanical A-1.4.3

1.2. Abuse	Cause	Information needed on cause	Where to get information
1.2.1. High load disposal of waste	- PLC manipulation	1. surveillance information	a. from the surveillance

B-2. External effects

2.1. Wastewater characteristics	Cause	Information needed on cause	Where to get information
2.1.1. Nature of pollutants	- wastes with substantial fat content - blockage by different materials	1. amount of grease and fat 1. nature of sewer deposit	a. from *in situ* sampling and measurements a. from *in situ* sampling and measurements

2.2. Extreme events	Cause	Information needed on cause	Where to get information
2.3.1. High discharge	- floods, natural water catastrophes (*e.g.* tsunami)	1. occurrence of the events	a. from historical records
2.3.2. Ground movement	- earthquakes, landslides *etc.*	1. occurrence of the events	a. from historical records

B.3. Human error & External effects

3.1. Control system failure	Cause	Information needed on cause	Where to get information
3.1.1. Power system failure	- *e.g.* thunder strike	1. reported failures	a. from the pump operators
3.1.2. PLC malfunction	- *e.g.* short circuiting; manipulation .	1. reported failures	a. from the pump operators

LIST OF SYMBOLS

SYMBOL	UNIT	PROPERTY
A	m	true value for the measured distance
a, b, c	m^{-1}	coefficients defining the plane of the reflection board
b_0, b_1	-	estimated regression coefficients
$b_{x_{FRONT}}$	m	x coordinates of a point as observed on the optical sensor of cam_{FRONT}
$b_{y_{FRONT}}$	m	y coordinates of a point as observed on the optical sensor of cam_{FRONT}
$b_{x_{BACK}}$	m	x coordinates of a point as observed on the optical sensor of cam_{BACK}
$b_{y_{BACK}}$	m	y coordinates of a point as observed on the optical sensor of cam_{BACK}
$C_{xx}(\phi)$	mHz^{-1}	sample spectrum
C_s	various	skewness
C_v	various	coefficient of variation
c_i	-	decrease of the spatial resolution
c_x, c_y	pixel	x, y camera optical centre
$camoff_x$	m	camera offset in the x direction
$camoff_y$	m	camera offset in the y direction
$camoff_z$	m	camera offset in the z direction
$class_{avg}$	-	average classification over the length
D_h	m	hydraulic diameter
d_i	m	distance between stationary laser stand and reflection board for laser distance meters $i = 1, 2, 3$ in coordinate system $\mathfrak{R}^{(3)}$
$d_{z_{FRONT}}$	m	distance between laser sheet and lens plane for cam_{FRONT}
$d_{z_{BACK}}$	m	distance between laser sheet and lens plane for cam_{BACK}
E	-	allowed difference between the estimated mean value and the 'true' value
$e_{(i)}$	various	PRESS residuals
$e_{z_{FRONT}}$	m	distance between optical sensor and lens plane for cam_{FRONT}
$e_{z_{BACK}}$	m	distance between optical sensor and lens plane for cam_{BACK}
F	-	cumulative distribution of Z1
F_h	N	horizontal force
F_v	N	vertical force
$F_{v,max}$	N	cracking force (occurrence of the first crack)
f	-	Darcy-Weisbach friction factor
f_e	-	equivalent Darcy friction factor of the pipe
f_x, f_y	pixel	x, y camera focal length
G	-	cumulative Gaussian distribution
g	m/s^2	gravitational acceleration

H	m	height of the pipe
h	m	water depth in the pipe
h_f	m	Darcy-Weisbach head loss
h_λ	m	mean range height
K	-	camera intrinsic matrix
k_1, k_2, k_3	-	radial distortion coefficients of the camera-lens
k_s	m	Nikuradse's equivalent sand-grain roughness
L	m	length of the conduit
M	m	measured distance
N	-	number of data points of the sample spectrum
N_1, N_2	-	sample sizes for the group 1 and 2
N_C	-	number of scanned objects consistant with measurements using calliper
$N(h)$	-	number of data pairs for given distance
N_T	-	total number of scanned objects
n	-	Manning's coefficient
n_e	-	equivalent Manning's coefficient of the pipe
n_s	-	sampling size
o, p, n	m	three vectors define the orthogonal base for the coordinate system $\Psi^{(3)}$
o_n, p_n, n_n	-	normalised orthogonal basis for the coordinate system $\Psi^{(3)}$
PRESS	various	statistics derived from the predicted residual sum of squares
p_1, p_2	-	tangential distortion coefficients of the camera-lens
p_i	m	wetted perimeter in each region i
$p_{\Psi^{(2)}_{c2_{i=1,2,3}}}$	m	x, y location of the projection of laser $i = 1, 2, 3$ in the coordinate system $\Psi^{(2)}$
$p_{\mathfrak{R}^{(2)}_{c2_{i=1,2,3}}}$	m	x, y location of the projection of laser $i = 1, 2, 3$ in the coordinate system $\mathfrak{R}^{(2)}$
$p^{(2)}_{\mathfrak{R}_{reference,1\rightarrow2}}$	m	vector between the x and y coordinates of lasers 1 and 2 in the coordinate system $\mathfrak{R}^{(2)}$
$p^{(2)}_{\mathfrak{R}_{1\rightarrow2}}$	m	vector between the x and y coordinates of the projected points of lasers 1 and 2 in the coordinate system $\mathfrak{R}^{(2)}$
pixel	m	pixel size
Q	m^3/s	discharge in a partially filled pipe
Q_{full}	m^3/s	full pipe discharge
R	-	3D rotation of the camera
$\bar{R}$	-	run test statistic
R_1, R_2	-	sums of the ranks assigned to the group 1 and 2
R^2	-	coefficient of determination
R^2_{PRESS}	-	predicted coefficient of determination
R_C	-	measurment consistency rate
R_h	m	hydraulic radius
R_e	-	Reynolds number

$\underline{\underline{R}}_{z(2)}$	-	two-dimensional rotation matrix for the z-axis
$\underline{\underline{R}}_{z(3)}$	-	three-dimensional rotation matrix for the z-axis
$\underline{\underline{R}}_{\Psi(2)}$	-	transformation matrix in coordinate system $\Psi^{(2)}$
$\underline{\underline{R}}_{\Psi(3)}$	-	transformation matrix in coordinate system $\Psi^{(3)}$
$\mathfrak{R}^{(2)}$	-	reference coordinate system in 2 dimensions ($z = 0$)
$\mathfrak{R}^{(3)}$	-	reference coordinate system in 3 dimensions
$S_{SCANNED}$	m	the dimensions of the object measured with laser profiler
$S_{MEASURED}$	m	the dimensions of the object measured with calliper
s	various	initial estimate for the standard deviation
s_x, s_y	-	the number of pixels per world unit in the x, y direction
s_{FRONT}	-	scaling factor for cam_{FRONT}
$s_{x_{FRONT}}$	-	scaling factor in the x direction for cam_{FRONT}
$s_{y_{FRONT}}$	-	scaling factor in the y direction for cam_{FRONT}
s_{BACK}	-	scaling factor for cam_{BACK}
$s_{x_{BACK}}$	-	scaling factor in the x direction for cam_{BACK}
$s_{y_{BACK}}$	-	scaling factor in the y direction for cam_{BACK}
T	-	translation of the camera relative to the world coordinate system
TSS	various	total sum of squares
t	-	length of series of the sample spectrum
U_1, U_2	-	Mann-Whitney statistic for the group 1 and 2
V_f	-	full resolution of the validation sample
V_i	-	decreased resolution of the validation sample
v	m/s	flow velocity in a partially filled pipe
$\bar{v}$	m/s	average flow velocity
$\underline{v}$	various	vector containing all the measured variables for the uncorrected projected points
$\underline{v}_c$	various	vector containing all the measured variables for the corrected projected points
v_{full}	m/s	full pipe velocity
w	-	arbitrary homogeneous coordinates scale factor
X, Y, Z	m	world coordinates of a point
X1, Y1, Z1	m	raw-sample-data coordinates
X2, Y2, Z2	m	interpolated-sample-data coordinates
x, y, z	m	coordinates
x_i, y_i	m	x, y location of laser i =1, 2, 3 in the reference coordinate system $\mathfrak{R}^{(3)}$
$x_{distorted}$	m	distorted pixel location x
$y_{distorted}$	m	distorted pixel location y
Z_{OK}	m	ordinary kriging estimate
Zt_{score}	-	residual divided by kriging standard error
Zt	-	normal-score transformation of Z1 coordinates
$Z_{\alpha/2}$	-	value from standard normal distribution corresponding to desired confidence level
α	-	significance level

α_{misal}	rad	misalignment of the lasers
γ	-	relative confidence interval
$\hat{\gamma}(h)$	m^2	semivariance
Δ	-	sampling interval of the sample spectrum
Δx	m	x-shift of the camera platform in $\mathfrak{R}^{(2,3)}$
Δy	m	y-shift of the camera platform in $\mathfrak{R}^{(2,3)}$
Δz	m	z-shift of the camera platform in $\mathfrak{R}^{(3)}$
$\underline{\Delta}_{orig}$	m	vector containing Δx, Δy and Δz
$\theta_x, \theta_y, \theta_z$	rad	pitch (x-axis), yaw (y-axis) and roll (z-axis) rotation angle
κ	-	kernel smoothening weight
$\lambda(u)$	-	kriging weight of each observation
λ_c	-	centroidal wavelength
μ	various	mean
σ	various	standard deviation
σ_i	various	standard deviation in parameter i
σ_{in}	m	spatial interpolation uncertainty
σ_m	m	measured uncertainty
$\sigma_{misaligment}$	rad	laser misaligment uncertainty
σ_{OK}	m	corresponding ordinary kriging prediction standard deviation
σ_{tot}	m	total uncertainty
$\sigma_{wall\ loss}$	m	uncertainty of loss of wall thickness
$\sigma_x, \sigma_y, \sigma_z$	m	uncertainty in the x, y and z direction
Φ_c	Hz	centroid frequency
ϕ	Hz	frequency
$\chi^{2(\beta)}_{n_s-1}$	-	β quantile for chi-squared distribution with n_s-1 degrees of freedom
$\Psi^{(2)}$	-	moving platform coordinate system in 2 dimensions (z = 0)
$\Psi^{(3)}$	-	moving platform coordinate system in 3 dimensions

BIBLIOGRAPHY

Ackers, P. (1961). The hydraulic resistance of drainage conduits. *Proc. Inst. Civ. Eng., 19*(3), 307-336.

Ackers, P., Crickmore, M. J., & Holmes, M. J. (1964). Effects of use on the hydraulic resistance of drainage conduits. *Proc. Inst. Civ. Eng., 28*(3), 339-360.

Akhtar, S. (2013). Review of Nondestructive Testing Methods for Condition Monitoring of Concrete Structures. *Journal of construction engineering*, (Vol. 2013), Article ID 834572, 1-11.

Ali, S., & Uijttewaal, W. S. J. (2012). Flow Resistance of Vegetated Weirlike Obstacles During High Water Stages. *Journal of Hydraulic Engineering, 139*(3), 325-330.

Ana, E., & Bauwens, W. (2007, September). *Sewer Network Asset Management Decision Support Tools: A Review.* Paper presented at the International Symposium on New Directions in Urban Water Management, UNESCO Paris, France.

Arsénio, A. M., Vreeburg, J., & Rietveld, L. (2013). Quantitative non-destructive evaluation of push-fit joints. *Urban Water Journal, 11*(8), 657-667.

Ashley, R., Blackwood, D., Butler, D., Davies, J. Jowitt, P., & Smith, H. (2003). Sustainable decision making for the UK water industry. *Engineering Sustainability, 156*, 41-49.

Ashley, R., & Hopkinson, P. (2002). Sewer systems and performance indicators–into the 21st century. *Urban water, 4*, 123-135.

Baranowski, L. (2013). Equations of motion of a spin-stabilized projectile for flight stability testing. *Journal of theoretical and applied mechanics, 51*(1), 235-246.

Beekhuizen, J., Heuvelink, G. B. M., Biesemans, J., & Reusen, I. (2011). Effect of DEM uncertainty on the positional accuracy of airborne imagery. *Geoscience and Remote Sensing, IEEE Transactions on, 49*(5), 1567-1577.

Bennis, S., Bengassem. J., & Lamarre, P. (2003). Hydraulic performance index of a sewer network. *Journal of hydraulic engineering, 129*(7), 504-510.

Bertrand-Krajewski, J. (2008). *Programme rw123etalo: 1st, 2nd and 3rd order polynomial Williamson regression with uncertainties in both variables for sensor calibration*. INSA Lyon, LGCIE, Villeurbanne, France.

Bielecki, R., & Schremmer, H. (1987). *Biogene Schwefelsäure-Korrosion in teilgefüllten Abwasserkanälen (Biogene sulfuric acid corrosion in partially filled sewers)*. Leichtweiβ-Institut, Braunschweig.

Bivand, R. S., Pebesma, E. J., Gómez-Rubio, V., & Pebesma, E. J. (2008). *Applied spatial data analysis with R*. New York, NY: Springer.

Boden, J.B., Nath, P., Trott, J.J., & Farrar, D.M. (1975). *Research on underground pipelines at the Transport and Road Research Laboratory*. Paper presented at the symposium on R&D sewerage and drainage design, Institution of Public Health Engineers.

Brachman, R. W., Moore, I., & Rowe, R. (2000). The design of a laboratory facility for evaluating the structural response of small-diameter buried pipes. *Canadian Geotechnical Journal, 37*, 281-295.

Burian, S. J., & Edwards, F. G. (2002, September). *Historical perspectives of Urban Drainage.* Paper presented at the 9th International Conference on Urban Drainage, Portland, Oregon, United States.

Butler, D., & Davies, J. W. (2004). Urban drainage (2nd ed.). London: Spon Press.

Carrión, A., Solano, H., Gamiz, M. L., & Debón, A. (2010). Evaluation of the reliability of a water supply network from right-censored and left-truncated break data. *Water resources management, 24,* 2917-2935.

Chan, T. W. S. (2011). *Inspectie & Beoordelingsplan van vrijverval riolering 2011-2015 (Inspection & Assessment Plan of gravity sewer 2011-2015)*. The Hague, the Netherlands: Municipality of The Hague.

Civieltechnisch Centrum Uitvoering Research en Regelgeving. (2000). *Onderzoek aan de betonconstructie (Research on the concrete structure)*. (CUR 74). Gouda, the Netherlands: CUR.

Clemens, F. H. L. R. (2001). *Hydrodynamic models in urban drainage: application and calibration*. PhD thesis, Delft University of Technology, Delft, The Netherlands.

Clemens, F. H. L. R., Stanić, N., van der Schoot, W., Langeveld, J. G., & Lepot, M. (2015). Uncertainties associated with laser profiling of concrete sewer pipes for the quantification of the interior geometry. *Structure and Infrastructure Engineering, 11*(9), 1218-1239.

Comery, W. (2007). Urban and Community Forestry in the Northeast: *Tree Roots versus Sidewalks and Sewers*. In J. E. Kuser (Ed.). New York, NY: Springer

Costello, S. B., Chapman, D. N., Rogers, C. D. F., & Metje, N. (2007). Underground asset location and condition assessment technologies. *Tunnelling and Underground Space Technology, 22,* 524-542.

Cressie, N. (1988). Spatial prediction and ordinary kriging. *Mathematical Geology, 20*(4), 405-421.

Davies, J. P., Clarke, B. A., Whiter, J. T., & Cunningham, R. J. (2001a). Factors influencing the structural deterioration and collapse of rigid sewer pipes. *Urban Water, 3,* 73-89.

Davies, J. P., Clarke, B. A., Whiter, J. T., Cunningham, R. J., & Leidi, A. (2001b). The structural condition of rigid sewer pipes: a statistical investigation. *Urban Water, 3,* 277-286.

de Belie, N., Monteny, J., Beeldens, A., Vincke, E., Van Gemert, D., & Verstraete, W. (2004). Experimental research and prediction of the effect of chemical and biogenic sulfuric acid on different types of commercially produced concrete sewer pipes. *Cement and Concrete Research, 34*(12), 2223-2236.

de Borst, R., Crisfield, M. A., Remmers, J. J. C., & Verhoosel, C. V. (2012). *Non-Linear Finite Element Analysis of Solids and Structures*. (2nd ed.), Wiley series on computational mechanics. ISBN 978-0-470-66644-9

de Borst, R., Kusters, G., Nauta, P., & De Witte, F. (1985). DIANA - a comprehensive but flexible finite element system. *Finite Element System Handbook*. Berlin, Germany: Springer-Verlag.

Delleur, J. W., Reyna, S., & Vanegas, J. (1998). Sewerage rehabilitation. In J. Marsalek, C. Maksimović, E. Zeman & R. Price (Eds.), *Hydroinformatics Tools for Planning, Design, Operation and Rehabilitation of Sewer Systems* (Vol. 44, pp. 415-450). Dordrecht: Kluwer Academic.

de Silva, D., Davis, P., Burn, L. S., Ferguson, P., Massie, D., Cull, J., Eiswirth, M., & Heske, C. (2002, May). *Condition assessment of cast iron and asbestos cement pipes by in-pipe probes and selective sampling for estimation of remaining life*. Paper presented at the NODIG 2002 International Conference, Copenhagen, Denmark.

Deutsch, C. V., & Journel, A. G. (1998). *GSLIB: Geostatistical Software Library and User's Manual*: Oxford University Press, New York, NY.

Dirksen, J., Baars, E. J., Langeveld, J. G., & Clemens, F. H. L. R. (2012). Settlement as a driver for sewer rehabilitation. *Water Science and Technology, 66,* 1534-1539.

Dirksen, J., & Clemens, F. H. L. R. (2008). Probabilistic modeling of sewer deterioration using inspection data. *Water Science and Technology, 57*(10), 1635-1641.

Dirksen, J., Clemens, F. H. L. R., Korving, H., Cherqui, F., Le Gauffre, P., Ertl, T., Plihal, H., Müller, K., & Snaterse, C. T. M. (2013). The consistency of visual sewer inspection data. *Structure and Infrastructure Engineering, 9*, 214-228.

Dirksen, J., Goldina, A., Ten Veldhuis, J. A. E., & Clemens, F. H. L. R. (2009). The role of uncertainty in urban drainage decisions: uncertainty in inspection data and their impact on rehabilitation decisions. In H. Alegre & M. do Ceu Almeida (Eds.), *Strategic Asset Management of Water Supply and Wastewater Infrastructures* (pp. 273). London: IWA.

Dirksen, J. Pothof, I, Langeveld, J. G., & Clemens, F. H. L. R. (2014). Slope profile measurement of sewer inverts. *Automation in construction, 37*, 122-130.

Duran, O., Althoefer, K., & Seneviratne, L. D. (2002). State of the art in sensor technologies for sewer inspection. *Sensors Journal, IEEE, 2*, 73-81.

Duran, O., Althoefer, K., & Seneviratne, L. D. (2003). Pipe inspection using a laser-based transducer and automated analysis techniques. *IEEE/ASME Transactions on Mechatronics, 3*, 401-409.

Duran, O., Althoefer, K., & Seneviratne, L. D. (2007). Automated pipe defect detection and categorization using camera/laser-based profiler and artificial neural network. *IEEE Transactions on Automation Science and Engineering, 4*(1), 118-126.

Einstein, H. A. (1934). Der hydraulische oder profil-radius (The hydraulic or cross-section radius). *Schweizerische Bauzeitung, Zurich, 103*(8), 89-91.

Elachachi, S. M., Breysse, D., & Vasconcelos, E. (2006, June). *Uncertainties, quality of information and efficiency in management of sewer assets*. Paper presented at the Joint International Conference on Computing and Decision Making in Civil and Building Engineering, Montréal, Canada.

Elsen, J. (2006). Microscopy of historic mortars - a review. *Cement and Concrete Research, 36*, 1416-1424.

Emery, X. (2006). Ordinary multigaussian kriging for mapping conditional probabilities of soil properties. *Geoderma, 132*(1), 75-88.

English, L. P. (1999). *Improving data warehouse and business information quality: methods for reducing costs and increasing profits*. New York, NY: John Wiley & Sons.

Environmental Protection Agency. (2010). *Report on condition assessment of wastewater systems*. EPA/600/R-10/100.

European Committee for Standardization. (2002). *Concrete pipes and fittings, unreinforced, steel fibre and reinforced*. (EN 1916). Brussels, Belgium: CEN.

European Committee for Standardization. (2003). *Conditions of drain and sewer systems outside buildings - Part 2: Visual inspection coding system*. (EN 13508-2). Brussels: CEN.

European Committee for Standardization. (2012). *Testing hardened concrete - Part 1: Shape, dimensions and other requirements for specimens and moulds*. (EN 12390-1). Brussels, Belgium: CEN.

European Committee for Standardization. (2009a). *Testing concrete in structures - Part 1: Cored specimens - Taking, examining and testing in compression*. (EN 12504-1). Brussels, Belgium: CEN.

European Committee for Standardization. (2009b). *Testing hardened concrete - Part 3: Compressive strength of test specimens*. (EN 12390-3). Brussels, Belgium: CEN.

European Committee for Standardization. (2009c). *Testing hardened concrete - Part 5: Flexural strength of test specimens*. (EN 12390-5). Brussels, Belgium: CEN.

European Committee for Standardization. (2009d). *Testing hardened concrete - Part 6: Tensile splitting strength of test specimens*. (EN 12390-6). Brussels, Belgium: CEN.

European Committee for Standardization. (2009e). *Testing hardened concrete - Part 7: Density of hardened concrete*. (EN 12390-7). Brussels, Belgium: CEN.

European Committee for Standardization. (2011). *General requirements for components used in drains and sewers* (EN 476). Brussels: CEN.

European Committee for Standardization. (2013). *Common rules for precast concrete products*. (EN 13369). Brussels, Belgium: CEN.

Faber, M. H., & Stewart, M. G. (2003). Risk assessment for civil engineering facilities: critical overview and discussion. *Reliability engineering and System safety, 80*, 173-184.

Faugeras, O. (1993).*Three-dimensional computer vision: a geometric viewpoint*: MIT press.

Feldman, L. J. (1984). Regulation of root development. *Annual review of plant physiology, 35*(1), 223-242.

Feng, Z., Horoshenkov, V., Tareq, M., & Tait, S. (2012, April). *An Acoustic Method for Condition Classification in Live Sewer Networks*. Paper presented at the 18^{t}h World Conference on Non-destructive Testing, Durban, South Africa.

Fenner, R. A. (1990). Excluding groundwater infiltration into new sewers. *Water and Environment Journal, 4*, 544-551.

Fenner, R. A. (1991). Influence of sewer bedding arrangements on infiltration rates on soil migration. *Proceedings of Institution of Civil Engineers - Municipal Engineer* (Vol. 8) (pp. 105-117). London: ICE Publishing.

Frosdick, S. (1997). The techniques of risk analysis are insufficient in themselves. *Disaster Prevention and Management, 6*, 165-177.

Gemeente Den Haag. (2011). *Gemeentelijk Rioleringsplan Den Haag 2011-2015: Goed riool, gezonde leefomgeving (Municipal Sewer Plan Hague 2011-2015: Good sewer, healthy environment)*. The Hague, the Netherlands: Municipality of The Hague.

Gooch, R. M. Clarke, T. A., & Ellis. T. J. (1996). A semi-autonomous sewer surveillance and inspection vehicle. *Proceedings IEEE Intelligent Vehicles*, (pp. 64-89).

Goovaerts, P. (1997). *Geostatistics for natural resources evaluation*, New York, NY: Oxford University Press.

Gregory, P. J. (1988). Growth and functioning of plant roots. In A. Wild (Ed.), *Russell's soil conditions and plant growth*. (11th ed., pp. 113-167).

Gruber, D. (2000, September). *The mathematics of the 3D rotation matrix*. Paper presented at the Xtreme Game Developers Conference, Santa Clare, California, United States.

Guo, W., Soibelman, L., & Garrett Jr, J. (2009). Automated defect detection for sewer pipeline inspection and condition assessment. *Automation in Construction, 18*(5), 587-596.

Hahn, M. A., Palmer, R. N., Merill, M. S., & Lukas, A. (2002). Expert system for prioritizing the inspection of sewers: Knowledge base formulation and evaluation. *Journal of Water Resources Planning and Management, 128*(2), 121-129.

Halfawy, M. R., Dridi, L., & Baker, S. (2008). Integrated decision support system for optimal renewal planning of sewer networks. *Journal of Computing in Civil Engineering, 22*, 360.

Hamilton, J. D. (1994). *Time series analysis*, (Vol. 2). Princeton, NJ: Princeton university press Princeton.

Hao,T., Rogers, C. D. F, Metje, N., Chapman, D. N., Muggleton, J. M., Foo, K. Y., Wang, P., Pennock, S. R., Atkins, P. R., Swingler, S. G., Parker, J., Costello, S. B., Burrow, M.P.N., Anspach, J. H., Armitage, R. J., Cohn, A. G., Goddard, K., Lewin, P. L., Orlando,G., Redfern, M. A., Royal, A. C .D., & Saul, A.J. (2012). Condition assessment of the buried utility service infrastructure. *Tunneling and Underground Space Technology, 28*, 331-344.

Heikkila, J. & Silvén, O. (1997). A four-step camera calibration procedure with implicit image correction (*Proceedings., 1997 IEEE Computer Society Conference on Computer Vision and Pattern Recognition*), 1106-1112.

Hengl, T. (2007). *A practical guide to geostatistical mapping of environmental variables*, (Vol. 140) Ispra, Italy: European Commission. Joint Research Centre. Institute for Environment and Sustainability.

Hobbs, D. (2001). Concrete deterioration: causes, diagnosis, and minimising risk. *International Materials Reviews, 46*, 117-144.

Holiday, D. B., Ballard, J. E., & McKeown, B. C. (1995). PRESS-related statistics: regression tools for cross-validation and case diagnostics. *Medicine and Science in Sports and Exercise, 27*(4), 612-620.

Hvitved-Jacobsen, T., Vollertsen, J., & Tanaka, N. (2000). An integrated aerobic/anaerobic approach for prediction of sulfide formation in sewers. *Water Science and Technology, 41*(6), 107-115.

Ibrahim, M., Cherqui, F., Le Gauffre, P., & Werey, C. (2009, October). *Sewer asset management: From visual inspection survey to dysfunction indicators*. Paper presented at the 2nd Leading-Edge Conference of Strategic Asset Management, Lisbon, Portugal.

International Organization for Standardization. (2010). *Geometrical Product Specifications (GPS) – acceptance and reverification tests for coordinate measuring machines (CMM) – Part 5: CMMs using multiple-stylus probing systems*. (10360-5), Geneva, Switzerland: ISO.

International Organization for Standardization. (1971). *ISO system of limits and fits – Part II : Inspection of plain workpieces*. (ISO 10360-5). Geneva, Switzerland: ISO.

International Organization for Standardization. (2004). *Testing of concrete – Part 6: Sampling, preparing and testing of concrete cores*. Geneva, Switzerland: ISO.

INTRON. (1997). *Classificatiemethode toestand betonnen rioolbuizen Den Haag (Classification method of sewer pipes concrete conditions - The Hague)*. the Netherlands: Instituut voor materiaal en milieu-onderzoek b.v.

Isaaks, E. H., & Srivastava, R. M. (1989). *Applied geostatistics*, (Vol. 2). New York, NY: Oxford University Press.

JCGM 104. (2009). *Uncertainty of measurement - Part 1: Introduction to expression of uncertainty in measurement*. Geneva, Switzerland: ISO/IEC Guide 98-1.

Juran, J. M. (1964). *Managerial Breakthrough*. New York, NY: McGraw-Hill.

Kahn, B. K., Strong, D.M., & Wang, R. Y. (2002). Information quality benchmarks: product and performance. *Communications of the ACM, 45*(4), 184-192.

Kang, J., Parker, F., & Yoo, C. H. (2007). Soil-structure interaction and imperfect trench installations for deeply buried concrete pipes. *Journal of Geotechnical and Geoenvironmental Engineering, 133*, 277-285.

Kim, J., O'Connor, S., Nadukuru, S., Lynch, J. P., Michalowski, R., Green, R. A., Pour-Ghaz, M., Weiss, W. J., & Bradshaw, A. (2010, March). *Behavior of full-scale concrete segmented pipelines under permanent ground displacements*. Paper presented at SPIE Smart Structures and Materials + Nondestructive Evaluation and Health Monitoring, San Diego, California, United States.

Kirkham, R., Kearney, P. D., Rogers, K. J., & Mashford, J. (2000). PIRAT - a system for quantitative sewer pipe assessment. *The International Journal of Robotics Research, 19*(11), 1033-1053.

Kirwan, B. (1992). Human error identification in human reliability assessment. Part 1: Overview of approaches. *Applied Ergonomics, 23*, 299-318.

Kleijwegt, R. A. (1993). On the prediction of sediment transport in sewers with deposits. *Water Science and Technology, 27*(5-6), 69-80.

Korving, H. (2004). *Probabilistic assessment of the performance of combined sewer systems*. PhD thesis, Delft University of Technology, Delft, The Netherlands.

Korving, H., & Clemens, F. H. L. R. (2004, November). *Reliability of coding of visual inspections of sewers*. Paper presented at the 4th International Conference on Sewer Processes and Networks, Funchal, Portugal.

Korving, H., Van Noortwijk, J. M., Van Gelder, P., & Parkhi, R. S. (2003). Coping with uncertainty in sewer system rehabilitation. In T. Bedford & P. H. A. J. M. van Gelder (Eds.), *Safety and Reliability*. Lisse: Swets & Zeitlinger.

Krige, D. G. (1951). A statistical approach to some basic mine valuation problems on the Witwatersrand. *Journal of Chemical, Metallurgical, and Mining Society of South Africa, 52*, 119-139.

Krizek, R. J., & McQuade, P. V. (1978). Behavior of buried concrete pipe. *Journal of Geotechnical and Geoenvironmental Engineering, 104* (ASCE 13899 Proceeding).

Kumar, R. (2005). Research methodology: A step-by-step guide for beginners (2nd ed.). London: Sage Publications Limited.

Le Gauffre, P., Joannis, C., Vasconcelos, E., Breysse, D., Gibello, C., & Desmulliez, J. J. (2007). Performance indicators and multicriteria decision support for sewer asset management. *Journal of Infrastructure Systems, 13*, 105-114.

Long, R., & Faram, M. G. (2014, October). *SewerBatt® - using sound to assess the condition of sewers and drains*. Paper presented at the 8th European Waste Water Management Conference, Manchester, UK.

Louangrath, P. T. (2014, May). *Sample Size Determination for Non-Finite Population*. Paper presented at the International Conference on Discrete Mathematics and Applied Science, Bangkok, Thailand.

Makar, J. M. (1999). Diagnostic techniques for sewer systems. *Journal of Infrastructure Systems, 5*, 69-78.

Marquardt, D. W. (1963). An algorithm for laser-squares estimation of nonlinear parameters. *Journal of the Society for Industrial and Applied Mathematics, 11*(2), 431-441.

Marsalek, J., & Schilling, W. (1998). Operation of sewer systems. In J. Marsalek, C. Maksimović, E. Zeman & R. Price (Eds.), *Hydroinformatics Tools for Planning, Design, Operation and Rehabilitation of Sewer Systems* (Vol. 44, pp. 393-414). Dordrecht Kluwer: Academic.

Matheron, G. (1971). *The theory of regionalized variables and its applications*, (Vol. 5). Paris, France: Ecole nationale supÃ©rieure des mines de Paris.

McPherson, E. G., & Pepér, P. J. (1995). Infrastructure repair costs associated with street trees in 15 cities. In G. W. Watson & D. Neely (Eds.), *Trees and building sites* (pp. 49-63). Champaign, IL: International Society of Arboriculture.

Minoshima, K. & Matsumoto, H. (2000). High-accuracy measurement of 240-m distance in an optical tunnel by use of a compact femtosecond laser. *Applied Optics, 39*(30), 5512-5517.

Montague, D. F. (1990). Process risk evaluation – What method to use? *Reliability Engineering and System Safety, 29*(1), 27-53.

Myers, R. (1990). Classical and Modern Regression with Applications (2nd ed.). Boston, MA: Duxbury Press.

Naumann, F., & Rolker, C. (2000, October). *Assessment methods for information quality criteria*. Paper presented at the 5th Conference on Information Quality, Cambridge, MA.

Nederlands Normalisatie Instituut. (2004a). *Buitenriolering - Classificatiesysteem bij visuele inspectie van objecten (Sewerage systems outside buildings - Classification system for visual inspection of objects)*. (NEN 3399). Delft, the Nehterlands: NEN.

Nederlands Normalisatie Instituut. (2004b). *Buitenriolering - Onderzoek en toestandsbeoordeling van objecten (Sewerage systems outside buildings - Diagnostic research and assessment of the condition of objects)*. (NEN 3398). Delft, the Nehterlands: NEN.

Nederlands Normalisatie Instituut. (2004c). *Buizen en hulpstukken van ongewapend, gewapend en staalvezelbeton (Concrete pipes and fittings, unreinforced, steel fibre and reinforced)*. (NEN 7126). Delft, the Netherlands: NEN.

Neville, A. M. (1995). *Properties of Concrete* (4th ed.). Harlow, UK: Longman Group.

Nikuradse, J. (1933). Strömungsgesetze in rauhen Röhren (Laws of flow in rough pipes). *VDI-Forschungsheft, 361*.

O'Connell, M., McNally, C., & Richardson, M. G. (2010). Biochemical attack on concrete in wastewater applications: A state of the art review. *Cement and Concrete Composites, 32*, 479-485.

Oksanen, J., & Sarjakoski, T. (2005). Error propagation of DEM-based surface derivatives. *Computers and Geosciences, 31*(8), 1015-1027.

Olhoeft, G.R. (2000). Maximizing the information return from ground penetrating radar. *Journal of Applied Geophysics, 43*, 175-187.

Oosterom, G. E., & Hermans, R. H. J. J. (2005). *The Sewerage Atlas*. Ede, the Netherlands: RIONED.

Oranjewoud. (2009). *Bemalingsadvies: Wooneilanden Talmastone en riolering Talmastraat Breda (Land drainage advice: Residential Islands Talma Zone and sewer Talmastraat Breda)*. (189027). Breda, The Netherlands: Oranjewoud.

Oualit, M., Jauberthie, R., Rendell, F., Melinge, Y., & Abadlia, M. (2012). External corrosion to concrete sewers: a case study. *Urban Water Journal, 9*, 429-434.

Parande, A. K., Ramsamy, P. L., Ethirajan, S., Rao, C. R. K., & Palanisamy, N. (2006). Deterioration of reinforced concrete in sewer environments. textitProceedings of the Institution of Civil Engineers: Municipal Engineer, 159(1), 11-20.

Park, H., & Lee, I. K. (1998). Existing sewer evaluation results and rehabilitation strategies: The city of Seoul, Korea. Environmental Technology, 19, 733-739.

Pegram, G. G. S., & Pennington, M. S. (1996). *A method for estimating the hydraulic roughness of unlined bored tunnels*. (WRC 579/1/96), Water Research Commission, Department of Civil Engineering, University of Natal. Johannesburg, South Africa.

Plihal, H., Kretschmer, F., Bin Ali, M. T., See, C. H., Romanova, A., Horoshenkov, K. V., & Ertl, T. (2015). A novel method for rapid inspection of sewer networks: combining acoustic and optical means. *Urban Water Journal*, 1-12.

Pipino, L. L., Lee, Y. W., & Wang, R. Y. (2002). Data quality assessment. *Communications of the ACM, 45*, 211-218.

Polder, R. (1987). *Duurzaamheid rioolleidingen - Een literatuurstudie naar Aantastingsmechanismen (Sustainable Sewers - A Literature Study on Deterioration Mechanisms)*. TNO, The Hague, The Netherlands.

Pomeroy, R., & Parkhurst, J. (1977). Forecasting of sulfide buildup rates in sewers. *Progress in water technology, 9*, 621-628.

Popovics, J. S., & Rose, J. L. (1994). A survey of developments in ultrasonic NDE of concrete. *IEEE Trans. Ultrason. Ferroelectr. Freq. Control 41*(1), 140-143.

Randrup, T. B., McPherson, E. G., & Costello, L. R. (2001). Tree root intrusion in sewer systems: Review of extent and costs. *Journal of infrastructure systems, 7*(1), 26-31.

Redman, T. C. (1996). *Data quality for the information age*. Boston: Artech House.

RILEM. (1988). CPC-18 Measurement of hardened concrete carbonation depth. *Materials and Structures*, 21, 453-455

RIONED. (2004). *Inspectie en beoordeling (Inspection and assessment)*. Ede, the Netherlands: RI-ONED.

RIONED. (2007). *Kostenkengetallen rioleringszorg (Key cost figures for sewerage management)*. D1100. Ede, the Netherlands: RIONED.

RIONED. (2009). *Urban drainage statistics 2009-2010*. Ede, the Netherlands: RIONED.

Romanova, A. (2014). *Acoustic monitoring of hydraulic resistance in partially full pipes*. PhD thesis. University of Bradford, Bradforf, UK.

Sægrov, S., Melo Baptista, J. F., Conroy, P., Herz, R. K., Le Gauffre, P., Moss, G., Oddevald, J. E., Rajani, B. & Schiatti, M. (1999). Rehabilitation of water networks: Survey of research needs and on-going efforts. *Urban Water, 1*(1), 15-22.

Sousa, V., Ferreira, F., Almeida, N., Saldanha, J., Martins, J., & Teixeira, A. (2009). A simplified technical decision support tool for the asset management of sewer networks. *Water Asset Management International, 5*, 3-9.

Stanić, N., de Haan, C., Tirion, M., Langeveld, J. G., & Clemens, F. H. L. R. (2013a). Comparison of core sampling and visual inspection for assessment of concrete sewer pipe condition. *Water Science and Technology, 67*(11), 2458-2466.

Stanić, N., van der Schoot, W., Kuijer, B., Langeveld, J. G. & Clemens, F. H. L. R. (2013b, August). *Potential of laser scanning for assessing structural condition and physical roughness of concrete sewer pipes*. Paper presented at the 7th International SPN Conference, Sheffield, UK.

Stanić, N., Langeveld, J. G., & Clemens, F. H. L. R. (2014a). HAZard and OPerability (HAZOP) analysis for identification of information requirements for sewer asset management. *Structure and Infrastructure Engineering, 10*(11), 1345-1356.

Stanić, N., Salet, T., Langeveld, J. G., & Clemens, F. H. L. R. (2014b, September). *Design of a laboratory set-up for evaluating structural strength of deteriorated concrete sewer pipes*. Paper presented at the 13th IWA/IAHR International Conference on Urban Drainage, Kuching, Malaysia.

Stein, D. (2001). *Rehabilitation and maintenance of drains and sewers*, Berlin, Germany: Ernst & Sohn.

Stark, J., & Bollmann, K. (1999). *Delayed ettringite formation in concrete*. Paper presented at the Nordic Concrete Research Meeting, Oslo, Norway.

Straub, L. G., & Morris, H. M. (1950). *Hydraulic tests on concrete culvert pipes*. Minneupolis, MN: St. Anthony Falls Hydraulic Laboratory, University of Minnesota.

Stone, S. L., Dzuray, E. J., Meisegeier, D., Dahlborg, A. S., & Erickson, M. (2002). textitDecision-support tools for predicting the performance of water distribution and wastewater collection systems: US EPA.

Titterton, D. & Weston, J. (2004). *Strap down Inertial Navigation*. ISBN 0-86341-358-7.

Thomson, J., Morrison, R. S., & Sangster, T. (2010). *Inspection Guidlines for Wastewater Force Mains*. (04-CTS-6URa). Alexandria, VA: Water Environment Research.

Trautmann, C. H., & O'Rourke, T. D. (1985). Lateral force-displacement response of buried pipe. *Journal of Geotechnical Engineering, 111*(9), 1077-1092.

Tsai, R.Y. (1987). A versatile camera calibration technique for high-accuracy 3D machine vision metrology using off-the-shelf TV cameras and lenses. *Robotics and Automation, IEEE Journal of, 3*(4), 323-344.

Tuncan, M., Arioz, O., Ramyar, K., & Karasu, B. (2008). Assessing concrete strength by means of small diameter cores. *Construction and Building Materials, 22*, 981-988.

van der Schoot, W. (2015). *Laser profiling of sewer pipes*. M.Sc thesis, Delft University of Technology, Delft, The Netherlands.

Waisel, Y., Eshel, A., & Kafkafi, U. (1991). *Plant Roots: The Hidden Half*. New York: Marcel Dekker.

Walder, T. C. (2011). Financing of the Dutch water systems. *Netherlands Water Partnership.*

Wang, R. Y. (1998). A product perspective on total data quality management. *Communications of the ACM, 41*, 58-65.

Wang, R. Y., & Strong, D. M. (1996). Beyond accuracy: What data quality means to data consumers. *Journal of Management Information Systems, 12*, 5-33.

Water Environment Federation (1994). Existing sewer evaluation and rehabilitation. *WEF manual of practice FD-6, ASCE manual and report on engineering practice. No. 62* (2nd ed.). Alexandria, VA: WEF Press.

Water Services Association and Foundation for Water Research (1993). *Materials selection manual for sewers, pumping mains and manholes. London*: (WSA/FWR-04) WSA/FWR.

Wirahadikusumah, R., Abraham, D. M., Iseley, T., & Prasanth, R. K. (1998). Assessment technologies for sewer system rehabilitation. *Automation in Construction, 7*(4), 259-270.

Wright, D., Greve, P., Fleischer, J. & Austin, L. (1992). Laser beam width, divergence and beam propagation factor-An international standardization approach. *Optical and quantum electronics, 24*, 993-1000.

Wu, J., Norvell, W., & Welch, R. (2006). Kriging on highly skewed data for DTPA-extractable soil Zn with auxiliary information for pH and organic carbon. *Geoderma, 134*(1), 187-199.

Zhang, Z. (2000). A flexible new technique for camera calibration, *Pattern Analysis and Machine Intelligence, IEEE Transactions on, 22*(11), 1330-1334.

Zhang, L., De Schryver, P., De Gusseme, B., De Muynck, W., Boon, N., & Verstraete, W. (2008). Chemical and biological technologies for hydrogen sulfide emission control in sewer systems: A review. *Water Research, 42*(1-2), 1-12.

SUMMARY

Asset management is a tool for maintaining the required level of serviceability of urban drainage systems, which are costly to construct and in some cases even more costly to replace. The required asset management effort to achieve a certain level of service is unclear due to a limited knowledge on sewer failure mechanisms and due to scarcity of information on the functioning and conditions of urban drainage systems. An important question is: what information of what quality is necessary for cost-effective sewer asset management? In The Netherlands the majority of urban drainage systems are made of concrete elements (about 72%), including nearly all main sewers > 500 mm, thus making the information on the concrete sewer pipes of significant importance.

This research aims at (*i*) identifying the required information on the structural and hydraulic performance of the sewer pipes, (*ii*) quantifying the uncertainties of information and (*iii*) improving the quality of this information in order to further understand the changes in processes/status. Sewer failure mechanisms explain the structural and/or operational failures of sewer elements. In order to be able to identify the main processes and defects responsible for the structural and/or operational failures of sewer elements, as well as the possibility of obtaining the information about them, a HAZard and Operability (HAZOP) approach was applied. This technique was demonstrated to be applicable for analysing the information needed for sewer asset management. Structural strength and hydraulic capacity are two essential parameters in the assessment of the need for sewer rehabilitation.

In sewer systems where corrosion is the dominant failure mechanism, visual inspection by closed circuit television (CCTV) and core sampling are among the methods mostly applied to assess sewer pipe condition. A study was carried out on visual inspection and drill core analysis in order to enhance a further understanding of the limitations and potentials of both methods and the added value of combining the information from both sources. Both methods have been applied on a selected sewer reach in the city of The Hague, which was reportedly subject to pipe corrosion. The results show that both methods, visual inspection and core sampling, are associated with large uncertainties and that there is no obvious correlation between the results of visual inspection and the results of drill core analysis. The conclusion is that information of a certain quality (depending on the circumstances) on the actual status of the assets is a prerequisite for adequate sewer asset management.

For instance, especially concrete pipes suffer from loss of wall thickness due to biochemical corrosion and, consequently, a decreasing structural strength along with an increase in hydraulic roughness. Unfortunately, routinely used visual inspection methods do not allow a quantification of the internal pipe geometry, which would enable not only detection but also the quantification of the progress of biochemical corrosion. Advances in laser technology and digital cameras theoretically allow a cost-effective application of laser profilers to measure the interior geometry of sewer pipes. An analysis of associated uncertainties revealed that the position and alignment of the laser in commonly used laser profiling techniques are the main sources of measurement errors. A full-scale laboratory set-up demonstrated, based on tests on a new and an 89 year old corroded sewer pipe, that laser profiling is indeed capable of measuring the interior geometry accurately enough to determine wall thickness losses for corroded pipes, provided that the position and alignment of the laser and camera are accounted for.

Further, drill core samples are taken for an analysis of the material characteristics of concrete pipes in order to improve the quality of decision making on rehabilitation actions. It was shown in this study that core sampling is associated with a significant uncertainty. The results of core samples are compared with the results of full-scale pipe cracking lab experiments. It is shown that the concrete of deteriorated sewer pipes shows a significant variability in material characteristics.

Further it is shown that the formation of ettringite due to biochemical sulphuric corrosion is not necessarily limited to the crown of the pipe and that also degradation of pipe material, measured by the carbonation depth, is occurring at the inside and outside of the pipe. It is concluded that tensile splitting strength and carbonation depth (*i.e.* loss of 'healthy' wall thickness) are material property parameters of core sampling with a sufficiently high correlation ($R^2 > 0.90$) with the constructive strength of the pipe. The thickness of the remaining healthy concrete material is the optimal parameter in terms of correlation with collapse strength, as this requires the smallest sampling size.

Furthermore, in sewer asset management, decision making on rehabilitation or replacement should preferably be based on the actual functionality of a sewer system. In order to judge the ability of a sewer system to transport sewage, hydrodynamic models are used: hydraulic roughness is one of the key parameters. For new pipes, the hydraulic properties are well known, but for aged pipes, with uneven deterioration along the cross section, information on the hydraulic roughness is lacking. The potential of laser profiling methods for accurate, non-invasive and non-intrusive assessment of the hydraulic roughness of concrete sewer pipes is described, demonstrated and discussed. Processing of raw scanned data consists of two steps: (*i*) spatial interpolation with uncertainty analysis and (*ii*) statistical analysis for estimating the hydraulic roughness. Moreover, a statistical analysis was carried out to determine the minimal scanning resolution required in order to yield results accurate enough for subsequent modelling uses. The results show a promising potential of the laser scanning approach for a simple and fast quantification of the hydraulic roughness in a sewer system.

A Prototype v1.0 (in this study) of an unbiased laser profiler was developed to improve the accuracy of collected information. However, there is a need for more accurate apparatus. The new design of the Prototype v2.0 presented provides accurate measurements ($\sigma < 2$ mm) of the cross section and, from frame to frame, an accurate 3D image of a pipe. The potential applications of the improved laser profiling technique are comprehensive *e.g.* enhancement of inaccurate visual inspection, deposit measurements, roughness measurements. The combination of the two methods, *i.e.* to use the laser profiler to determine the pipe interior geometry as well as to identify representative patches where roughness should be measured, is an opportunity to strengthen laser profiling as a method that may partially replace a CCTV inspection as a dominantly applied sewer investigation technique. Additionally to achieve a higher accuracy, there are several improvements that can be applied to a potential third version of the prototype. Currently the amount of raw data that is generated during the experiment over 1 m of pipe length is around 4.86 GB: the data flow is too high for an embedded application but this can be significantly reduced. There are still some improvements to be done with the presented hardware to make the data acquisition faster and easier.

Future work will concentrate on the development and improvement of the laser profiling technique accuracy and possibilities for its use - Prototype v3.0. The results of this research will be used for future development of inspection strategies using core sampling. For sewer rehabilitation decisions, it is necessary to be able to calculate the remaining strength of the soil-pipe construction environment for deteriorated pipes. Further research will concentrate on simulations with a Finite Element Method (FEM), with the pipe geometry information provided by laser profiling and material properties by core sampling. The model will be used to determine the remaining load-bearing capacity of a sewer pipe and to determine the type of information needed to further enhance the decision making process.

SAMENVATTING

Kosteneffectief beheer van de riolering heeft als doel een bepaald minimum service niveau te garanderen tegen minimale/acceptabele kosten. Om dit te bereiken is informatie nodig over de actuele functionaliteit en kennis van faalmechanismen. De kennis over deze faalmechanismen is echter beperkt en de in de praktijk beschikbare informatie is beperkt. Daarom is het niet altijd mogelijk om tot een efficiënte manier van werken te komen. Een belangrijke vraag in dit verband is: welke informatie van welke kwaliteit is er nodig voor kosteneffectief rioleringsbeheer? Het meest gebruikte buismateriaal voor riolering in Nederland is beton (ongeveer 72%). Om deze reden is in het hier gepresenteerde onderzoek uitgegaan van betonnen rioolbuizen.

Dit onderzoek richt zich op (*i*) het identificeren van de vereiste informatie over de constructieve en hydraulische karakteristieken van rioolbuizen, (*ii*) het kwantificeren van de onzekerheden van deze informatie en (*iii*) de verbetering van de kwaliteit van deze informatie om het inzicht in faalmechanismen en de actuele staat van een buis te kunnen vergroten. Deze faalmechanismen beschrijven zowel het constructief als het operationele falen van riolen. Om in staat zijn om de belangrijkste processen en gebreken die verantwoordelijk zijn voor constructief en/of operationeel falen te beschrijven, en de informatie die noodzakelijk is voor de kwantificering ervan, is een HAZOP (Hazard and Operability) benadering toegepast. Constructieve sterkte en hydraulische capaciteit zijn de twee essentiële parameters bij de beoordeling van de noodzaak tot vervanging/reparatie van een riool.

In situaties waar corrosie het dominante faalmechanisme is, zijn visuele inspectie via een gesloten tv-circuit (CCTV) en boorkern analyse de meest toegepaste methoden om de staat van riolen te beoordelen. Onderzocht is of en in hoeverre beide methoden onderling consistente resultaten opleveren en of het combineren van de beide methoden tot meerwaarde leidt. Dit onderzoek is uitgevoerd op een rioolstreng in de gemeente Den Haag, waar sprake was van aantasting van het buismateriaal. De resultaten van dit onderzoek laten zien dat er geen duidelijke relatie is te leggen tussen de informatie uit de visuele inspectie en de analyseresultaten van de genomen boorkernen.

Met name betonnen buizen (maar ook andere cementgebonden materialen) lijden aan verlies van wanddikte door biochemische corrosie. Als gevolg daarvan treedt een afname van de constructieve sterkte op in combinatie met een toename van hydraulische ruwheid en daardoor een afname van de hydraulische capaciteit. Helaas is het zo dat met de tegenwoordig toegepaste visuele inspectie technieken een nauwkeurige *in situ* bepaling van de interne geometrie van een buis niet mogelijk is. Ontwikkelingen in de laser- en camera technologie maken het mogelijk om juist deze binnen geometrie nauwkeurig in te meten. Uit een analyse van de bijbehorende onzekerheden bleek dat het nauwkeurig kennen van de positie en de oriëntatie van de meetapparatuur een belangrijke voorwaarde is om tot bruikbare resultaten te komen. In een laboratoriumopstelling is op basis van experimenten op een nieuwe en een 89 jaar oude rioolbuis aangetoond dat het met laser profilering mogelijk is om de binnen geometrie dusdanig nauwkeurig in te meten dat de resterende wanddikte tot op enkele millimeters nauwkeurigheid te bepalen is.

Het uitvoeren van een boorkernanalyse bij betonnen buizen is een veel gebruikte methode om informatie te verkrijgen over de constructieve sterkte van riolen. In dit onderzoek is nagegaan in hoeverre boorkernanalyse bruikbare informatie oplevert. Aangetoond is dat, zeker in oudere buizen, sprake is van een grote spreiding in de resultaten (samenhangend met een grote inhomogeniteit van het buismateriaal). De splijtsterkte van boorkernen en de carbonatatiediepte blijken de beste informatiebronnen te zijn ten aanzien van constructieve sterkte. Tevens is aangetoond dat, om een voldoende betrouwbare schatting van relevante parameters te verkrijgen, een zeer groot aantal monsters genomen moet worden. In bepaalde gevallen wordt dit aantal dus-

danig groot dat dit praktisch en financieel onhaalbaar wordt. Verder is gebleken dat ettringiet vorming vrijwel overal in het buismateriaal voorkomt.

Een rioolstelsel dient er in de eerste plaats voor om (afval)water in te zamelen en af te voeren. Daarom is de hydraulische capaciteit van een riool een belangrijke parameter bij het beoordelen van de functionaliteit. Naast lokale hydraulische verliezen speelt ook de ruwheid van de buiswand hierbij een rol. Als gevolg van corrosie van beton neemt deze ruwheid gedurende de gebruiksfase van een riool toe in combinatie met een toename van het doorstroomprofiel. Om de actuele hydraulische capaciteit van een riool te kunnen bepalen is dus zowel een meting van de binnen geometrie als een bepaling van de wandruwheid noodzakelijk. In dit onderzoek is een combinatie van respectievelijk laser profiling en laserscanning toegepast om beide parameters nauwkeurig te meten. De verwerking van ruwe gescande gegevens bestaat uit twee stappen: (*i*) de ruimtelijke interpolatie met onzekerheidsanalyse en (*ii*) statistische analyse voor het schatten van de hydraulische ruwheid. Bovendien werd een statistische analyse uitgevoerd om de minimale scanresolutie te bepalen die vereist is om bruikbare resultaten te verkrijgen. De resultaten tonen aan dat met behulp van de gebruikte technieken een betrouwbare schatting van de hydraulische capaciteit mogelijk is.

In dit onderzoek is begonnen met een eenvoudig Prototype v1.0 laser profiler, waarbij via een zelf ontwikkelde methode werd gecorrigeerd voor positie en oriëntatie van de profiler in de rioolbuis. Aan de hand van een analyse van de resultaten en een onderzoek naar de bronnen van onnauwkeurigheid, is een verbeterd Prototype v2.0 ontwikkeld waarmee een 3D beeld met een aantoonbare nauwkeurigheid van 2 mm verkregen kan worden. Met de ontwikkelde technieken is het mogelijk om objectieve informatie met een bekende nauwkeurigheid te genereren ten aanzien van twee belangrijke parameters die direct aan het functioneren van de riolering raken, namelijk constructieve sterkte en hydraulische capaciteit. Om te komen tot praktijktoepassingen dient nog het een en ander te worden onderzocht/ontwikkeld, bijvoorbeeld het systeem van positiebepaling en de verwerking van de gegevensstroom. Momenteel is de hoeveelheid ruwe data die wordt gegenereerd tijdens een experiment ongeveer 4.86 GB per strekkende meter riool: deze datastroom te hoog is voor een praktijk toepassing. Inmiddels heeft het gebruik van datacompressietechnieken en aanpassingen in de hardware geleid tot een aanzienlijke reductie van deze datastroom.

Toekomstig onderzoek zal zich concentreren op de ontwikkeling en verbetering van de laser profilering techniek, met name het verder vergroten van de nauwkeurigheid en de mogelijkheden voor het praktisch gebruik moeten hierbij aandacht krijgen. De resultaten van dit onderzoek zullen gebruikt worden voor de ontwikkeling van inspectie strategieën door middel van boorkern analyse. Daarnaast is er nog veel onbekend over de interactie tussen buis en de omringende grond, verder onderzoek moet leiden tot niet-destructieve methoden aan de hand waarvan, gecombineerd met de hier gepresenteerde technieken, de constructieve sterkte van een riool nauwkeurig kan worden bepaald, denk hierbij bijvoorbeeld aan toepassing van simulaties gebaseerd op de Eindige Elementen Methode (EEM).

LIST OF PUBLICATIONS

Peer-Reviewed Journal Publications

Stanić, N., de Haan, C., Tirion, M., Langeveld, J. G., & Clemens, F. H. L. R. (2013). Comparison of core sampling and visual inspection for assessment of concrete sewer pipe condition. *Water Science and Technology, 67*(11), 2458-2466.

Stanić, N., Langeveld, J. G., & Clemens, F. H. L. R. (2014). HAZard and OPerability (HAZOP) analysis for identification of information requirements for sewer asset management. *Structure and Infrastructure Engineering, 10*(11), 1345-1356.

Clemens, F. H. L. R., Stanić, N., van der Schoot, W., Langeveld, J. G., & Lepot, M. (2015). Uncertainties associated with laser profiling of concrete sewer pipes for the quantification of the interior geometry. *Structure and Infrastructure Engineering, 11*(9), 1218-1239.

Stanić, N., Langeveld, J. G., Salet, T., & Clemens, F. H. L. R. (2015). Relating the structural strength of concrete sewer pipes and material properties retrieved from core samples. *Structure and Infrastructure Engineering*: under review.

Stanić, N., Clemens, F. H. L. R., Lepot, M., & Langeveld, J. G. (2015). Estimation of hydraulic roughness of concrete sewer pipes by laser scanning. *Journal of Hydraulic Engineering*: under review.

Stanić, N., Lepot, M., Catieau, M., Langeveld, J. G., & Clemens, F. H. L. R. (2015). A new and collaborative technology for sewer pipe inspection (Part 1): design, calibrations, corrections and potential application of a laser profiler. *Automation in Construction*: under review.

Lepot, M., Stanić, N., & Clemens. F. H. L. R. (2015). A new and collaborative technology for sewer pipe inspection (Part 2): assessment of robustness and accuracy in laboratory. *Automation in Construction*: under review.

Conference proceedings

Stanić, N., Langeveld, J. G., & Clemens, F. H. L. R. (2012, September). *Identification of the information needs for sewer asset management by assessing failure mechanisms*. Paper presented at the 9th International Conference on Urban Drainage Modelling, Belgrade, Serbia.

Stanić, N., de Haan, C., Tirion, M., Langeveld, J. G., & Clemens, F. H. L. R. (2012, September). *Comparison of core sampling and visual inspection for assessment of concrete sewer pipe condition*. Paper presented at the 9th International Conference on Urban Drainage Modelling, Belgrade, Serbia.

Stanić, N., van der Schoot, W., Kuijer, B., Langeveld, J. G. & Clemens, F. H. L. R. (2013, August). *Potential of laser scanning for assessing structural condition and physical roughness of concrete sewer pipes*. Paper presented at the 7th International SPN Conference, Sheffield, UK.

Stanić, N., Langeveld, J. G., & Clemens, F. H. L. R. (2014, September). *Potential of laser scanning for quantification of sediment deposits in sewer*. Paper presented at the 13th IWA/IAHR International Conference on Urban Drainage, Kuching, Malaysia.

Stanić, N., Salet, T., Langeveld, J. G., & Clemens, F. H. L. R. (2014, September). *Design of a laboratory set-up for evaluating structural strength of deteriorated concrete sewer pipes*. Paper presented at the 13th IWA/IAHR International Conference on Urban Drainage, Kuching, Malaysia.

van Riel, W. A. P., Stanić, N., Langeveld, J. G., & Clemens, F. H. L. R. (2014, October). *Pipe quality information in sewer asset management:. Use and uncertainties*. Paper presented at the 9th World Congress on Engineering Asset Managemen, Pretoria, South Africa.

Lepot, M., Stanić, N., Catieau, M., & Clemens, F. H. L. R. (2015, September). *Laser profiling: a promising technique to accurately assess pipe state and roughness*. Paper presented at the 10th International Urban Drainage Modelling Conference, Mont Saint-Anne, Canada.

National publications

Stanić, N., Langeveld, J. G., & Clemens, F. H. L. R. (2012). Identificatie van de benodigde informatie voor het beoordelen van faalmechanismen bij het rioleringsbeheer. *WT Afvalwater, 12*(4), 293-302.

Stanić, N., de Haan, C., Tirion, M., Langeveld, J. G., & Clemens, F. H. L. R. (2013). Een vergelijking van boorkernenanalyse en visuele inspectie ter beoordeling vna de conditie van rioolbuizen. *WT Afvalwater, 13*(1), 9-18.

ABOUT THE AUTHOR

Nikola Stanić was born in Kragujevac (44° 0′ 40″ N, 20° 54′ 40″ E), Serbia on September 26th 1983. He received his graduate degree in hydraulic engineering from the Faculty of Civil Engineering, University of Belgrade, Serbia in 2007 and spent a year working as a junior design engineer in the small engineering consultancy firm CEKIBEO d.o.o., Belgrade. He moved in 2008 to Delft to complete a MSc in Water Supply Engineering at UNESCO-IHE Institute for Water Education. After obtaining his MSc at UNESCO-IHE in 2010 he stayed at the Institute and worked on the projects *i.e.* Arsenic adsorption with ferritin and ASREM-Serbia as a research fellow. In May 2011, he joined Urban Drainage group, Sanitary Engineering Section at Delft University of Technology as a PhD candidate. His research focuses have been on structural and hydraulic conditions of concrete sewer pipes, inspection techniques, information quality, sewer asset management and failure mechanisms; his work resulted in this thesis.